Spatiotemporal Variability of Extreme Low Wind Power Events in Great Britain



Panit Potisomporn
Kellogg College
University of Oxford

A thesis submitted for the degree of
Doctor of Philosophy
Trinity Term 2024

Acknowledgements

To my supervisors–Prof. Thomas Adcock and Dr. Christopher Vogel–I extend my deepest thanks for the opportunity to embark on this unparalleled academic journey. Your guidance, dedication, time, and immense support have been pivotal to the completion of this research. One truly could not ask for better supervisors.

To my friends–exceptional mathematicians, statisticians, engineers, scientists, lawyers, literary scholars, finance practitioners, golfers, and poker enthusiasts–I express my sincere appreciation for the unfailing counsel and encouragement in the face of challenges. Your companionship has made my experience in Oxford enormously joyful, fulfilling, and memorable.

To my family, I offer my boundless gratitude. Your love has been, and always will be, the foundation of all my achievements. I owe you everything.

Abstract

In the United Kingdom, wind energy assumes a pivotal role in the decarbonisation of the electricity system as part of the Net Zero Strategy. However, the intermittency and variability of the wind resource are key challenges for its integration into the electricity system. A clear manifestation of such an issue occurred in March 2021, when the country experienced one of the longest cold, calm spells in a decade. For eleven consecutive days, the Great British wind farm fleet operated at 11% of its rated capacity, during a period when low temperatures drove up electricity demand. Although infrequent, such events represent the foremost challenge to the decarbonisation of the British electricity system. This thesis is concerned with quantifying the likelihood of these extreme low wind events.

A Great Britain-wide evaluation is conducted on ERA5 reanalysis data to ensure its suitability in representing low wind power events. Results show that events longer than 12 hours are well described by ERA5, but addressing the dataset's significant positive mean wind speed bias is still necessary to improve this representation. The findings are then used to inform the simulation of nationally aggregated wind power output over a 72-year period, from 1950 to 2021. Taking motivation from hydrology, runs analysis is used to define and identify low wind power events from the power output time series. Compared to a simple constantly-below-threshold approach, the concurrent application of pooling procedures to identify such events results in a definition for extreme wind events that is more statistically robust as well as more relevant to the balancing of wind energy supply and electricity demand. Results suggest that the duration for which extreme wind events impact the electricity system is, in fact, longer than previously estimated; using a 0.1 capacity factor threshold, the longest event identified from the 72-year record has a duration of 26 days.

This methodology is applied to the nationally aggregated wind power output time series simulated from the current, near-future, and potential far-future wind farm distributions. An extreme value analysis is conducted on each set of identified low wind power events to quantify their risk. The current Great British fleet is expected to experience a 2-week low wind power event once every 10 years. By 2030, this recurrence interval is projected to increase to 30 years, but the risk of shorter events does not exhibit substantial reduction. The exploration of various wind farms distribution scenarios for the year 2050 underscores the need for greater spatial diversification by deploying wind farms farther offshore and into less developed regions like the West, Northwest, and Southwest. Achieving this strategic deployment is critical to enhancing the resilience of the future electricity system.

Nomenclature

Abbreviations

3D-VAR	Three-dimensional Variational
4D-VAR	Four-dimensional Variational
AMS	Annual Maximum Series
CDF	Cumulative Distribution Function
CDF-t	Cumulative Distribution Function transform
CF	Capacity Factor
CoV	Coefficient of Variation
DNW	Demand-net-wind
ECMWF	European Centre for Medium-range Weather Forecast
EEZ	Exclusive Economic Zone
ERA5	European Centre for Medium-range Weather Forecast 5th Generation Reanalysis
FES	Future Electricity Scenarios
GB	Great Britain
IET	Inter-event Time
MA	Moving Average
MIDAS	Met Office Integrated Data Archive System
NAO	North Atlantic Oscillation
PDS	Partial Duration Series
PDF	Probability Density Function
PV	Projected Values
REPD	Renewable Energy Planning Database
RMSE	Root Mean Square Error
SD	Spatial Distribution
SPA	Sequent Peak Algorithm
StDev	Standard Deviation
UK	United Kingdom
UTC	Coordinated Universal Time

Variables

θ_{CF}	Capacity factor threshold
σ	Standard deviation
CF	Capacity Factor
u	Wind speed
$\overline{u}$	Mean wind speed
$()_{ERA}$	Quantities associated with ERA5 data
$()_{OBS}$	Quantities associated with observed data

Common units

GWh	Gigawatt-hour
GW	Gigawatt
km^2	Square kilometre
m	Metre
m/s	Metre per second
MW	Megawatt
TWh	Terawatt-hour

Chapter 2

λ	Weibull scale factor
k	Weibull shape factor
$P(u < 4)$	Percentage frequency of wind speed lower than 4 m/s
u_i	Wind speed component in the i direction
$()_{ERROR}$	Quantities associated with ERA5 errors with respect to observed data

Chapter 3

α_i	The i^{th} coefficient of regression
θ	Five-parameter logistic function parameters set
μ_e	Target mean wind speed
σ_e	Target wind speed standard deviation
CDH	Cooling degree hour
D	Hourly electricity demand
HDH	Heating degree hour
P_{5PL}	Five-parameter logistic function
T	Country-averaged hourly 2-m temperature
u^*_{ERA}	Bias-corrected ERA5 wind speed
$()_{AMS}$	Annual maximum series of a variable
$()_{PDS}$	Partial duration series of a variable

Chapter 4

α	Partial duration series truncation level
δ	Binary indicator for whether a time series is below a threshold
σ	Severity of an excess event
γ	Duration of an excess event
γ_r	Inter-event ratio threshold
γ_t	Inter-event time threshold
c	Wind farm capacity
cf	Single-farm capacity factor
d	Duration of a low wind event
D	Discrete series of low wind event duration
$E[L]$	Inter-arrival time
$E[T]$	Recurrent interval
s	Severity of a low wind event
S	Discrete series of low wind event severity
w	Cumulative deficit time series

Contents

1 Introduction **1**
- 1.1 Renewable energy . . . 2
  - 1.1.1 Renewable energy in the United Kingdom . . . 3
- 1.2 Wind energy . . . 4
  - 1.2.1 Spatiotemporal variability of the wind resource . . . 4
  - 1.2.2 Extreme low wind events . . . 7
- 1.3 Wind energy in the United Kingdom . . . 10
  - 1.3.1 Climatology . . . 10
  - 1.3.2 Spatiotemporal variability . . . 11
  - 1.3.3 Extreme low wind events . . . 13
  - 1.3.4 Sensitivity of extreme low wind events to wind farm spatial distribution 16
- 1.4 Review of Methodologies . . . 17
  - 1.4.1 Reanalysis data usage . . . 17
  - 1.4.2 Modelling wind power output and electricity demand from reanalysis data . . . 19
  - 1.4.3 Frequency and extreme value analyses . . . 20
- 1.5 Thesis objectives . . . 22
- 1.6 Thesis outline . . . 25

2 Evaluating ERA5 reanalysis predictions of low wind speed events around the UK **33**
- 2.1 Introduction . . . 34
- 2.2 Methodology and Data . . . 37
  - 2.2.1 Reanalysis Data . . . 37
  - 2.2.2 Observation Data . . . 37
  - 2.2.3 Methodology . . . 39
- 2.3 Results and Discussions . . . 42
  - 2.3.1 Errors . . . 42
  - 2.3.2 Sources of Uncertainty . . . 48
- 2.4 Conclusion . . . 53

3 Modelling Great Britain wind power output and electricity demand **59**
- 3.1 Introduction . . . 60
- 3.2 GB-aggregated power output model . . . 61
  - 3.2.1 Bias correction . . . 62
  - 3.2.2 Extrapolation of wind speed to hub height . . . 65
  - 3.2.3 Wind farm power curve modelling . . . 68
  - 3.2.4 Validation . . . 72
- 3.3 Electricity demand model . . . 73
- 3.4 Conclusions . . . 76

4 Extreme value analysis of low wind power events in Great Britain 82
4.1 Introduction . . . 83
4.2 Data sources and processing . . . 85
4.2.1 Reanalysis data description and evaluation . . . 86
4.2.2 GB wind farms and spatial interpolation . . . 87
4.2.3 Extrapolation of wind speed to hub height . . . 87
4.2.4 Power output modelling . . . 88
4.2.5 GB-aggregated CF and validation . . . 88
4.3 Application of pooling procedures to low wind power events . . . 89
4.3.1 Runs analysis . . . 89
4.3.2 Pooling procedures . . . 90
4.3.3 Sensitivity to pooling procedure . . . 94
4.3.4 Frequency, duration, and severity of low wind power events . . . 96
4.4 Extreme value analysis: a 72-year case study of low wind power events in Great Britain . . . 98
4.4.1 Extreme value models . . . 98
4.4.2 Extreme value distribution evaluation . . . 101
4.4.3 Return periods and confidence intervals . . . 104
4.5 Discussion . . . 106
4.5.1 Implications for the electricity system . . . 106
4.5.2 Model limitations . . . 110
4.6 Conclusions . . . 111

5 Spatial variability of extreme wind events: Implications for the future electricity system 117
5.1 Introduction . . . 118
5.2 Near-future analysis . . . 120
5.2.1 Data and Methods . . . 120
5.2.2 Fleet . . . 120
5.2.3 Capacity factor . . . 123
5.2.4 Low wind power events . . . 123
5.3 Far-future analysis . . . 125
5.3.1 Data and methods . . . 125
5.3.2 Wind energy supply . . . 127
5.3.3 Electricity system . . . 142
5.4 Conclusions . . . 144

6 Conclusions 156
6.1 Summary and Conclusions . . . 157
6.2 Future work . . . 160
6.2.1 Power output modelling . . . 160
6.2.2 Weather regimes . . . 161
6.2.3 Climate change . . . 161
6.3 Concluding remarks . . . 162

CHAPTER 1

Introduction

Characterised by rising global temperatures, sea-level rise, and an increase in the frequency and severity of extreme weather events, climate change presents an urgent and global challenge, demanding decisive action to mitigate its effects through the reduction of greenhouse gas emissions. Central to these efforts is the decarbonisation of the electricity system, which is responsible for 40% of all such emissions globally [1]; importantly, this also supports the decarbonisation of other sectors like transport and heating, thus impacting a broader range of emissions beyond just the electricity sector. Hence, a transition to renewable-energy-based power production is necessary. The United Kingdom (UK) has committed to these goals, currently generating approximately 40% of its electricity from renewable sources [2], and due to the country's geographical advantage, wind energy represents a key component. As of 2024, the UK's wind energy capacity reached 30 GW, with wind power generation accounting for up to 33.8% of the nation's electricity generation. In pursuit of future goals as part of the broader Net Zero Strategy, the UK government aims to expand this capacity to over 50 GW by 2030, with projected capacity in 2050 ranging from 100 to 160 GW. These initiatives highlight the pivotal role of wind energy in the UK's strategy to achieve a sustainable, low-carbon future and combat climate change while ensuring energy security.

However, the intermittency and variability of the wind resource are a key challenge for its integration into the wider electricity system. A clear manifestation of this issue occurred in March 2021 when Great Britain (GB) experienced one of the longest cold calm spells in over a decade. As illustrated in Figure 1.1, the national wind farms fleet operated at merely 11% of its rated capacity for 11 consecutive days, during a period when electricity demand was significantly elevated by low temperatures. In response to this substantial reduction in wind power generation, dispatchable fossil fuel generation was increased to compensate for the shortfall. Although such events are not frequent, they

represent one of the foremost challenges to the complete decarbonisation of the electricity system. Therefore, as the proportion of wind energy within the energy mix continues to rise, it is critical to rigorously characterise the risk of these extreme events and their implications for the resilience of the future GB electricity system.

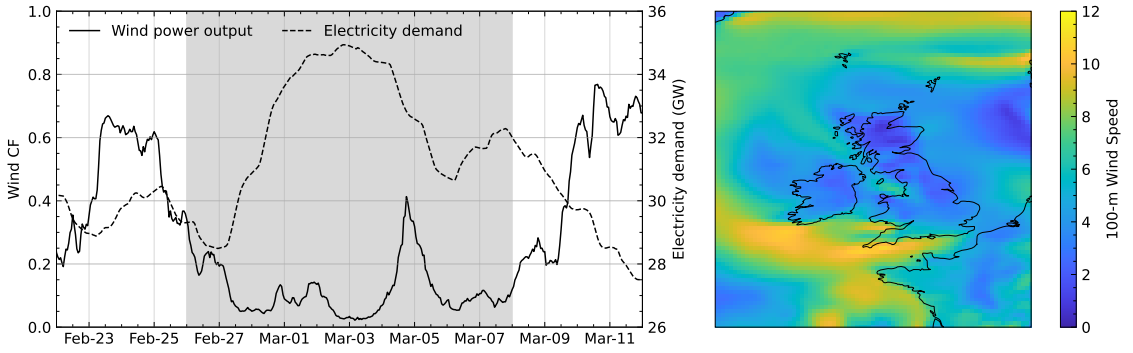


Figure 1.1: (Left) Time series of GB hourly wind power output and 48-hour rolling mean of electricity demand four days before and after the March 2021 event based on data obtained from [3]. The 11-day period of the event is shaded in grey. (Right) Spatial plot of 100-m wind speed across the UK on 2nd March 2021.

1.1 Renewable energy

The global response to climate change is shaped by the recognition that reducing greenhouse gas emissions is critical to limiting global warming to 1.5°C above pre-industrial levels, as stipulated in the Paris Agreement [4]. This target requires a significant reduction in global emissions by 2030 and achieving net-zero emissions by mid-century. Given that the power sector is responsible for approximately 40% of global greenhouse gas emissions [1], the decarbonisation of the electricity system through the deployment of renewable energy plays a central role in this endeavour. Renewable energy sources are derived from natural resources that are inexhaustible and naturally renewable over time, producing little to no greenhouse gas emissions during operation, thereby making them essential components of a low-carbon energy system. The deployment of renewable energy technologies such as wind, solar, and hydroelectric power can significantly reduce CO_2 emissions and drive the achievement of these global climate targets.

Significant progress has been made on this front globally. Currently, approximately

30% of global electricity is generated from renewable sources and this share is projected to increase substantially to 77% by 2050 [1]. Although major contributions have come from large-scale hydroelectric projects, the last decade has seen rapid expansion in renewable capacity, primarily driven by the growth of solar and wind power. However, their inherent variability and intermittency, coupled with their increasing capacity in the energy mix, means that the integration of such resources into the electricity system poses considerable challenges to electricity system planning and operations. One of the foremost challenges is maintaining grid reliability and stability. Unlike conventional power plants which provide predictable power output, variable renewable energy sources produce power that fluctuates with weather-driven variations. Such fluctuations can result in periods of surplus energy during peak production times or more critically, significant energy shortages during low production periods, posing severe risks to energy supply reliability [5].

1.1.1 Renewable energy in the United Kingdom

The UK has set ambitious goals to achieve net-zero greenhouse gas emissions by 2050, as outlined in its Net Zero Strategy [6]. Central to achieving these climate goals is the decarbonisation of the electricity system, which has achieved a remarkable 78% reduction in greenhouse gas emissions since 1990, the highest reduction across all UK sectors [7]. The growth of renewable energy sources (as shown in Figure 1.2), driven by the country's unique geographical advantages and robust policy framework, plays a crucial role in this remarkable feat. As of 2024, renewable energy sources have a total installed capacity of over 57 GW and account for over 50% of electricity generation [7], with a target to reach 100% by 2035. The country's renewable energy portfolio is diverse, featuring a mix of wind, solar, biomass, and hydroelectric power. More mature technologies like solar, biomass, and hydroelectric power collectively make significant contributions, representing 30% of total electricity generated by renewable sources in 2023 [7]. But emerging technologies like tidal power also hold great potential, as strong tidal currents make the UK one of the few locations globally with both the geographical and technological capacity to exploit this more predictable and reliable energy source.

The most important contributor to the UK's renewable energy portfolio, however, is

wind energy. The country's exposure to the strong and consistent winds of the North Atlantic, combined with its extensive coastline and relatively shallow territorial waters, provides optimal conditions for harnessing wind power efficiently, both onshore and offshore. As of 2023, the UK's installed wind power capacity stood at 30 GW, accounting for over 60% of the electricity generated from renewable sources [7], with an additional 38 GW of capacity expected to be deployed by 2030 [8]. Moreover, the UK is one of the global leaders in offshore wind capacity, hosting the world's largest offshore wind farms and pioneering floating wind technology. These achievements and rapid expansions in wind energy not only significantly contribute to reducing carbon emissions but also offer a compelling case study for the integration of wind energy into an electricity system.

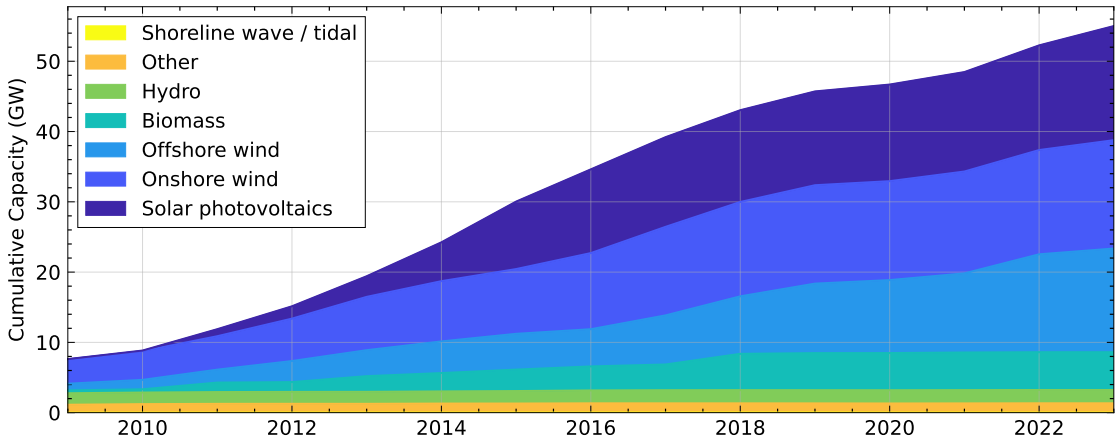


Figure 1.2: Cumulative capacity of renewable energy sources in the UK [7].

1.2 Wind energy

1.2.1 Spatiotemporal variability of the wind resource

Wind is an inherently intermittent resource with limited predictability in both the temporal and spatial domains. Such characteristics are widely recognised as a key challenge for the operation of an electricity system with a high penetration of wind energy [9, 10]. This intermittency arises from various scales of variation in wind speed, ranging from the micro-scale to the macro-scale. On the micro-scale, topographically-induced atmospheric turbulence can cause rapid fluctuations in wind speed and direction at a time scale of

seconds to several minutes and at a spatial scale of metres to hundreds of metres. Variations on such a scale are important for voltage and frequency regulation due to the low system inertia provided by wind turbines [11]. In contrast, at the global climatic scale, variations of the wind resource stem from long-period climatic variations, i.e., the change in the mean and variability of the climate that persists for an extended period, typically decades or longer [12]. This scale of variability therefore concerns long-term policy planning for the integration of wind energy into the electricity system, as well as the evolving dynamics of the electricity system itself. Between these two scales, significant and widely acknowledged spatiotemporal variations of the wind resource can also be observed.

Diurnal variation in wind speed arises from the daily cycle of pressure gradients caused by the diurnal heating and cooling of the Earth's surface [13]. Onshore wind speeds are generally higher during daylight hours and lower at night. In contrast, the offshore domain typically shows a reversal of the onshore pattern, or a bimodal pattern with peaks in wind speed occurring in the early morning and before midnight [14]. Geographically, diurnal wind patterns also vary with latitude, as shown by marginal shifts in the hour of peak wind speed, representing a small degree of spatial variability [15]. Such consistency and predictability make the variability of wind speed at this scale significant in terms of the wind resource's complementarity with electricity demand and solar power. For example, during daylight hours, when solar power generation is at its peak, higher onshore wind speeds can provide additional energy, reducing reliance on other energy sources. At night, when solar power is not available, offshore wind patterns, with their characteristic nocturnal peaks, can compensate for the lack of solar energy [16].

Similarly, both offshore and onshore winds demonstrate fairly consistent and predictable variations on a seasonal scale. However, unlike diurnal variation, seasonal variation in wind speed exhibits significant spatial differences influenced by geographical location and climate type. High-latitude regions experience greater variability in winter due to the stronger polar jet stream, resulting in higher wind speeds, while summer winds are generally weaker due to the reduced temperature gradient [17]. Mid-latitude areas are influenced by shifting high- and low-pressure systems, with pronounced winter westerlies contributing to significant seasonal wind variations [18]. Tropical regions, affected by mon-

soonal systems, show distinct seasonal wind patterns with strong winds during the summer monsoon and relatively calm conditions during the winter monsoon [19]. But similar to diurnal variation, these seasonal variations are typically predictable for a given location. Therefore, the variability of the wind resource at this time scale is similarly significant in terms of its complementarity to electricity demand and other variable energy sources, particularly for high-latitude regions where seasonality is more pronounced.

Driven by large-scale atmospheric patterns and regional climatic factors on time scales ranging from several months to several years, inter-annual variability of wind speed also varies significantly across different parts of the world. One major driver of this variability is teleconnection patterns, such as the North Atlantic Oscillation (NAO) or the El Niño-Southern Oscillation (ENSO), which describe large-scale atmospheric pressure anomalies that influence weather and climate conditions far from their origin [20]. However, compared to diurnal and seasonal variations, inter-annual variability of wind speed is much less predictable [21]. Consequently, it holds substantial importance regarding the uncertainty in wind energy yield estimations and project planning. Of equally great importance is the variability due to weather regimes. These are variations in weather patterns on a time scale of more than five days to a few weeks [22], which can be partially driven by the different phases of teleconnection patterns. While short- to medium-term forecasts can help predict the occurrences of these regimes, their predictability is not consistent. Therefore, this scale of wind variability is crucial for the short- to medium-term balancing of wind energy supply and electricity demand.

An overarching theme among these different scales of variations is the spatial variability of the wind resource. As previously mentioned, at the micro-scale, spatial variability is influenced by local topography, such as surface roughness or the presence of geographical features, which can cause substantial differences in wind speed and direction over short distances. At the meso-scale, larger regional geographical features like mountain ranges can also determine the spatial variability of the wind resource, but the variation in weather regimes is also a major driver [23]. At the macro-scale, large-scale atmospheric circulation and climate zones determine the overall wind climate of a region where high- and low-pressure systems, jet streams, and prevailing wind directions influence the spatial

variability of wind speed [24].

However, central to the concept of spatial variability at all scales is the fact that the correlation between wind speed at any given two sites decreases with distance [25–27], as shown in Figure 1.3. The crucial implication here is that temporal variability can be mitigated by averaging wind energy production over a number of geographically distributed wind farms. For example, at the smallest scale, short-duration fluctuations in wind speed can be smoothed out by aggregating wind energy production from multiple geographically dispersed wind farms [28]. Similarly, on a continental scale, the correlation in wind power has also been shown to decrease as the distance between countries increases, highlighting the necessity of cross-country and cross-continent interconnector capacity [29].

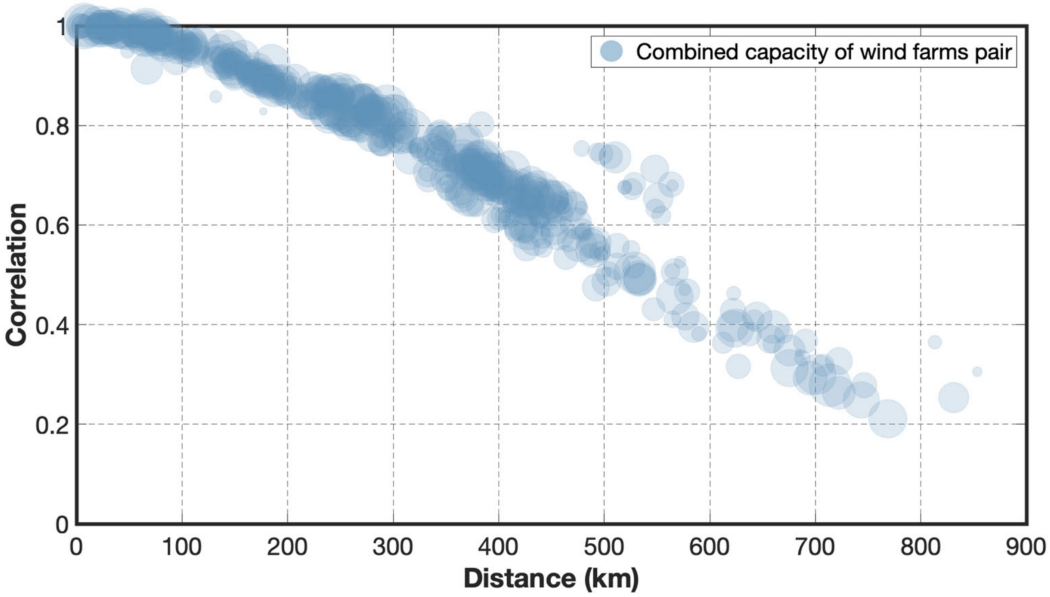


Figure 1.3: Distance-correlation scatter plot for the UK offshore wind farm pairs [26].

1.2.2 Extreme low wind events

A statistical extreme is defined as an observation or data point that lies in the tails of a dataset's distribution, significantly deviating from the median of the data points, and is often characterised by its rarity and potential impact on statistical analysis [30]. Historically, extremes in the context of wind energy were primarily associated with high wind loads, which posed significant challenges to the structural integrity and reliability of wind turbines. However, due to the increasing penetration of wind energy into electricity sys-

tems around the world, extremes in the context of low wind events and their potential impacts on the resilience of electricity systems have gained considerable attention in recent years. Given the evidently multidimensional nature of such events, there are several definitions of extremes in this context. These definitions can be categorised into two broad classifications, namely *extreme low wind power events* and *extreme electricity system stress events*. In this thesis, both types of events are referred to as *extreme low wind events*. These events are the focus of this research.

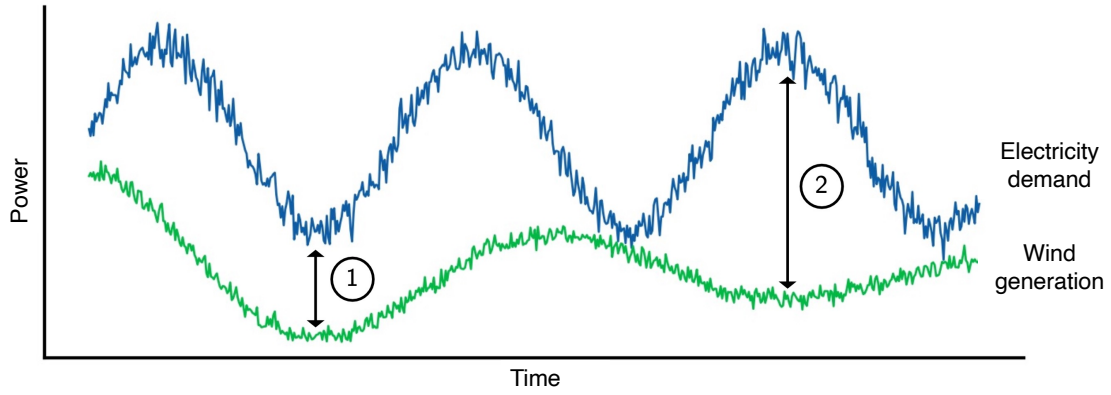


Figure 1.4: An illustration of a hypothetical wind generation and electricity demand time series. Instances 1 and 2 illustrate *low wind power events* where wind power output is reduced for a prolonged period. Instance 2 illustrates an *electricity system stress event.* where a prolonged period of low wind power output occurs concurrently with a period of high electricity demand.

Low wind power events (or *low wind speed events* in the case where only wind speed is considered) refer to prolonged periods of low wind speeds resulting in reduced wind power output, as illustrated by instances 1 and 2 in Figure 1.4. Extreme low wind power events, therefore, denote those events whose durations fall within the upper tail of the distribution, indicating particularly prolonged instances of low wind power generation. The duration of these low wind power events can vary greatly, depending on the quantitative definition of such events and the location at which the analysis is carried out. In general terms, an event that lasts a few hours is often attributed to small-scale fluctuations in wind speed, while the more consequential extreme events are often associated with location-specific weather regimes and large-scale atmospheric patterns that lead to prolonged instances of low wind speeds [26, 31]. For example, in the Western United States, nation-wide low wind speed

conditions persisted from January to March 2015 due to the North Pacific Mode state, which reached its historical maximum during this period [32]. In Europe, extreme low wind power events are associated with blocked weather regimes where stationary high-pressure systems or anticyclones disrupt the prevailing westerly flow into Europe, leading to reduced wind speeds over the region for several days [22].

On the other hand, *electricity system stress events* can be considered as instances where low wind power events coincide with periods of high electricity demand, as illustrated by instance 2 in Figure 1.4. Similarly, their extremes refer to events whose durations fall within the upper tail of the distribution, indicating particularly prolonged instances where the electricity system is stressed by low wind power output. Such events are particularly critical for electricity systems where a large proportion of electricity generation is sourced from wind energy. Due to the additional dimension introduced by electricity demand, the drivers of these electricity system stress events are further varied and localised. For example, in Northern Europe, where electricity demand is higher during winter months due to heating demand, the occurrence of low wind power events is more likely to stress the electricity system than in summer [22]. In the Mediterranean-like climate of California characterised by hot, dry summers and mild, wet winters, electricity demand is driven primarily by cooling requirements during the summer months of July, August, and September. Consequently, the electricity system is particularly susceptible to low wind power events during this period of the year [33]. In Brazil, the tropical and equatorial climate means that electricity demand is less temperature-dependent. However, the reliance on hydropower makes dry spells problematic. While wind power in Northeastern Brazil is typically high during the dry season, low wind power events can further increase the stress on the electricity grid when hydroelectric generation is already reduced [34].

Several crucial implications arise from analysing extreme events of both classifications, the most prevalent of which is the necessity for robust electricity system management and energy planning. Energy storage systems such as batteries, pumped hydro storage, and compressed air energy storage can store excess energy generated during periods of high wind speeds and release it during low wind events, ensuring a stable and continuous power supply [35]. Enhanced grid management and integration strategies are also critical.

Advanced grid technologies, including smart grids and demand response systems, allow for better matching of supply and demand by adjusting consumption patterns in response to real-time data on wind power availability [36]. By shifting or reducing demand during low wind periods, these systems help maintain grid stability and reduce reliance on fossil-fuel backup power. A clear understanding and quantification of the frequency, duration, and risk of these extreme events are essential for providing robust guidance for future electricity system planning, especially with the increasing integration of wind energy.

1.3 Wind energy in the United Kingdom

1.3.1 Climatology

The climatology of the United Kingdom is characterised by a temperate maritime climate, heavily influenced by its geographical location and the surrounding Atlantic Ocean. The North Atlantic Drift, a powerful warm ocean current, plays a crucial role in moderating the UK's climate, leading to relatively mild temperatures year-round compared to other regions at similar latitudes. The UK experiences a considerable amount of precipitation distributed throughout the year, with notable regional variations. Western regions, particularly those in proximity to the Atlantic, receive higher levels of rainfall due to prevailing westerly winds and orographic effects. In contrast, the eastern regions are relatively drier. Seasonal variations are marked, with winters typically wet and cool, and summers moderately warm. However, the UK's climate is also subject to variability and extremes, including heatwaves, cold spells, and heavy rainfall events [37].

Of particular significance among these variabilities is the wind. Situated in one of the most common regions for atmospheric blocking and at the endpoint of a major mid-latitude storm track, the United Kingdom experiences one of the most variable wind climates in northwest Europe [38]. The primary drivers of wind variability in the UK include the North Atlantic Oscillation (NAO), which influences the strength and direction of westerly winds, and the jet stream, whose position and intensity can lead to significant changes in wind patterns [39]. During the positive phase of the NAO, the UK typically experiences stronger westerly winds, bringing mild and wet conditions, whereas the negative phase is associated

with weaker winds and colder, drier conditions. The jet stream, a fast-flowing current of air in the upper atmosphere, shifts north and south, influencing the path and intensity of storm systems that impact the UK. When the jet stream shifts south of its average position but remains over or near the UK, it tends to direct more storms towards the region, leading to increased wind speeds and variability [39]. Additionally, the presence of cyclonic and anticyclonic systems plays a crucial role in wind variability. Cyclonic systems, or low-pressure areas, are associated with stronger winds and stormy conditions as air converges and rises, leading to high wind speeds. Conversely, anticyclonic systems, or high-pressure areas, typically bring calmer weather with lighter winds as air diverges and descends [40, 41]. These variations have immense implications for wind energy production in the UK, affecting the variability of the wind at different time scales.

1.3.2 Spatiotemporal variability

The spatiotemporal variability of wind speed in the United Kingdom is influenced by geographical features and complex climatic patterns. Diurnal and seasonal variations in wind speed follow a consistent pattern. Onshore wind exhibits a distinct diurnal variation, where wind speed is generally higher during daylight hours, reaching its maximum in the afternoon, and lower at night, reaching its minimum in the morning [25]. In contrast, the offshore domain typically shows a reversed diurnal pattern, with wind speeds higher at night and lower during the day [26]. On an annual time scale, both offshore and onshore wind also demonstrate clear seasonal variations; wind speed in the UK is generally lower during the summer months than in winter [25] due to the prevalence of high-pressure systems and easterly winds associated with calm conditions [42]. Additionally, the diurnal variation of wind speed, particularly in the offshore domain, exhibits seasonal changes, where the patterns in winter and autumn differ from those in summer and spring [26].

Significant inter-annual variations in the UK primarily stem from the North Atlantic Oscillation [43]. Positive phases of the NAO are generally associated with stronger westerly winds and increased storminess over the UK, leading to higher wind power generation, while negative phases can lead to calmer conditions and reduced wind power output [44]. For example, in Scotland, variations in wind power can reach 10-15% [45], while for the

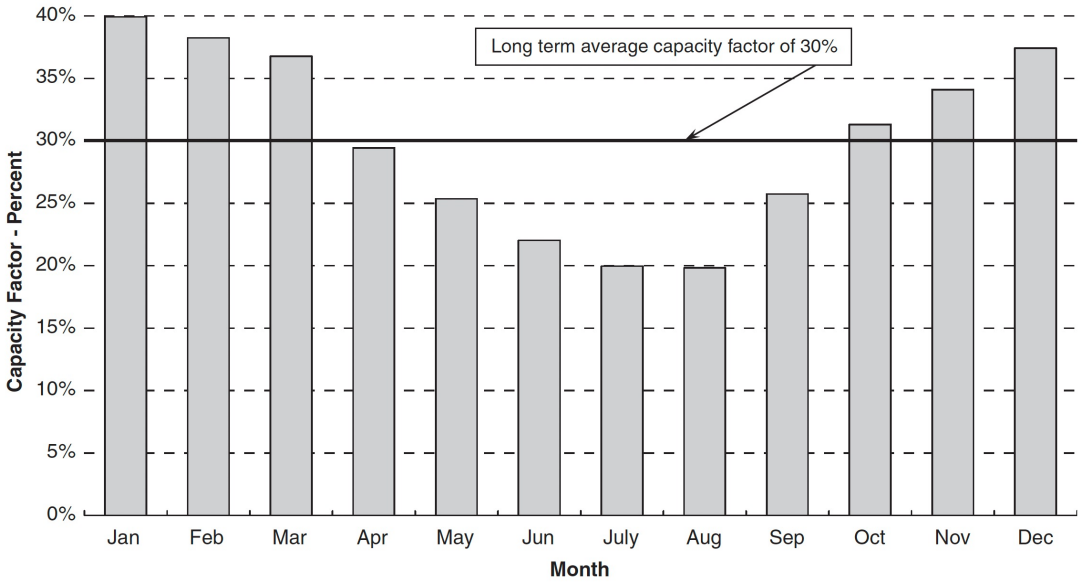


Figure 1.5: Monthly capacity factor of the UK onshore wind farm fleet averaged over 1970-2003 [25].

UK onshore farms fleet, the variability in annual energy yield was found to be 7.4% [25]. Although the UK's offshore domain is reported to exhibit lower variability, with an inter-annual variability of 4% [26], these figures have been noted to be more significant than climate-change-induced non-stationarity [46], and therefore, represent substantial variability in total annual energy supplied to the electricity system.

Variability due to atmospheric weather systems or weather regimes in the UK follows that of its Northern European counterparts. High-pressure systems, known as blocking regimes, typically lead to reduced wind speeds and lower wind power generation. These blocking regimes are associated with stationary anticyclones that disrupt the westerly flow into Europe, reducing near-surface winds over large areas of the country [22, 44]. Conversely, cyclonic regimes or low-pressure systems enhance near-surface winds and increase wind power output due to stronger atmospheric circulation [22]. The transition between different weather regimes in the UK can cause wind power output to vary by up to 20% from the long-term mean and hence, has significant implications on the balance of supply of wind energy and electricity demand [47].

1.3.3 Extreme low wind events

Low wind power event duration in the UK can vary greatly; an event can last a mere few hours or, in extreme cases, up to a week, with lower frequency and duration observed in the offshore domain [26, 48, 49]. As previously mentioned, while events lasting a few hours are caused by small-scale fluctuations in wind speed, extreme low wind power events are associated with stationary high-pressure systems that disrupt the prevailing westerly flow into Europe [22]. Therefore, the frequency of shorter events is naturally higher and decreases with increasing duration, approximating an exponential decay [48], as shown in Figure 1.6. Given that the frequency of these blocked regimes is higher in summer, a higher occurrence of low wind power events is observed in the UK during this period, with extreme events also showing a tendency to last longer during these summer months. Furthermore, although the spatial scale of these regimes means they often affect a large area, Potisomporn and Vogel [26] showed that the likelihood of a low wind power event occurring simultaneously at any two given locations decreases with their distance, indicating that spatial diversification of wind farms can lead to a reduction in the frequency and duration of these extreme low wind power events.

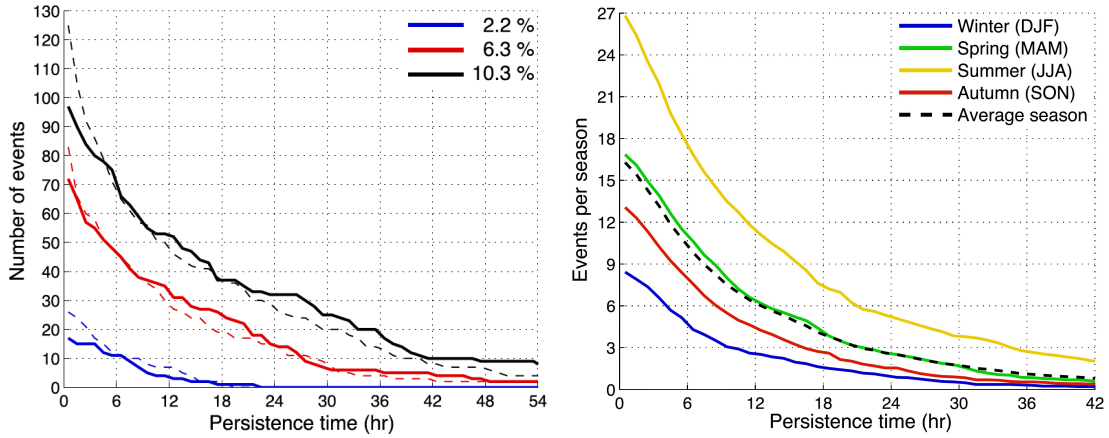


Figure 1.6: (Left) Annualised frequency-duration curves of low wind power events, as identified by runs analysis, in Great Britain corresponding to different CF thresholds. (Right) Annualised frequency-durations curves of low wind power events corresponding to a CF threshold of 6.3%. Both plots were taken from a 33-year case study of GB CF time series based on the MERRA-2 reanalysis [48]

Historically, electricity system stress events in the UK have been primarily driven by the

relationship between near-surface temperature and electricity demand; low temperatures lead to high heating demand, which in turn increases the strain on the electricity system [50]. However, the increasing penetration of renewable energy into the electricity system increases the sensitivity of energy supply to weather systems, with Bloomfield et al. [51] suggesting that GB's electricity network may have already transitioned from a temperature-dominated regime to one primarily influenced by wind. Although low wind power events are most frequent in the summer and spring months when the frequency of blocking regimes is highest, their impacts on the electricity system are limited by lower heating demands during this period of the year. In winter, however, the presence of high-pressure systems poses a significant challenge to the electricity system. For example, during a weather regime like Greenland blocking (see Figure 1.7), a high-pressure system develops over Greenland, causing a disruption in the typical zonal flow into Europe. This setup often leads to cold, stagnant air masses over Great Britain, characterized by clear skies, light winds, and low temperatures. These conditions result in reduced wind speeds, limiting wind power generation, while simultaneously driving up electricity demand for heating due to the cold weather, creating significant stress on the electricity system. Nevertheless, it should be noted that such trends are expected to change. Firstly, increasing electrification of the gas network by 2050 will likely increase winter electricity demand due to widespread adoption of heat pumps, re-establishing temperature as a dominant driver of electricity system stress [52]. Secondly, rising global temperatures are expected to significantly increase summer electricity demand in the UK due to a surge in cooling requirements, shifting the current winter-dominated demand profile. [53]

On the climatic scale, winters with higher electricity demand and lower wind power supply than average tend to occur during periods of stronger negative NAO signals due to the same condition of lower temperatures and reduced wind speed [54]. Therefore, in addition to the relatively short event time-scales discussed above, multi-year periods of low wind have also been noted by The Royal Society [55] as critical challenges for energy systems increasingly reliant on wind energy. While less frequent, such prolonged events have the potential to create sustained deficits in wind power generation, compounding issues for electricity systems already facing seasonal demand peaks.

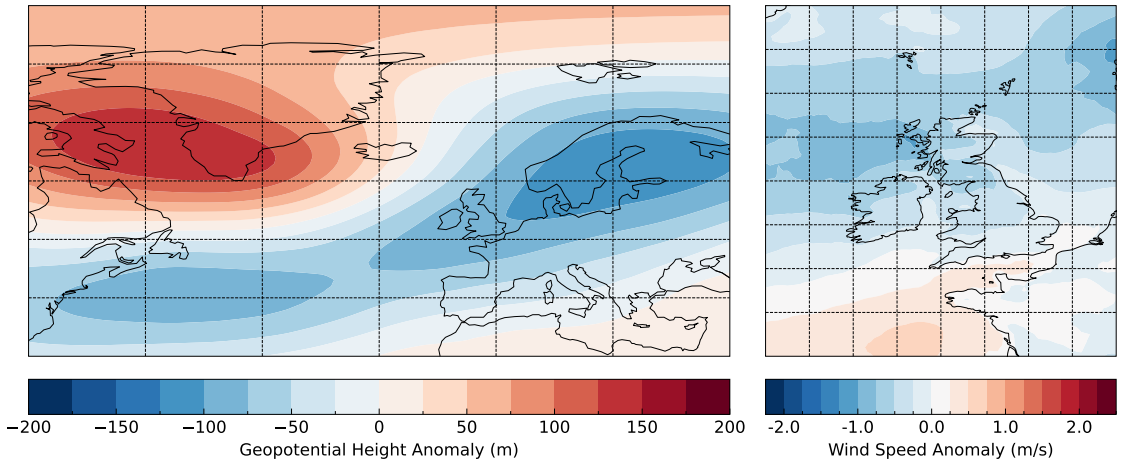


Figure 1.7: (Left) Time-averaged geopotential height anomaly during the Greenland blocking regime. (Right) Wind speed anomaly around the UK during the Greenland blocking regime in winter. Classification methods from Grams et al. [22] were used to identify and illustrate this weather regime using ERA5 data from 1979 to 2018. Both illustrations correspond to time-averaged values taken from time steps classified to be in such a regime.

It is evident that low wind power events occur across a wide range of timescales, from short-term fluctuations lasting hours to prolonged periods spanning weeks or even years. Storage technology is critical in addressing these variations, as it provides the necessary flexibility to balance supply and demand during periods of low wind power availability. Different technologies are suited to different event scales: short-duration storage solutions, such as lithium-ion batteries, are effective for addressing rapid fluctuations but are limited in capacity, while mid-duration technologies, like advanced compressed air energy storage and liquid air energy storage, offer more extended energy release capabilities but fall short for managing prolonged low wind periods. For long-duration storage, the Royal Society highlights hydrogen storage as the most promising solution for the UK, utilizing the country's significant potential for underground storage in salt caverns to handle seasonal and long-term energy variations [55]. Given the UK's ambitious goals of decarbonising the electricity system, quantifying the frequency, duration, and severity of low wind power events across these timescales is therefore, crucial for understanding these energy storage requirements. Equally important is the need to employ methods to quantify these events that align with the specific requirements of storage technologies, ensuring their relevance and effectiveness in meeting energy system needs.

1.3.4 Sensitivity of extreme low wind events to wind farm spatial distribution

The spatial variability of wind speed, as discussed earlier, plays a key role in the mitigation of these extreme low wind events. Since wind speed correlations decrease with distance, a geographically diverse wind farm fleet can ensure more consistent and reliable power output [25, 26, 56]. However, achieving a spatially balanced portfolio is both economically and technically challenging, underscoring the importance of a strategic approach to wind farm deployment to minimize the impacts of extreme low wind events on the electricity system. For example, on a continental scale, Grams et al. [22] highlights the potential for strategic spatial deployment of wind farms across Europe, particularly in regions with contrasting responses to weather regimes (e.g., Balkans vs. North Sea), to minimise output variability and increase fleet-wide reliability during extreme electricity system stress events. Such findings are corroborated by Wohland et al. [57]'s study, which reiterates the importance of transnational cooperation in Europe to achieve geographically optimized siting of renewable energy infrastructure to effectively reduce the impact of multidecadal variability of wind speed.

In GB/UK, Giddings et al. [58] demonstrated that a uniform distribution of wind farms significantly reduces inter-annual, monthly, and daily generation variability, resulting in fewer extreme ramping events and persistent low-generation periods compared to the current wind farm distribution. Similarly, a report from Regen [59] highlighted that allocating wind farm capacity to the less-developed Western regions of the UK to achieve an East-West balance can halve the maximum duration of low wind power events, albeit with only a marginal increase in annual energy yield. Additionally, Abdelaziz et al. [60] demonstrated that the East and North offshore regions of the UK face higher risks of low wind power events, while the Southern region remains the most resilient, showing stable or reduced risks under projected future climate conditions. While all studies agree on the benefits of spatial diversification of wind farms, there is still no clear consensus on the optimal wind farm distribution, underscoring the need for further research to refine deployment strategies that account for these extreme low wind power events.

1.4 Review of Methodologies

1.4.1 Reanalysis data usage

Obtaining wind power output data is the first step in the investigation of the spatiotemporal variability of the wind resource and extreme low wind events. Such data can be most directly obtained from electricity systems datasets, which provide nationally aggregated wind power output and electricity demand data. An alternative approach is to obtain wind power output data from wind farms or to model wind power output from observed wind speed. The advantage of these datasets is that they provide real-world measurements, offering a high degree of accuracy and minimising potential biases. Hence, a number of studies have been carried out on the variability of the wind resource and extreme wind events using these observed data [25, 45, 61]. However, there are several drawbacks to this approach. Firstly and most importantly, the rarity of extreme events necessitates the use of long-term datasets which span several decades to increase the sample size of such events and hence, reduce the associated uncertainty. Observed electricity system data and wind power output data are often available for limited temporal coverage, and so only a small number of extreme events can be identified from such datasets. Secondly and similarly, the limited spatial coverage of wind farm power output data and observed wind speed data, especially in the offshore domain, means that it is difficult to accurately model the wind farm distribution and its constant evolution. Thirdly, measurement equipment can be prone to malfunctions and replacements, leading to frequent occurrences of missing data. Therefore, it can be unreliable and can often be situated in locations that are susceptible to topographically-induced anomalous wind speeds, limiting its applicability to wind energy modelling.

In the past decade, reanalysis data has increasingly been used as a substitute for observed data [26, 44, 48, 62]. Reanalysis datasets are comprehensive sets of meteorological and climate data created by combining historical observational data with numerical weather prediction models through data assimilation techniques [63]. This process generates a continuous, consistent record of atmospheric, oceanic, and surface conditions, facilitating retrospective analysis and research in climate science. Therefore, reanalysis datasets adequately

address the aforementioned issues associated with observed data. Firstly, most reanalysis datasets provide extensive spatiotemporal coverage, often encompassing global scales and spanning several decades [64]. For example, the European Centre for Medium-range Weather Forecasts 5th generation reanalysis (ERA5) has global coverage (as illustrated in Figure 1.8) and extends back to 1940. Therefore, a significantly larger sample of extreme low wind events can be identified from these longer datasets while permitting flexibility in modelling aggregated wind power output for any wind farm distribution. Secondly, reanalysis datasets offer near-perfect spatiotemporal consistency, meaning that there are no gaps in the data coverage, providing a comprehensive and uninterrupted record over the entire study period. Hence, compared to observed data, reanalysis datasets represent the more suitable candidate for the analysis of extreme low wind events.

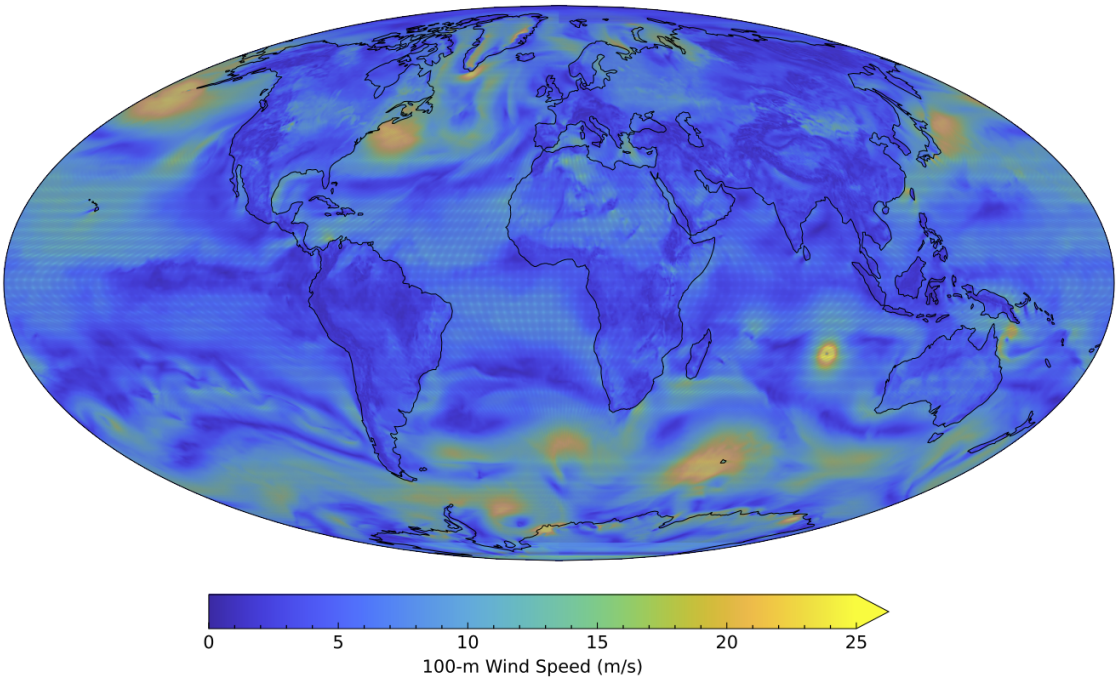


Figure 1.8: Global map of ERA5 100-m wind speed to illustrate the comprehensive data provided by reanalysis models for assessing global wind patterns and variability

Despite the significant advantages of reanalysis datasets, three main shortcomings are widely acknowledged. First, due to the need to provide extensive spatiotemporal coverage using finite computational resources, reanalysis datasets are limited in their spatiotemporal resolution. Many state-of-the-art global reanalysis datasets offer a maximum temporal resolution of hourly intervals, while spatial resolution reaches only up to 0.20° [65]. Al-

though the hourly temporal resolution may be adequate for investigating extreme events lasting days or weeks, the limited spatial resolution means that wind speeds in complex topographical areas, such as coastal regions, may not be accurately resolved. Second, significant biases in mean wind speed have been reported across various reanalysis datasets [66–68]. These biases arise because reanalysis datasets rely on numerical weather prediction models, which are prone to systematic errors introduced by both the models and the data assimilation processes used to integrate observational data. While these biases are often confined to a magnitude of a tenth of a metre per second, they can result in up to 20% error in energy yield calculations [69]. Third, reanalysis datasets are inherently limited to historical data, which means that any simulation of future wind power output based on these datasets requires the assumption that past statistics are indicative of future conditions. This assumption is crucial because it does not account for potential changes in climate patterns or other factors that may alter future wind characteristics. Therefore, although reanalysis datasets offer a robust alternative data source for studying extreme low wind events, these limitations are crucial and should be acknowledged and addressed prior to usage.

1.4.2 Modelling wind power output and electricity demand from reanalysis data

The use of reanalysis datasets as a substitute for observed datasets necessitates the modelling of wind power output from reanalysis wind speed data. Approaches used in the literature can vary significantly in granularity and scope: some focus on the overall dynamics of an electricity system with renewable energy, using simple conversions from wind speed to power output [70–72], while others concentrate on detailed, physics-based models of turbine wakes and farm-scale resistance, which are more computationally intensive [73–75]. Studies that lie between these extremes often model wind power generation on a national scale, using elaborate but not overly granular methods suitable for large numbers of wind farms [26, 48, 62, 76]. Regardless, the typical modelling procedure involves these steps. First, some studies apply bias correction to the input wind speed data [66, 44]. For those using wind speed at low altitudes, extrapolation to the turbine hub height is

required, often using conventional methods like the logarithmic wind profile or power law [76]. Finally, wind speed at hub height is converted to power output, frequently through the use of manufacturer's turbine power curves or calibrated curves for greater accuracy [77].

In studies considering the electricity system, the relationship between wind energy supply and electricity demand is often represented by a demand-net-wind time series, reflecting the level of electricity demand not met by wind power generation [62]. Similarly to the challenges associated with observed wind power output, the limited temporal coverage of electricity demand data is insufficient to provide an adequate sample size for extreme events. However, it is widely recognized that near-surface temperature is the most significant meteorological factor influencing electricity demand in Great Britain [44, 42, 78]. A commonly used approach is conceptually summarised by that of Bloomfield et al. [44], where a multiple linear regression model captures the relationship between electricity demand and temperature, as well as time. The resulting demand model is typically linearly mean-scaled to align with the electricity demand level during a period of interest. While this is a standard approach, it should be noted that it is based on the major assumption that the demand profile remains constant. Although this may be sufficient for modelling electricity demand for the present period, the electrification of the gas networks is expected to introduce substantial variability in demand profiles that challenges the assumption of a constant profile [52, 79].

1.4.3 Frequency and extreme value analyses

The definition and frequency analysis of low wind events are rooted in *runs analysis*, a time series method developed and widely used in the field of hydrology [80]. The technique, in its simplest form, defines the duration of a hydrological drought as the number of consecutive time steps a stream flow series is under a specified threshold or the duration of a flood as the number of consecutive time steps a stream flow series is over a specified threshold. In some cases where the temporal resolution of the stream flow time series is high, *minor events* and *mutually dependent events* are present in the identified set of events. These types of events are problematic in that they can introduce dependencies between events and

distort the perceived severity of extreme events as shown in Figure 1.9. To mitigate this, techniques such as pooling procedures are used to aggregate minor events and help achieve independence of identified events, providing a more statistically robust representation of the data [81].

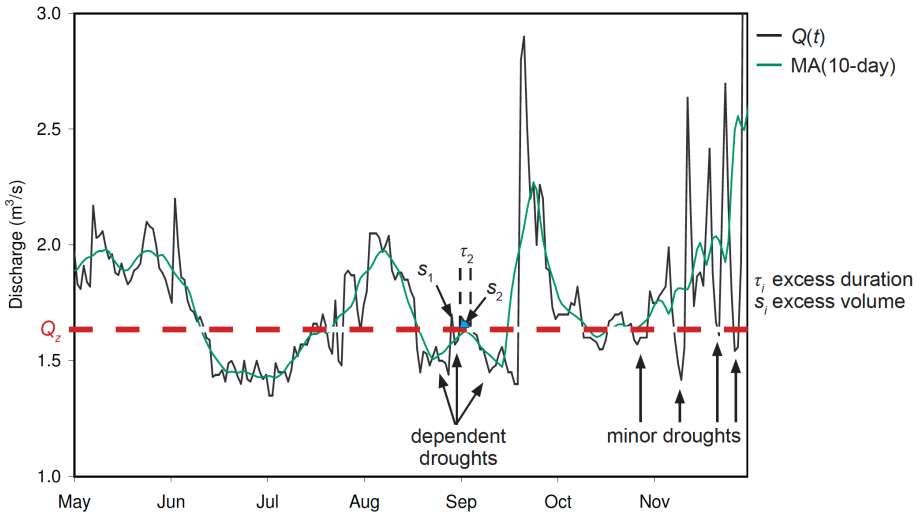


Figure 1.9: Illustration of the pooling of mutually dependent droughts and the treatment of minor droughts by a 10-day moving average filter [81].

These analogies between hydrological droughts and low wind power events, and that between floods and electricity system stress events, are leveraged by and form the basis of several wind-oriented studies in the frequency analysis of low wind events. For low wind power events, runs analysis can be applied to a wind power output time series to identify periods where the time series is continuously below a threshold [48, 26]. Runs analysis can also be applied to a wind speed time series in a similar manner, with the subtle difference being that in such a case, the operational aspects of a wind turbine e.g., cut-in and cut-off speeds, are not taken into account [61]. Similarly, for electricity system stress events, runs analysis is applied to a demand-net-wind time series, i.e., the level of electricity demand not met by wind power generation, to identify prolonged periods where demand-net-wind is higher than a specified threshold [62]. For both classifications of events, a commonly used pooling procedure in the wind energy context is the application of a simple moving average to the underlying time series [62, 76]. As such, the identified events signify periods where the moving mean is below a predefined threshold, demonstrating the subtle distinctions

presented by the different definitions of these events.

The quantification of the risk of extreme events sampled from the upper tail of the identified events' distribution is carried out using extreme value analysis. The term *risk*, in this context, therefore refers to the likelihood of these extreme events in terms of return periods or recurrence intervals i.e., how frequently they are expected to occur within a given period of time. The methodology involved in an extreme value analysis follows a standardised procedure: first, a set of extreme events is identified from the distribution of events; second extreme value distributions are fitted to the identified set of extreme events to provide a means of interpolation and extrapolation from the observed data; and last, return periods are calculated from the fitted distribution for the return level of interest [82]. Again, this process has been widely used in the field of hydrology to quantify the risk of droughts and floods [83, 84]. More recently, this hydrological extreme value analysis has also been adapted and applied in the context of wind energy on low wind power events [49, 61], as well as on electricity system stress events [62].

1.5 Thesis objectives

The increasing reliance of GB's electricity system on wind energy necessitates a thorough and statistically robust investigation and quantification of the wind farm fleet and the system's risk to extreme low wind events. This thesis aims not only to contribute to the growing body of literature on this topic but also to address key aspects of extreme events analyses that may have been acknowledged peripherally but could have significant ramifications on the findings. This overarching aim is addressed through three primary objectives. The first objective focuses on modelling GB power output and electricity demand using reanalysis data. The second objective involves developing statistically robust frequency and extreme value analyses for extreme low wind events and applying them to the GB wind farms fleet. The third objective concerns the impacts of spatial variability of extreme low wind events.

Throughout this thesis, the scope shifts between the UK and GB as deemed appropriate, considering the specific context and relevance of the information presented. The evaluation

of ERA5 was conducted for the UK to gain a comprehensive understanding of the dataset's limitations and uncertainties over the entire geographical domain. Policies and territories are also discussed with respect to the UK rather than GB due to the former's complete geopolitical representation. However, the scope of analyses related to the electricity system, which primarily denotes the supply of wind energy and electricity demand, is placed on GB. This focus is due to the fact that GB constitutes the main geographical area for wind energy supply and electricity consumption within the UK, thus allowing the consideration of an isolated system without the complexities introduced by interconnectors. Note that since Northern Ireland's electricity system is integrated into the all-Ireland Single Electricity Market, it is considered to be a separate entity from the GB grid.

Objective 1: GB wind power output and electricity demand modelling from reanalysis data

ECMWF's state-of-the-art ERA5 global reanalysis, distinguished by its high spatiotemporal resolution and advanced data assimilation model, forms the basis of GB wind power output model output and electricity demand modelling in this study. But due to the widely acknowledged drawbacks of reanalysis datasets, a UK-wide evaluation of ERA5's inaccuracies and sources of uncertainties, the first of its kind for this specific dataset, must first be carried out. In addition to examining commonly used error metrics, it is necessary for this evaluation to focus specifically on metrics related to low wind speed events due to their importance to the objectives of this thesis. Additionally, the insights gained from the evaluation will provide valuable information for future studies, helping to improve the accuracy and reliability of reanalysis data applications in wind power and electricity demand modelling.

Subsequently, a model is to be developed based on the evaluated ERA5 datasets, taking the identified limitations into account. The primary goal of the model is to use ERA5 wind speed at a given wind farm location as input, along with other climate variables, and convert it into farm power output. In the literature, a simple approach is often used to model this power conversion, resorting to conventional methods like the logarithmic wind profile to vertically extrapolate wind speed or the manufacturer's power curve to

obtain farm power output. In contrast, the second part of this objective is to investigate and address the limitations of these conventional approaches and develop a model that can better capture GB-aggregated wind power output. Temperature-dependent demand modelling will also be explored to further model DNW time series. Similarly, findings from this investigation may be useful in informing the modelling process for future studies.

Objective 2: Frequency and extreme value analyses of low wind power events

The second objective of this thesis is to quantify the frequency of extreme low wind events and their risks in terms of return periods for the 2022 GB wind farm distribution. Frequency and extreme value analyses, prevalent in the hydrology literature, are increasingly applied to extreme events in the context of wind energy to quantify the risk of low wind events. However, these applications to wind energy events are often based on events identified through a simple runs analysis. This approach presents two problems. Firstly, a simple runs analysis does not address instances where a brief exceedance of a predefined threshold leads to the fragmentation of what should be considered a single continuous event, resulting in an underestimation of the duration of a low wind power event. Secondly, the fragmentation of these continuous events means that it does not achieve independence of events, which is a key assumption in extreme value analysis. Therefore, this second objective aims not only to quantify the risk of extreme low wind events but also to contribute to the refinement and development of these methodologies for future research endeavours.

Objective 3: Spatial variability of extreme low wind power events

The spatial variability of the wind resource means that one of the key guiding factors for wind farm deployment is their geographical placement. Not only is this factor crucial for optimising energy production, but it has also been shown to determine the resilience of the electricity system to extreme low wind events [26]. While previous studies may have focused only on the effects of wind's spatial variability on energy yield or regional extreme low wind events, the objective of this research is to study the spatial variability of extreme low wind events through the investigation of GB wind farm distributions, addressing current, near-

term, and long-term changes. The aim is to employ the extreme value methodologies developed as part of Objective 2 on the current and future wind farm fleets and to assess the sensitivity of risk profiles to wind farm distributions. This objective is to be further satisfied through the exploration of various long-term wind farm distribution scenarios, seeking to offer insights into how best to allocate additional resources spatially.

1.6 Thesis outline

The contents of this thesis are organised and presented in an integrated format, i.e., a combination of published academic articles and thesis chapters. Therefore, each section in this thesis is presented as a self-contained document, complete with its own abstract, literature review, contents, and bibliography, contributing to the overarching narrative of the research. Published academic articles were preserved as faithfully as possible, with only minor adjustments to the formatting, terminology, and content for consistency with the rest of this thesis. Naturally, repetition of certain information was necessary to maintain the independence and coherence of each section while ensuring minimal duplication.

Chapter 2 was adapted from an academic article published in the *Energy Reports* journal titled *Evaluating ERA5 reanalysis predictions of low wind speed events around the UK* [85]. It presents a nationwide evaluation of the ERA5 reanalysis wind speed dataset against both onshore and offshore observed wind speed data obtained from meteorological masts and weather buoys. Focus is placed on fundamental error metrics as well as ERA5's representation of low wind speed events. Furthermore, sources of uncertainty in the dataset, as well as their inherent limitations, are discussed.

Chapter 3 was adapted from the supplementary information section of an academic article published in the *Renewable Energy* journal titled *Extreme value analysis of wind droughts in Great Britain* [86], and presented as a thesis chapter. It outlines the process of modelling GB-aggregated wind power output and electricity demand from reanalysis data, which includes the bias correction of ERA5 using output from Chapter 2, the vertical extrapolation of wind speed, and the conversion of wind speed to power output, as well as the modelling of hourly weather-dependent electricity demand. A validation of the

resultant GB-aggregated power output against observed electricity system data is also presented.

Chapter 4 was adapted from an academic article published in the *Renewable Energy* journal titled *Extreme value analysis of wind droughts in Great Britain* [86]. It investigates the different methods of defining and identifying low wind power events and discusses the advantages and disadvantages of each with respect to its practicality and statistical robustness. Subsequently, findings from a frequency analysis and an extreme value analysis of the identified low wind power events are then presented for the 2022 distribution of GB wind farms, quantifying the risk of extreme low wind events in terms of return periods.

Chapter 5 was written as a regular thesis chapter and is currently being adapted for publication. It focuses on the spatial variability of extreme events and their impacts on the future electricity system. The chapter begins by comparing the risk profile of the 2022 distribution of GB wind farms with that of the projected 2030 distribution, using the methodology developed in Chapter 4. Looking further into the future, the second part of the chapter explores the distribution of GB wind farms in 2050 under various possible scenarios. It aims to provide insights on wind farm siting strategies that promote the fleet's resilience to extreme low wind events.

Chapter 6 presents the main conclusions of the thesis and offers detailed suggestions for further work and future research directions.

References

[1] International Renewable Energy Agency (IRENA). *World Energy Transitions Outlook: 1.5°C Pathway*. International Renewable Energy Agency, Abu Dhabi, 2023.

[2] Department for Energy Security and Net Zero. Energy Trends June 2024, 2024. URL `https://www.gov.uk/government/statistics/total-energy-section-1-energy-trends`. Accessed: 2024-07-02.

[3] Elexon. Elexon generation data. URL `https://www.elexonportal.co.uk/`.

[4] UNFCCC. *Paris Agreement*. United Nations Framework Convention on Climate Change, 2015.

[5] P. Denholm and M. Hand. Grid flexibility and storage required to achieve very high penetration of variable renewable electricity. *Energy Policy*, 39(3):1817–1830, 2011.

[6] UK Government. Net Zero Strategy: Build Back Greener, 2021. URL `https://www.gov.uk/government/publications/net-zero-strategy`. Accessed: 2024-07-19.

[7] Department for Energy Security and Net Zero. Renewable electricity capacity and generation (ET 6.1 - quarterly), 2024. URL `https://www.gov.uk/government/statistics/energy-trends-section-6-renewables`. Accessed: 2024-07-19.

[8] Department for Energy Security and Net Zero. Renewable Energy Planning Database, 2022. Accessed: 2022-12-15.

[9] B. Li, S. Basu, S. J. Watson, and H. W. Russchenberg. Quantifying the predictability of a 'Dunkelflaute' event by utilizing a mesoscale model. In *Journal of Physics: Conference Series*, volume 1618, page 062042. IOP Publishing, 2020.

[10] S. M. Fisher, J. T. Schoof, C. L. Lant, and M. D. Therrell. The effects of geographical distribution on the reliability of wind energy. *Applied Geography*, 40:83–89, 2013.

[11] D. R. Drew, D. J. Cannon, D. J. Brayshaw, J. F. Barlow, and P. J. Coker. The impact of future offshore wind farms on wind power generation in Great Britain. *Resources*, 4(1):155–171, 2015.

[12] M. Babiker, P. Zhai, H.-O. Pörtner, D. Roberts, J. Skea, P. R. Shukla, A. Pirani, W. Moufouma-Okia, C. Péan, R. Pidcock, S. Connors, J. B. R. Matthews, Y. Chen, X. Zhou, M. I. Gomis, E. Lonnoy, T. Maycock, M. Tignor, and T. Waterfield. Global Warming of 1.5 degree Celcius: An IPCC Special Report, 2018.

[13] D.-L. Zhang and W.-Z. Zheng. Diurnal cycles of surface winds and temperatures as simulated by five boundary layer parameterizations. *Journal of Applied Meteorology and Climatology*, 43(1):157–169, 2004.

[14] A. Lapworth. The diurnal variation of the marine surface wind in an offshore flow. *Quarterly Journal of the Royal Meteorological Society*, 131(610):2367–2387, 2005.

[15] Y. Ashkenazy and H. Yizhaq. The diurnal cycle and temporal trends of surface winds. *Earth and Planetary Science Letters*, 601:117907, 2023.

[16] M. A. Delucchi and M. Z. Jacobson. Providing all global energy with wind, water, and solar power, Part II: Reliability, system and transmission costs, and policies. *Energy policy*, 39(3):1170–1190, 2011.

[17] X. Zhang, Y. Wang, J. Li, and Q. Liu. Climatology of near-surface wind speed from observational, reanalysis and high-resolution regional climate model data over the Tibetan Plateau. *Climate Dynamics*, 2021.

[18] D. Wang, D. Li, A. D. Ziegler, and L. Dong. A continuous decline of global seasonal wind speed range over land since 1980. *Journal of Climate*, 2021.

[19] X. Huang, M. Zhang, S. Wang, and H. Xin. Spatiotemporal variation of upper-air and surface wind speed and its influencing factors in northwestern China during 1980–2012. *Theoretical and Applied Climatology*, 2021.

[20] D. W. Thompson and J. M. Wallace. Regional climate impacts of the Northern Hemisphere Annular Mode. *Science*, 293(5527):85–89, 2001.

[21] S. C. Pryor, T. J. Shepherd, and R. J. Barthelmie. Interannual variability of wind climates and wind turbine annual energy production. *Wind Energy Science*, 3(2): 651–665, 2018.

[22] C. M. Grams, R. Beerli, S. Pfenninger, I. Staffell, and H. Wernli. Balancing Europe's Wind-Power Output Through Spatial Deployment Informed by Weather Regimes. *Nature Climate Change*, 7:557–562, 2017.

[23] C. K. Wikle, R. F. Milliff, and W. G. Large. Surface wind variability on spatial scales from 1 to 1000 km observed during TOGA COARE. *Journal of the Atmospheric Sciences*, 56(13):2222–2231, 1999.

[24] G. Luzia, A. N. Hahmann, and M. J. Koivisto. Evaluating the mesoscale spatio-temporal variability in simulated wind speed time series over northern Europe. *Wind Energy Science*, 7(6):2255–2270, 2022.

[25] G. Sinden. Characteristics of the UK wind resource: Long-term patterns and relationship to electricity demand. *Energy Policy*, 35:112–127, 1 2007.

[26] P. Potisomporn and C. R. Vogel. Spatial and temporal variability characteristics of offshore wind energy in the United Kingdom. *Wind Energy*, 25(3):537–552, 2022.

[27] S. M. Robeson and K. A. Shein. Spatial coherence and decay of wind speed and power in the north-central United States. *Physical Geography*, 18(6):479–495, 1997.

[28] R. Goić, J. Krstulović, and D. Jakus. Simulation of aggregate wind farm short-term production variations. *Renewable Energy*, 35(11):2602–2609, 2010.

[29] A. Malvaldi, S. Weiss, D. Infield, J. Browell, P. Leahy, and A. M. Foley. A spatial and temporal correlation analysis of aggregate wind power in an ideally interconnected Europe. *Wind Energy*, 20(8):1315–1329, 2017.

[30] S. Coles, J. Bawa, L. Trenner, and P. Dorazio. *An introduction to statistical modeling of extreme values*, volume 208. Springer, 2001.

[31] D. J. Brayshaw, A. Troccoli, R. Fordham, and J. Methven. The impact of large scale atmospheric circulation patterns on wind power generation and its potential predictability: A case study over the UK. *Renewable Energy*, 36(8):2087–2096, 2011.

[32] L. Lledó, O. Bellprat, F. J. Doblas-Reyes, and A. Soret. Investigating the effects of Pacific sea surface temperatures on the wind drought of 2015 over the United States. *Journal of Geophysical Research: Atmospheres*, 123(10):4837–4849, 2018.

[33] A. H. Mejia, J. Brouwer, and D. A. Copp. Performance and dynamics of California offshore wind alongside Western US onshore wind and solar power. *Renewable Energy Focus*, 47:100490, 2023.

[34] P. C. S. Borba, W. C. Sousa, M. Shadman, and S. Pfenninger. Enhancing drought resilience and energy security through complementing hydro by offshore wind power—The case of Brazil. *Energy Conversion and Management*, 277:116616, 2023.

[35] X. Luo, J. Wang, M. Dooner, and J. Clarke. Overview of current development in electrical energy storage technologies and the application potential in power system operation. *Applied Energy*, 137:511–536, 2015.

[36] P. Cappers, C. Goldman, and D. Kathan. Demand response in US electricity markets: Empirical evidence. *Energy*, 35(4):1526–1535, 2010.

[37] Royal Meteorological Society. What is the UK's climate like?, 2024. URL `https://www.metlink.org/resource/what-is-the-uks-climate-like/`. Accessed: 2024-07-21.

[38] T. Woollings. Dynamical influences on European climate: An uncertain future. *Philosophical Transactions of the Royal Society A: Mathematical, Physical and Engineering Sciences*, 368(1924):3733–3756, 2010.

[39] N. Earl, S. Dorling, R. Hewston, and R. Von Glasow. 1980–2010 variability in UK surface wind climate. *Journal of Climate*, 26(4):1172–1191, 2013.

[40] J. M. Garrido-Perez, C. Ordóñez, D. Barriopedro, R. García-Herrera, and D. Paredes. Impact of weather regimes on wind power variability in western Europe. *Applied Energy*, 264:114731, 2020.

[41] R. Vautard. Multiple weather regimes over the North Atlantic: Analysis of precursors and successors. *Monthly Weather Review*, 118(10):2056–2081, 1990.

[42] H. E. Thornton, A. A. Scaife, B. J. Hoskins, and D. J. Brayshaw. The relationship between wind power, electricity demand and winter weather patterns in Great Britain. *Environmental Research Letters*, 12:064017, 6 2017.

[43] C. Justus, K. Mani, and A. Mikhail. Interannual and month-to-month variations of wind speed. *Journal of Applied Meteorology and Climatology*, 18(7):913–920, 1979.

[44] H. C. Bloomfield, D. J. Brayshaw, and A. J. Charlton-Perez. Characterizing the winter meteorological drivers of the European electricity system using targeted circulation types. *Meteorological Applications*, 27(1):e1858, 2020.

[45] W. G. Früh. Long-term wind resource and uncertainty estimation using wind records from Scotland as example. *Renewable Energy*, 50:1014–1026, 2013.

[46] S. C. Pryor, R. J. Barthelmie, M. S. Bukovsky, L. R. Leung, and K. Sakaguchi. Climate change impacts on wind power generation. *Nature Reviews Earth & Environment*, 1 (12):627–643, 2020.

[47] K. van der Wiel, H. C. Bloomfield, R. W. Lee, L. P. Stoop, R. Blackport, J. A. Screen, and F. M. Selten. The influence of weather regimes on European renewable energy production and demand. *Environmental Research Letters*, 14(9):094010, 2019.

[48] D. J. Cannon, D. J. Brayshaw, J. Methven, P. J. Coker, and D. Lenaghan. Using reanalysis data to quantify extreme wind power generation statistics: A 33 year case study in Great Britain. *Renewable Energy*, 75:767–778, 2015.

[49] P. Patlakas, G. Galanis, D. Diamantis, and G. Kallos. Low wind speed events: persistence and frequency. *Wind Energy*, 20(6):1033–1047, 2017.

[50] H. Thornton, B. J. Hoskins, and A. Scaife. The role of temperature in the variability and extremes of electricity and gas demand in Great Britain. *Environmental Research Letters*, 11(11):114015, 2016.

[51] H. C. Bloomfield, D. J. Brayshaw, L. C. Shaffrey, P. J. Coker, and H. E. Thornton. The changing sensitivity of power systems to meteorological drivers: a case study of Great Britain. *Environmental Research Letters*, 13:054028, 2018.

[52] M. Deakin, H. Bloomfield, D. Greenwood, S. Sheehy, S. Walker, and P. C. Taylor. Impacts of heat decarbonization on system adequacy considering increased meteorological sensitivity. *Applied Energy*, 298:117261, 2021.

[53] N. D. Miranda, J. Lizana, S. N. Sparrow, M. Zachau-Walker, P. A. Watson, D. C. Wallom, R. Khosla, and M. McCulloch. Change in cooling degree days with global mean temperature rise increasing from 1.5 c to 2.0 c. *Nature Sustainability*, 6(11): 1326–1330, 2023.

[54] C. R. Ely, D. J. Brayshaw, J. Methven, J. Cox, and O. Pearce. Implications of the North Atlantic Oscillation for a UK–Norway renewable power system. *Energy Policy*, 62:1420–1427, 2013.

[55] The Royal Society. Large-scale Electricity Storage. Technical report, The Royal Society, 2023. URL `https://royalsociety.org/-/media/policy/projects/large-scale-electricity-storage/large-scale-electricity-storage-report.pdf`.

[56] T. Poulsen and H. G. Beyer. Spectral characteristics and spatial smoothing of wind power–a case study of the Faroe Islands. *Meteorologische Zeitschrift*, 29:427–438, 2020.

[57] J. Wohland, D. Brayshaw, and S. Pfenninger. Mitigating a century of European renewable variability with transmission and informed siting. *Environmental Research Letters*, 16(6):064026, 2021.

[58] J. Giddings, H. Bloomfield, R. James, and M. Blair. The impact of future UK offshore wind farm distribution and climate change on generation performance and variability. *Environmental Research Letters*, 19(6):064022, 2024.

[59] Regen. Go West! An analysis of the energy system benefits and implication of a more geographically diverse offshore wind portfolio. Technical report, 2022.

[60] S. Abdelaziz, S. N. Sparrow, W. Hua, and D. C. Wallom. Assessing long-term future climate change impacts on extreme low wind events for offshore wind turbines in the UK exclusive economic zone. *Applied Energy*, 354:122218, 2024.

[61] P. G. Leahy and E. J. McKeogh. Persistence of low wind speed conditions and implications for wind power variability. *Wind Energy*, 16(4):575–586, 2013.

[62] L. Dawkins and I. Rushby. Characterising adverse weather for the UK electricity system, including addendum for surplus generation events, 2020. URL `www.metoffice.gov.uk`.

[63] H. Hersbach, B. Bell, P. Berrisford, S. Hirahara, A. Horányi, J. Muñoz-Sabater, J. Nicolas, C. Peubey, R. Radu, D. Schepers, A. Simmons, C. Soci, S. Abdalla, X. Abellan, G. Balsamo, P. Bechtold, G. Biavati, J. Bidlot, M. Bonavita, G. D. Chiara, P. Dahlgren, D. Dee, M. Diamantakis, R. Dragani, J. Flemming, R. Forbes, M. Fuentes, A. Geer, L. Haimberger, S. Healy, R. J. Hogan, E. Hólm, M. Janisková, S. Keeley, P. Laloyaux, P. Lopez, C. Lupu, G. Radnoti, P. de Rosnay, I. Rozum, F. Vamborg, S. Villaume, and J. N. Thépaut. The ERA5 Global Reanalysis. *Quarterly Journal of the Royal Meteorological Society*, 146:1999–2049, 7 2020.

[64] G. Gualtieri. Analysing the uncertainties of reanalysis data used for wind resource assessment: A critical review. *Renewable and Sustainable Energy Reviews*, 167:112741, 2022.

[65] S. Saha, S. Moorthi, X. Wu, J. Wang, S. Nadiga, P. Tripp, D. Behringer, Y.-T. Hou, H.-Y. Chuang, M. Iredell, et al. The NCEP Climate Forecast System Version 2. *Journal of Climate*, 27(6):2185–2208, 2014.

[66] I. Staffell and S. Pfenninger. Using bias-corrected reanalysis to simulate current and future wind power output. *Energy*, 114:1224–1239, 11 2016.

[67] G. Gualtieri. Reliability of ERA5 reanalysis data for wind resource assessment: A comparison against tall towers. *Energies*, 14:4169, 7 2021.

[68] J. E. Stopa and K. F. Cheung. Intercomparison of wind and wave data from the ECMWF Reanalysis Interim and the NCEP Climate Forecast System Reanalysis. *Ocean Modelling*, 75:65–83, 2014.

[69] K. Gruber, P. Regner, S. Wehrle, M. Zeyringer, and J. Schmidt. Towards global validation of wind power simulations: A multi-country assessment of wind power simulation from MERRA-2 and ERA-5 reanalyses bias-corrected with the global wind atlas. *Energy*, 238:121520, 2022.

[70] D. Raynaud, B. Hingray, B. François, and J. D. Creutin. Energy droughts from variable renewable energy sources in European climates. *Renewable Energy*, 125:578–589, 2018.

[71] F. Kaspar, M. Borsche, U. Pfeifroth, J. Trentmann, J. Drücke, and P. Becker. A climatological assessment of balancing effects and shortfall risks of photovoltaics and wind energy in Germany and Europe. *Advances in Science and Research*, 16:119–128, 2019.

[72] O. Ruhnau and S. Qvist. Storage requirements in a 100% renewable electricity system: Extreme events and inter-annual variability. *Environmental Research Letters*, 17(4): 044018, 2022.

[73] R. J. Barthelmie, S. C. Pryor, S. T. Frandsen, K. S. Hansen, J. Schepers, K. Rados, W. Schlez, A. Neubert, L. Jensen, and S. Neckelmann. Quantifying the impact of wind turbine wakes on power output at offshore wind farms. *Journal of Atmospheric and Oceanic Technology*, 27(8):1302–1317, 2010.

[74] A. Kirby, F.-X. Briol, T. D. Dunstan, and T. Nishino. Data-driven modelling of turbine wake interactions and flow resistance in large wind farms. *Wind Energy*, 26 (9):968–984, 2023.

[75] A. Niayifar and F. Porté-Agel. Analytical modeling of wind farms: A new approach for power prediction. *Energies*, 9(9), 2016.

[76] N. Ohlendorf and W.-P. Schill. Frequency and duration of low-wind-power events in Germany. *Environmental Research Letters*, 15(8):084045, 2020.

[77] B. Kruyt, M. Lehning, and A. Kahl. Potential contributions of wind power to a stable and highly renewable Swiss power supply. *Applied Energy*, 192:1–11, 2017.

[78] J. W. Taylor and R. Buizza. Using weather ensemble predictions in electricity demand forecasting. *International Journal of Forecasting*, 19(1):57–70, 2003.

[79] I. G. Wilson, A. J. Rennie, Y. Ding, P. C. Eames, P. J. Hall, and N. J. Kelly. Historical daily gas and electrical energy flows through great britain's transmission networks and the decarbonisation of domestic heat. *Energy Policy*, 61:301–305, 2013.

[80] V. M. Yevjevich. An objective approach to definitions and investigations of continental hydrologic droughts. *Hydrology Papers Colorado State University*, 1967.

[81] A. K. Fleig, L. M. Tallaksen, H. Hisdal, and S. Demuth. A global evaluation of streamflow drought characteristics. *Hydrology and Earth System Sciences*, 10(4):535–552, 2006.

[82] J. Shiau. Return period of bivariate distributed extreme hydrological events. *Stochastic Environmental Research and Risk Assessment*, 17:42–57, 2003.

[83] L. M. Tallaksen, H. Madsen, and B. Clausen. On the definition and modelling of streamflow drought duration and deficit volume. *Hydrological Sciences Journal*, 42 (1):15–33, 1997.

[84] E. Zelenhasić and A. Salvai. A method of streamflow drought analysis. *Water Resources Research*, 23(1):156–168, 1987.

[85] P. Potisomporn, T. A. A. Adcock, and C. R. Vogel. Evaluating ERA5 reanalysis predictions of low wind speed events around the UK. *Energy Reports*, 10:4781–4790, 2023.

[86] P. Potisomporn, T. A. A. Adcock, and C. R. Vogel. Extreme value analysis of wind droughts in Great Britain. *Renewable Energy*, 221:119847, 2024.

CHAPTER 2

Evaluating ERA5 reanalysis predictions of low wind speed events around the UK

This chapter presents the evaluation of ERA5 reanalysis wind speed and its predictions of low wind speed events around the UK. The article has been accepted and published in Energy Reports *journal on 13th November 2023 [1].*

Low wind speed events represent one of the biggest challenges in fully decarbonising the electricity system due to the growing proportion of wind energy in the UK energy mix. While reanalysis products are a useful tool to study the spatiotemporal characteristics of these occurrences, their performance and limitations should be understood prior to usage. In this study, hourly 10 m ERA5 reanalysis wind speed data were evaluated against in-situ wind speed measurements from 205 onshore and offshore observation stations around the UK. It was found that ERA5 has biases in mean wind speed of 0.166 m/s and -0.136 m/s for onshore and offshore domains, respectively, and biases in hourly wind speed standard deviation of -0.354 m/s and -0.425 m/s for onshore and offshore domains respectively. Both errors are more pronounced in autumn and winter. These errors lead to an underestimation of the percentage frequency of short-duration low wind speed events. Furthermore, the findings suggest that the largest errors are from sites which are situated in coastal and mountainous regions where short-range topographical variability and local wind effects may not be resolved by ERA5. Despite these shortcomings, ERA5 nevertheless outperforms its global reanalysis counterparts in the UK domain and, therefore, can provide valuable information in the context of low wind speed events prediction.

2.1 Introduction

In March 2021, the United Kingdom experienced the longest "cold calm spell" in over a decade; for 11 consecutive days, wind farms operated at 11% of their rated capacity, in a month where low temperatures drove up heating and electricity demand. In response, the electricity system escalated gas power output to compensate for the lack of wind power generation, resorting to the very energy source that the country has been endeavouring to curb. Such an occurrence, neither an isolated incident nor limited to the UK, potentially represents one of the biggest challenges in fully de-carbonising the electricity system [2]. Hence, there is a growing need to characterise the UK's wind energy resource, particularly these low wind speed events.

A trend that has emerged in the past decade is the growing prevalence of reanalysis data being used as a substitute for observed wind speed or measured power output in the characterisation of low wind speed events [3–5]. A reanalysis dataset is a reconstruction of historical atmospheric or climate conditions derived from integrating observational data with a numerical weather prediction model. Data assimilation methods incorporate measurements from sources such as surface stations, radiosondes, satellites, and ship-based instruments into a computational framework governed by the physical equations of the atmosphere. Reanalyses offer advantages over observed data in two main aspects: data consistency and coverage, as they are provided as regularly gridded datasets that cover a large area, often the whole world, and are also provided at regular time steps. Such consistency overcomes the shortcomings of measured data which are irregularly spatially distributed and tend to decrease in number further into the past. These advantages thus allow reanalyses to perform two tasks that observed data do not permit: the consideration of long-term trends in wind speed and the investigation of the wind resource over a wide geographical domain.

However, several studies have highlighted a number of issues associated with using reanalysis data. First, significant biases in mean wind speed have been observed in reanalysis datasets which stem from underlying systemic model errors [4]. Second, generation variability represented by reanalyses tends to be underestimated over short time scales, which

may lead to misrepresentation of ramp events [3]. Third, the coarse spatial resolution of reanalyses is not able to resolve complex topography and the ensuing effects on airflow [5]. Fourth, global reanalyses are limited by uneven access to high-quality observations, leading to significant variability in their performance, with strong accuracy in well-observed regions but reduced reliability in areas with sparse or inconsistent observational coverage [6]. Hence, a thorough evaluation of a reanalysis dataset is necessary to understand and mitigate the uncertainties which arise from these issues.

Hence, a substantial number of evaluations of the accuracy of reanalysis wind speed have been conducted in various locations in both onshore and offshore environments. For example, Miao et al. [7] evaluated the accuracy of European Centre for Medium-Range Weather Forecasts Reanalysis Interim (ERA-Interim), Japanese 55-year Reanalysis (JRA-55), Climate Forecast System Reanalysis (CFSR), Modern-Era Retrospective analysis for Research and Applications 2 (MERRA-2), and National Centers for Environmental Prediction (NCEP) reanalyses against observed surface wind speed data in the Northern Hemisphere, Carvalho et al. [8] assessed the performances of ERA-Interim, CSFR, NCEP reanalysis 2, and MERRA reanalyses in Portugal and the Iberian Peninsula, Kumar and Anandan [9] evaluated NCEP reanalysis 2 in India, while Stopa and Cheung [10] similarly validated ERA-Interim and CSFR reanalysis in United States waters. Ideally 100 m wind speed would be used for validation as this is closer to the hub height of modern multi-MW wind turbines. However, the majority of these evaluations resorted to using observed wind speed from observations at 10 m for validation due to the much greater data availability at this elevation. Only a few validation studies of reanalysis wind speed at 100 m have been made [11, 12]. Regardless, while most studies have concluded that most reanalyses show a decent correlation (mean Pearson R $>$ 0.75) of wind speed with observed data, they also found significant mean biases of magnitude greater than 0.3 m/s and found RMSEs higher than 3 m/s.

Only a limited number of European Centre for Medium-Range Weather Forecasts Reanalysis 5 (ERA5) reanalysis wind speed evaluations exist in the literature due to its relatively recent release. Of those that have been performed, Gualtieri [13] validated ERA5 wind speed against 100 m tower observations in America, Europe, the Middle East, Africa,

and Oceania, Fan et al. [14] compared ERA5 against other reanalyses using more than 1,000 observation stations across all six continents, Kardakaris et al. [15] evaluated ERA5 wind speed against in-situ measurements in the Greek seas, while Soukissian and Sotiriou [16] compared the long-term variability of wind speed and direction in the Mediterranean Basin with results obtained from ERA-Interim. As with evaluations of other reanalysis datasets, these studies reported mean wind speed biases that range from -0.84 m/s to 2.28 m/s while RMSEs were found to reach as high as 3.69 m/s. Furthermore, significant spatial variations in mean wind speed bias were also observed on a global scale. However, due to the superior spatial resolution, these studies found that ERA5 globally exhibits better performance, with respect to mean wind speed bias and RMSE, compared to other reanalysis datasets.

There exist a number of gaps within these evaluations of reanalysis wind speed data that are relevant to the scope of this study. First, ERA5 wind speed has never been investigated on a large scale in the UK [17]. Second, only a few studies (e.g., [18]) have investigated the sources of errors which may stem from physical factors like topography or model uncertainties. Last and more importantly, the exclusive usage of error metrics like RMSE, mean wind speed bias, and Pearson correlation in most studies means the performance of ERA5 is only captured in very general terms. While this may be sufficient for applications like energy yield calculations, this study's focus on low wind speed events requires a further examination of the dataset in terms of low wind speed events, which is generally lacking in the literature. Studies that mention low wind speed validation only did so with respect to wind speed percentiles that do not stem from physical reasons, and although Cannon et al. [3] briefly touched on the comparison between MERRA reanalysis and observed sustained low wind speed events, it was not the main purpose of the study.

Therefore, the aim of this study is to provide a comprehensive evaluation of ERA5 wind speed in the UK. In addition to evaluating ERA5's performance using standard metrics for general accuracy of wind speed prediction, this study also presents an assessment focused on low wind speed events, as well as the sources of underlying uncertainties.

2.2 Methodology and Data

2.2.1 Reanalysis Data

Released in 2019, ERA5 [19] is the latest generation reanalysis model produced by ECMWF using a four-dimensional variational (4D-VAR) assimilation scheme. This offers significant advantages over a three-dimensional variational (3D-VAR) assimilation scheme of other widely used reanalyses such as MERRA-2 and CSFR [20] in terms of its ability to incorporate observations at the exact time of measurement. At a spatial resolution of 0.25° latitude-longitude, or approximately 27.5 km, and a maximum temporal resolution of 1-hourly time steps, ERA5 offers the highest spatiotemporal resolution out of all reanalyses that provide global coverage. The fact that ERA5 extends back to 1950 (now extended further to 1940, but limited to 1950 at the time of this analysis) is also advantageous because of the rarity of extreme low wind speed events which necessitates a long dataset and to capture inter-decadal variability in wind speeds. For example, the UK average wind speed during 1960-1980 was significantly lower than that in 1980-2000 [21]. Furthermore, in addition to wind data, which are available in the form of easterly and northerly wind speed components at 10 m and 100 m elevations, other meteorological variables such as 2 m temperature, boundary layer height etc. are also provided by ERA5. As the focus of the study is on the region containing the UK's wind farm fleet, the scope of ERA5 dataset used herein extends from 48°N to 61°N and from 10°W to 4°E in the form of gridded data as illustrated in Figure 2.1.

2.2.2 Observation Data

In this study, we use in-situ 10 m wind speed measurements taken from weather observation stations around the UK to validate the ERA5 reanalysis data. While it is preferable to validate ERA5 at 100 m, which is representative of the average wind turbine hub height, most wind speed measurements are typically taken at 10 m. The majority of the observed data were obtained from the British Atmospheric Data Centre's (BADC) Met Office Integrated Data Archive System (MIDAS) Land and Marine Surface Stations dataset [22], which comprises hourly weather measurements from the Met Office station network from

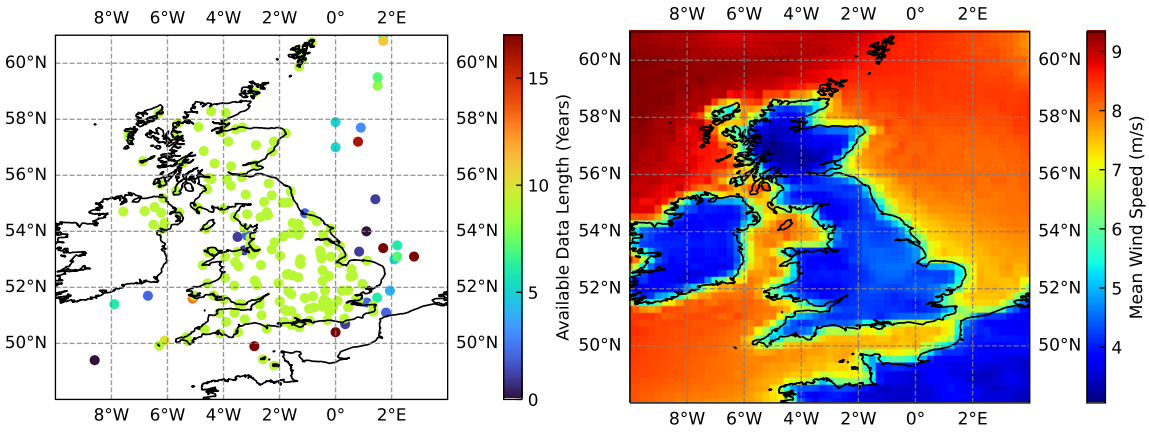


Figure 2.1: Primary datasets used in the study. (Left) Locations of meteorological observation stations from the MIDAS dataset and the Marine Data Exchange dataset. (Right) Mean 10-metre wind speed of the ERA5 dataset for 2000-2020.

1853 to the present, and represents the largest database of UK wind speed measurements available in public archives. Because most MIDAS stations are located onshore, additional station data were obtained from Crown Estate's Marine Data Exchange (MDE) database, which comprises weather data collected from met-masts near UK offshore wind farms.

Although the actual number of observation stations from these datasets exceeds 300, only those whose data length is longer than one year and with data availability greater than 90% were used so that seasonal variations could be observed. It is important to note that for those stations that met these criteria, while the available data record can extend to more than 40 years, MIDAS station anemometers had a cut-in wind speed of 4-5 m/s before the Met Office's upgrade campaign reduced the cut-in wind speed to 0.5 m/s in 1997 [23]. Since the focus of the present study is placed on low wind speed events, only data after 1997 were therefore used. The filtering procedure resulted in 205 time series with an average data length of 9.5 years within 1997-2020, 172 of which are from onshore stations and 33 from offshore stations whose locations are illustrated in Figure 2.1 and summarised in Table 2.1.

Due to the size of the dataset, the data cleaning process was automated based on the criteria employed by Staffell and Green [24]. First, data points that did not pass the Met Office's quality checks were removed. Second, non-zero identical repeated values that extended over 24 hours were deemed measurement instrument errors and, therefore, removed. Third, anomalously high readings, namely wind speeds above 125 knots, were

removed. Finally, data whose units were in knots were converted to m/s. For all 205 observation locations, data availability remained greater than 98% after the removal of data points by the quality check, especially data from the Marine Data Exchange dataset that are of consistently higher quality than those from the MIDAS dataset, both in terms of measurement precision and data completeness. Therefore, no effort was made to recreate missing or removed observations to avoid introducing uncertainty into the data.

In the present study, we treat this quality-controlled dataset of field measurements as a ground truth against which to compare the reanalysis data. However, despite the implemented data quality control process, there remains a number of limitations. First, the dataset includes observations from various sources, each with distinct measurement accuracies and practices, which can affect the homogeneity of the data. Second, surface wind measurements are sensitive to unknown local environmental conditions, such as terrain, vegetation, and nearby structures, and therefore, may not be representative of broader regional wind patterns or the grid-scale wind speeds captured by reanalysis datasets. Third, the MIDAS dataset is precise to one knot, as outlined in Table 2.1. This limited precision introduces an additional source of uncertainty when comparing MIDAS observations to ERA5 estimates. As a result, the calculated RMSE values for ERA5 should be considered conservative estimates, since the low precision of MIDAS inherently restricts the accuracy of the validation dataset.

Dataset	**Domain**	**Precision**	**No. of Stations**
MIDAS Land Observations	Onshore	0.51 m/s	172
MIDAS Marine Observations	Offshore	0.51 m/s	24
Marine Data Exchange	Offshore	0.01 m/s	9

Table 2.1: Observation station datasets used in the study. Note that 0.51 m/s corresponds to 1 knot, which is the precision of the MIDAS measurement devices.

2.2.3 Methodology

To evaluate the performance of ERA5 in capturing observed wind speed, the ERA5 wind speed time series was compared against the observed wind speed time series at the location of each of the 205 observation stations. This represents a total of 17,157,190 hourly

data points drawn from the period 1997-2020. ERA5 wind speed time series at each specific location was obtained by separately interpolating easterly and northerly wind speed components u_x and u_y from the grid points to the station's coordinates. Multiple interpolation schemes were considered: bi-linear interpolation, inverse distance weighting interpolation, and bi-cubic interpolation. However, it was found the choice of interpolation scheme does not significantly affect the resultant interpolated time series, and hence, the less computationally expensive bi-linear interpolation was used. Using four grid points $(x_1, y_1), (x_1, y_2), (x_2, y_1)$, and (x_2, y_2) whose corresponding wind speed components are $u_{i,11}, u_{i,12}, u_{i,21}, u_{i,22}$, the bi-linearly interpolated wind speed component u_i at (x, y) is given by:

$$\begin{aligned} u_i = &\frac{(x_2 - x)(y_2 - y)}{(x_2 - x_1)(y_2 - y_1)} u_{i,11} + \frac{(x - x_1)(y_2 - y)}{(x_2 - x_1)(y_2 - y_1)} u_{i,21} \\ &+ \frac{(x_2 - x)(y - y_1)}{(x_2 - x_1)(y_2 - y_1)} u_{i,12} + \frac{(x - x_1)(y - y_1)}{(x_2 - x_1)(y_2 - y_1)} u_{i,22}. \end{aligned} \tag{2.1}$$

The interpolated wind speed u and direction ϕ at the desired coordinate were then computed by:

$$u = \sqrt{u_x^2 + u_y^2}, \tag{2.2}$$

$$\phi = \frac{180}{\pi} \arctan\left(\frac{u_y}{u_x}\right). \tag{2.3}$$

At each observation station location, the observed wind speed time series u_{OBS} was compared against the interpolated ERA5 wind speed time series u_{ERA}, both of length N, using three metrics, namely: Root Mean Square Error (RMSE) as a general error metric, Mean Error to capture bias, and Standard Deviation Error to capture the hourly variability as given by:

$$\text{RMSE (m/s)} = \sqrt{\frac{\Sigma_{i=1}^{N} (u_{ERA,i} - u_{OBS,i})^2}{N}}, \tag{2.4}$$

$$\text{Mean Error (m/s)} = \overline{u}_{ERA} - \overline{u}_{OBS}, \tag{2.5}$$

$$\text{StDev Error (m/s)} = \sigma_{ERA} - \sigma_{OBS}. \tag{2.6}$$

Error metrics related to the Weibull distribution, which is given by

$$f(u,\lambda,k) = \begin{cases} \frac{k}{\lambda}(\frac{u}{\lambda})^{k-1}e^{-(u/\lambda)^k} & ;\ u \geq 0 \\ 0 & ;\ u < 0 \end{cases}, \tag{2.7}$$

which are associated with the distribution's two governing parameters, namely the scale factor λ and the shape factor k were also used as performance metrics as given by:

$$\text{Scale Factor Error } (\%) = \frac{\lambda_{ERA} - \lambda_{OBS}}{\lambda_{OBS}}, \tag{2.8}$$

$$\text{Shape Factor Error } (\%) = \frac{k_{ERA} - k_{OBS}}{k_{OBS}}. \tag{2.9}$$

Finally, to capture the discrepancy between observed wind speed and ERA5 wind speed concerning low wind speed events, the error in the percentage frequency of wind speed less than the typical cut-in wind speed of a wind turbine of 4 m/s was used as a metric:

$$P_{Error}(u \leq 4) = P_{ERA}(u \leq 4) - P_{OBS}(u \leq 4), \tag{2.10}$$

where P_i is the respective cumulative distribution function.

A caveat that comes with such an approach is that there is no physical basis to support the use of the Weibull distribution to approximate wind speed. In the context of the present study, this is often the case for observed wind speed distributions for which there is a non-zero frequency of calm conditions (below the cut-in threshold of measurement devices), whereas a zero frequency of 0 m/s wind speeds is enforced by the two-parameter Weibull distribution. Although this fact has been acknowledged, these distribution-based error metrics are predicated on the commonly adopted practice of using the Weibull distribution as a standard engineering tool to approximate wind speed distributions [25–27]. Hence, taking into account these limitations and given the scope of this study, the use of the Weibull distribution was deemed adequate.

2.3 Results and Discussions

2.3.1 Errors

Overview

Figure 2.2 provides an overview of the errors between the 205 observed–ERA5 wind speed time series pairs in terms of the relationship between mean error and RMSE. With a mean RMSE of 1.85 m/s and a mean of mean error of 0.12 m/s, a small but not insignificant positive bias is observed in ERA5 wind speed. While there is a correlation between RMSE magnitude and mean error, for locations that exhibit insignificant mean error, the non-zero RMSE when the mean wind speed error is 0 m/s shows that a significant proportion of RMSE is also driven by wind speed noise. The relationship presented also shows that the largest RMSEs exhibited are caused by the underestimation of wind speed by ERA5 and that such an effect is only observed in the onshore domain; all locations with an RMSE greater than 3.5 m/s were onshore.

While the error profile presented here indicates that the reanalysis dataset is imperfect, ERA5 demonstrates superior performance in terms of these error metrics when compared with other datasets. For example, ERA-Interim, CSFR, and MERRA reanalyses exhibit mean RMSEs and means of mean errors upwards of 2 m/s and 0.34 m/s, respectively, when validated against observations in Northern Europe, the Iberian Peninsula, and Portugal [8, 13, 28]. While these studies were conducted in different locations, a more direct comparison can be made between the present evaluation and the validation of the CSFR reanalysis dataset by Sharp et al. [18]. Like the present study, this was conducted in the UK against MIDAS station data. The study reported mean RMSE and mean of mean error of 2.35 m/s and 0.33 m/s respectively, both of which are significantly higher than the ERA5 errors presented in this study.

To further evaluate the performance of ERA5 in the UK, ranges and distributions of each error metric are presented in Figures 2.3 and 2.4. Moreover, due to the differences between onshore and offshore topography and weather regimes, it was also of interest to consider the performance of ERA5 separately in each environment. It was found that

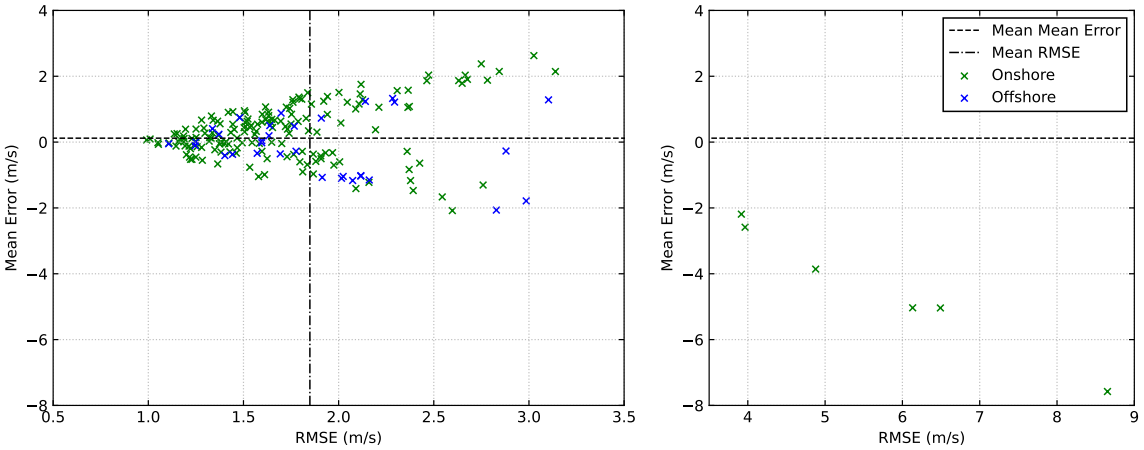


Figure 2.2: Mean errors plotted against Root Mean Square Errors for each observed-ERA5 time series pair. Each cross represents errors from a single validation site, with green crosses indicating onshore locations and blue crosses indicating offshore locations (colour online). Note the scaling of the x-axis on the right to clearly display extreme errors.

offshore sites demonstrate a smaller range of RMSEs due both to the extreme onshore errors previously mentioned and also that RMSE at the majority of sites lies between 1 and 2 m/s, with a mean of 1.89 m/s and a median of 1.63 m/s for onshore locations, and a mean of 1.84 m/s and a median of 1.77 m/s for offshore locations.

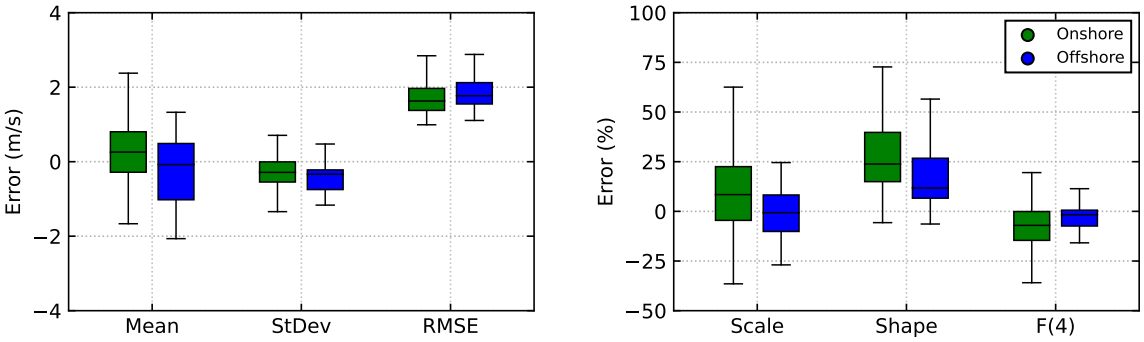


Figure 2.3: Onshore (green) and offshore (blue) errors of ERA5 wind speed compared to observations at 205 validation sites. The left plot shows hourly wind speed mean error, standard deviation error, and RMSE while the right plot shows errors in scale parameter, shape parameter, and percentage frequency of low wind speed. For all error metrics, subsets of 33 onshore station error values were repeatedly sampled with replacement to match the number of offshore stations, and the standard deviation was calculated for each sample; the results failed to reject the null hypothesis, indicating no statistically significant difference in variability between onshore and offshore errors.

There are two major differences in mean errors between onshore and offshore sites. First, offshore sites exhibit fewer extreme errors than their onshore counterparts and, second, while there is a 0.17 m/s positive bias of mean wind speed in the onshore environment,

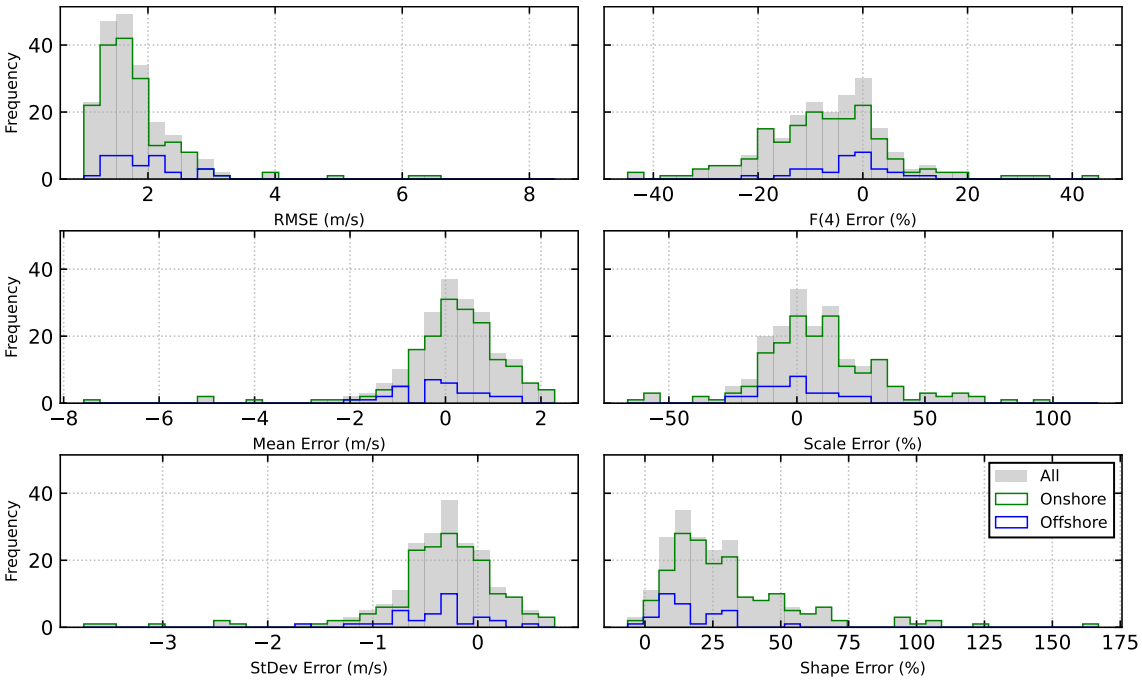


Figure 2.4: Distributions of onshore (green), offshore (blue), and combined (grey) errors of ERA5 wind speed compared to observations at 205 validation sites.

a 0.14 m/s negative bias is observed in the offshore environment. Furthermore, both the onshore and offshore mean error distributions are loosely centred around their respective mean, while also displaying considerable variance. This observation is also reflected in the error distribution of scale factor, as scale factor is approximately proportional to mean wind speed for a given location. Similarly, the distribution of standard deviation error are also loosely centred around their respective mean, while also displaying considerable magnitudes of variance, albeit centred on a value that is below zero for both the onshore and offshore environments. This is reflected in the shape error distribution, which shows a very low frequency of negative error, suggesting that ERA5 consistently underestimates the hourly variability of wind speed. As a result, the ERA5 wind speed time series shows a clear tendency, especially in the onshore environment, to underestimate the percentage frequency of low wind speeds, as shown in the distribution of $P(u \leq 4)$ errors whose magnitude can approach 50%.

Seasonal Variation

Seasonal variation of ERA5's predictions also has important implications on the reanalysis' ability to accurately simulate observed wind speed. Wind speed time series from all observation sites were sorted into each season as defined by a three-month period (spring starts on 1st of March and ends on 31st of May etc.), and the results are presented in Figure 2.5. There is a clear difference between errors present in spring and summer and those in winter and autumn, where the former have an average mean error of -0.05 and 0.00 m/s (-4.2% and -2.2% as normalised by the observed mean) whereas the latter pair's average mean errors are 0.28 m/s and 0.23 m/s (8.1% and 10.5%) respectively. At 1.78 m/s and 1.65 m/s, the RMSEs in spring and summer are also markedly lower than the RMSEs of 2.04 m/s and 1.90 m/s in winter and autumn. These RMSEs correspond to consistent Mean Absolute Percentage Error values of 40-46% across the four season, suggesting that seasonal differences in RMSE may be attributed to variations in the magnitude of wind speeds as well. As well as the similar pattern observed for standard deviation errors, these trends lead to the fact that the percentage frequency of low wind speed, defined as that below 4 m/s, is only underestimated on average by 0.29% and 0.42% in spring and summer, compared to 5.46% and 5.81% in autumn and winter.

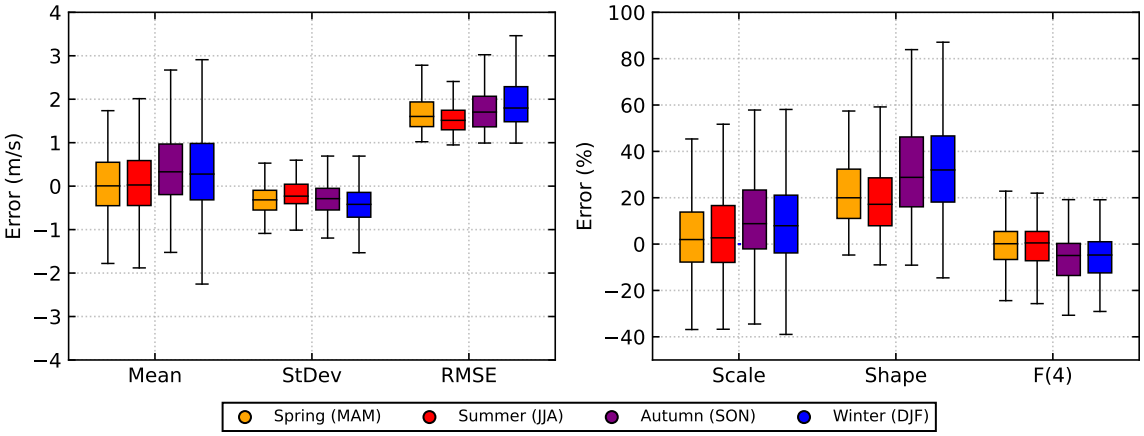


Figure 2.5: ERA5 errors sorted into seasons. The left plot shows hourly wind speed mean error, standard deviation error, and RMSE, while the right plot shows errors in scale parameter, shape parameter, and percentage frequency of low wind speed.

These results are not unexpected as wind speeds tend to be higher in winter and autumn than in spring and summer due to the increase in temperature gradient and, hence, the

pressure gradient between the approaching and the displaced air masses [29, 30]. Therefore, on average, ERA5 would be expected to predict higher wind speeds in these months. Such an error trend is significant because winter and autumn are the two seasons where low temperatures lead to high electricity demand for heating. Hence, the underestimation of low wind speed percentage frequency may lead to an overestimation of wind energy production's ability to match demand during these periods.

Low Wind Speed Events

$P(u \leq 4)$ error is included as an error metric as the focus of this study is on low wind speed events. Although the percentage frequency of low wind speed $P(u \leq 4)$ provides a convenient measure to compare the performance of ERA5 in terms of extreme events across multiple locations, the duration of these events is of greater importance, as long periods of wind droughts can have more significant impacts on wind energy production than multiple scattered short-term events. There are multiple ways to quantify these longer-term events, as presented in each row of Figure 2.6 for both the onshore and offshore environments.

First, low wind speed events, defined as periods where the wind speed is continuously below 4 m/s, from all 205 locations were sorted based on their duration and plotted against their number of observations. The first notable finding is the periodicity in the number of observations of onshore low wind speed events that is not seen in the offshore environment. This effect is explained by the clearer and more consistent diurnal variations of wind speed on land that arise from the presence of short time-scale changes in land temperature and their absence in sea surface temperature [31]. However, a more important trend that can be observed for both environments is that the number of observations of short-term (below 25 hours for onshore and 15 hours for offshore) low wind speed events is significantly underestimated by ERA5. For example, 1-hour events are underestimated by over 260,000 observations. On the other hand, the number of observations of longer low wind speed events is overestimated by ERA5, though by a smaller margin. For example, ERA5 overestimates the observations of a five-day-long low wind speed event by 53 observations.

A more useful representation of low wind speed events, which has been employed in previous studies [3, 32], is to present these events as a cumulative sum and as a percentage

of time rather than the raw number of observations, as illustrated in the second row of Figure 2.6. For example, for the onshore environment, low wind speed events that persist for at least 15 hours make up 1.1% of the data record. Here, it can be seen more clearly that considering the severity of events, the observed and ERA5 data show a decent level of agreement for wind speed events over 16 hours for onshore and 6 hours for offshore, while shorter wind speed events are significantly underestimated.

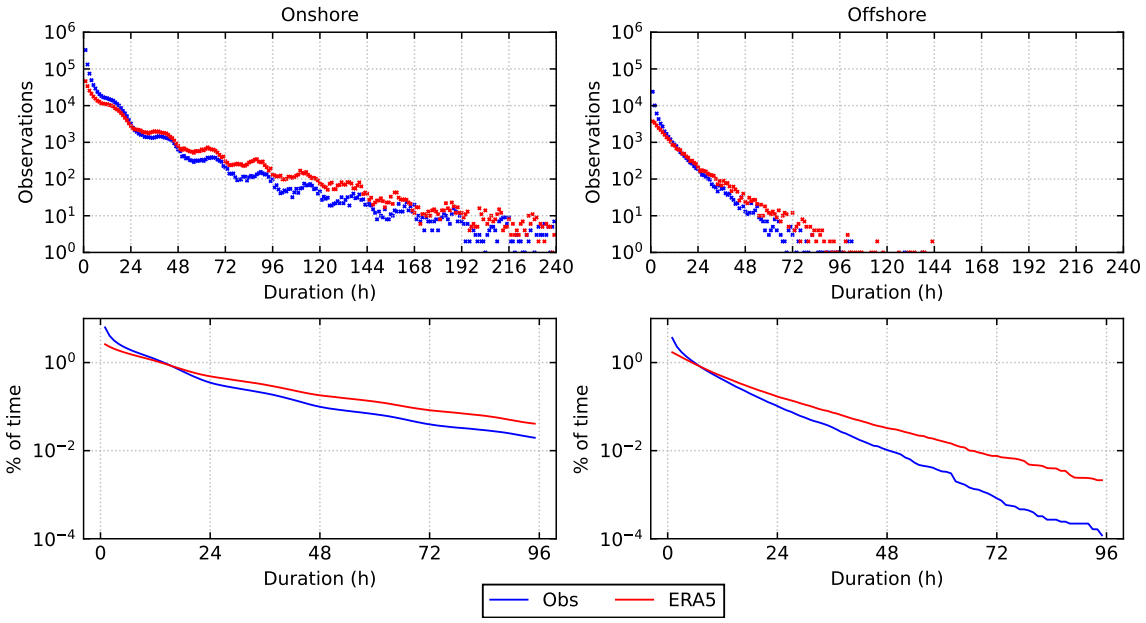


Figure 2.6: Errors in terms of the persistence of low wind speed events from observation (blue) and ERA5 (red) data. The left column shows errors from onshore locations, while the right column shows errors from offshore locations. The top row considers the raw frequency of these sustained low wind speed events, while the bottom row considers the cumulative frequency.

While the cumulative density at a low wind speed threshold ($P(u \leq 4)$) demonstrates that ERA5 tends to underestimate the number of observations of low wind speed, a further investigation into the duration of these events indicates that this discrepancy is heavily influenced by the underestimation of low wind speed events shorter than one day. This observed discrepancy can be explained by ERA5's underestimation of the hourly wind variability caused by small-scale fluctuations that are not captured by the macro-scale-driven ERA5 simulation, hence, the inability to capture small, frequent drops in wind speed that give rise to short events. Overall, it can be argued that ERA5's performance in capturing longer low wind speed events, which have a greater impact on wind energy

generation than short, intermittent ones, is more significant than its inability to capture the number of shorter events.

2.3.2 Sources of Uncertainty

Coastal and Elevated Sites

Figure 2.7 illustrates the spatial variation of the differences between ERA5 and observed wind speeds to gain insight into the errors and uncertainty associated with ERA5 reanalysis around the UK. While there is no apparent spatial pattern of error distribution across the UK, there exist some features of interest. First, a number of sites with high underestimation of mean and standard deviation, and hence high RMSE and overestimation of $P(u \leq 4)$, are observed onshore of North Western England and Western Scotland. This is a high-elevation region that typically experiences high wind speed but is represented by the lowest mean wind speed in ERA5, as shown in Figure 2.1. Second, sites with large magnitude of mean wind speed errors and hence, high errors in low wind speed percentage frequency are often situated along the coast, particularly Great Britain's Southern coast.

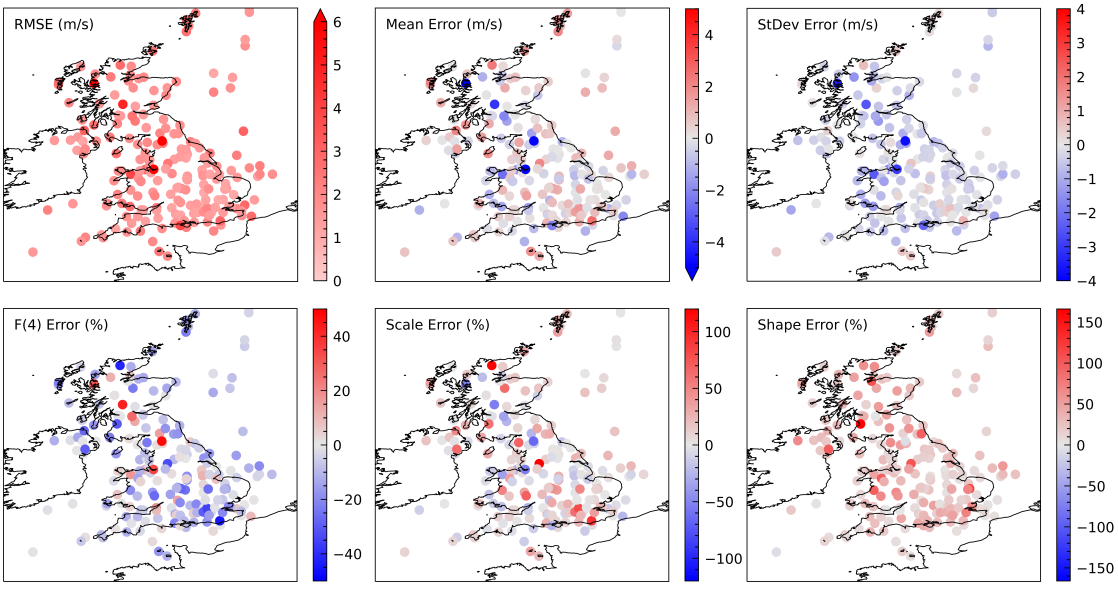


Figure 2.7: Spatial distribution of ERA5 errors around the UK. Each circle represents the location of the observation station used to validate ERA5 data in this study.

Two observed trends are that coastal and elevated areas give rise to particularly significant errors, consistent with Sharp et al. [18]'s evaluation of CFSR reanalysis wind speed.

To further clarify this observation, the 205 sites were sorted into four categories, namely coastal locations (45 sites), elevated locations (22 sites), both coastal and elevated locations (3 sites), and locations that are neither coastal nor elevated (135 sites), where coastal locations are defined as those within 27.5 km of the coastline (the resolution of ERA5) and elevated locations are those situated over 200 m above sea level. The results presented in Figures 2.8 and 2.9 corroborate this finding in a number of ways, as exemplified by the mean RMSE of non-coastal-non-elevated sites of 1.67 m/s compared to the RMSE of 3.17 m/s from sites in the other three categories.

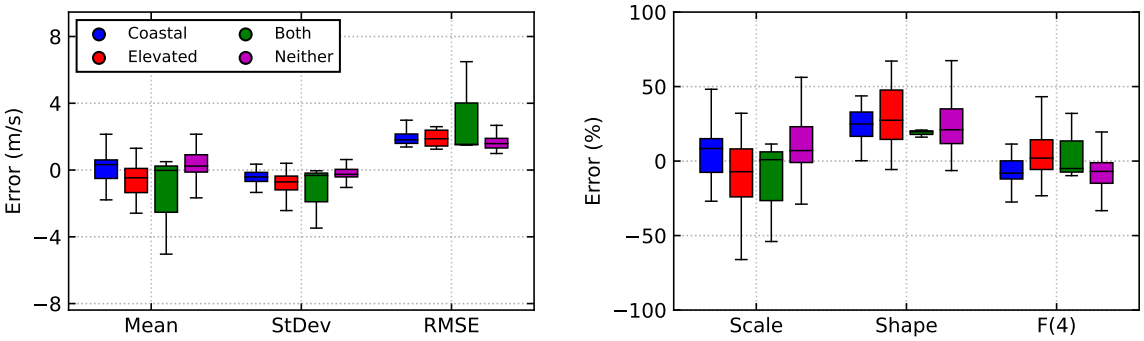


Figure 2.8: Errors according to the classification of each site which is one of: coastal (blue), elevated (red), coastal and elevated (green), and neither (purple). Coastal sites are defined as those within 27.5 km of the coastline (the resolution of ERA5) and elevated sites are defined as those over 200 m above sea level. The left plot shows hourly wind speed mean error, standard deviation error, and RMSE while the right plot shows errors in scale parameter, shape parameter, and percentage frequency of low wind speed. Note that for the *neither* group, the three data points correspond to the lower whisker, the median line, and the upper whisker.

First, elevated and elevated/coastal sites were found to be negatively biased, whereas it was previously observed that ERA5 wind speed tends to be positively biased in the UK. High elevation implies mountainous regions that are predominantly situated in Scotland (e.g., the Grampion mountains, the Maell Gorm peak, etc.) and some of the sites where ERA5 has the highest underestimation of mean wind speed are situated in such regions, therefore implying the effects of topography on these discrepancies. Wind in mountainous regions is subjected to both the ridge-acceleration effect, where wind layers are accelerated over a peak, and the Venturi effect, where passes and valleys parallel to the wind direction increase the wind speed [33]. However, these topographic features are too small to be captured by the resolution of ERA5 grids; hence, physical features affecting the flow are

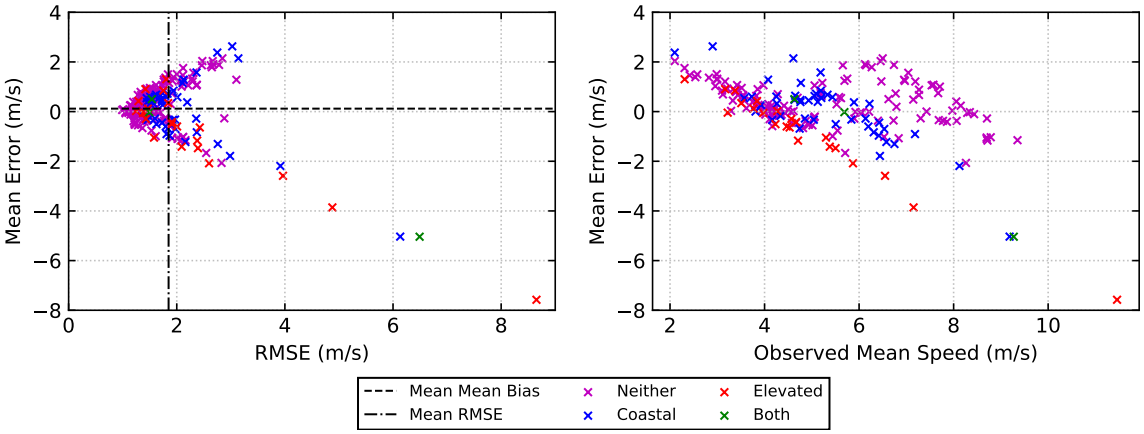


Figure 2.9: (Left) Relationship between mean error and RMSE. (Right) Relationship between mean error and observed mean speed. Each cross represents errors from a single validation site sorted into the classification of each site (coastal (blue), elevated (red), coastal and elevated (green), and neither (purple)). Coastal sites are defined as those within 27.5 of the coastline (the resolution of ERA5) and elevated sites are defined as those over 200 m above sea level.)

under-resolved, leading to the underestimation of wind speed in these regions. This is further corroborated by Figure 2.9 where underestimations of mean wind speed by ERA5 are more significant for elevated sites with higher observed wind speed than overestimations of mean wind speed at non-elevated sites with lower observed mean wind speed, hence implying localised, topography-induced acceleration. Therefore, rather than indicating a flaw in ERA5's performance, these outlying errors point to the placement of certain observation stations in locations where the winds are highly localised and greater resolution (e.g. through down-scaling) would be required. Regardless, it should be noted that these elevated sites, especially those with the largest errors in the North, are situated in remote mountainous regions that do not currently accommodate nor are particularly suitable for wind farms and so will not have significant effects on the analysis of the UK's wind resource.

Second, although coastal sites exhibit a similar range of mean wind speed errors to sites that are neither coastal nor elevated, they contain more extreme errors. Characterised by the variability of topography, surface roughness, and thermal gradient, coastal areas have always been regarded as a modelling challenge [34, 18]. This is, again, partly due to the resolution of reanalyses which cannot resolve the changes that occur over the short distance that is the interface between the offshore and the onshore environment. But unlike elevated sites whose terrains are not always suitable for wind farms, coastal regions, especially the

West coast, are home to several wind farms both offshore and onshore and hence, are more consequential when evaluating reanalysis data. However, at an average RMSE of 2.05 m/s, ERA5's performance in coastal areas already surpasses other global reanalyses [18].

Assimilation Window Error

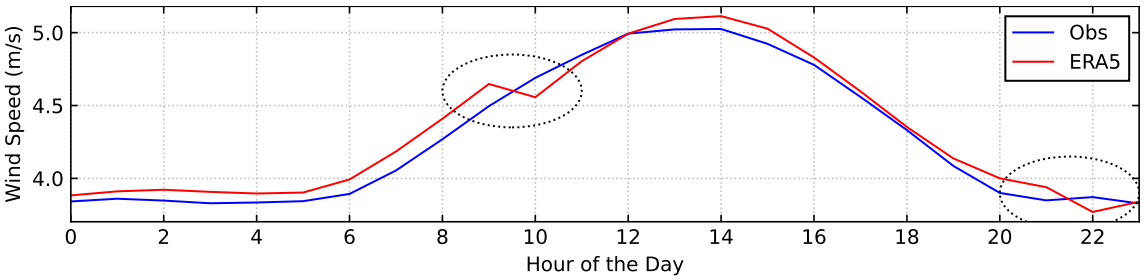


Figure 2.10: Diurnal variation of observed and ERA5 wind speed taken from a validation site at 50.86,-3.24, with the discontinuities at 0900-1000 and 2100-2200 highlighted.

Another major source of uncertainty stems from the underlying data assimilation model of ERA5 reanalysis. Reanalyses rely on the process of data assimilation to incorporate observed data to correct the forecasts made by the underlying weather prediction model. This process takes place in assimilation windows which extend for a short period of time, within which the cost function that captures the difference between the forecast and the observed data is minimised. In a 3D-VAR model where time is not involved, observations within the assimilation window are only used to correct a single point in the time domain [35]. However, in ERA5's underlying 4D-VAR assimilation model, including time as the fourth dimension means that the initial state of the assimilation window is adjusted in the process to optimise the forecast for the entire window [19]. More specifically, ERA5 utilises two 12-hour assimilation windows per 24-hour cycle where one begins at 1000 UTC and another at 2200 UTC. Since the initial state of these windows is also subjected to adjustments in a 4D-VAR model, discontinuities between 0900-1000 UTC and 2100-2200 UTC are present in several climate parameters, including u_x and u_y components of wind speed.

Although such an issue has been recognised by the ECMWF [36], to the author's knowledge, no previous evaluation of ERA5 wind speed has investigated the impacts that these discontinuities have on data reliability, especially in the context of low wind speed

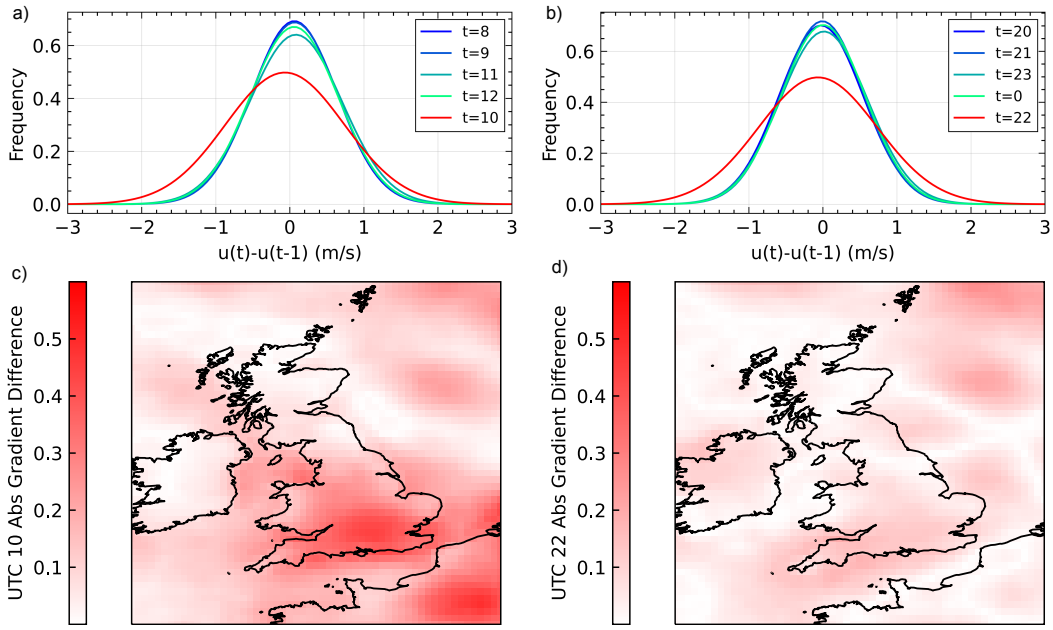


Figure 2.11: Distributions of hourly wind speed gradient from (a) 0700-1200 UTC (b) and 1900-0000 UTC. (Bottom) Spatial difference of mean gradient difference (c) between 0900-1000 UTC and the mean of 0700-0900 UTC and 1000-1200 UTC, and (d) between 2100-2200 UTC and the mean of 1900-2100 UTC and 2200-0000 UTC.

events. Hence, to observe such an effect on wind speed, Figure 2.10 illustrates the diurnal variation of wind speed from a typical observation site, averaged over the period 2010-2020, showing clearly the discontinuities in wind speed at the junction of these 12-hour assimilation windows. A question that arises is whether these discontinuities are the result of consistent drops in wind speed. The top row of Figure 2.11 shows the distribution of the hourly wind speed gradients at these two junctions. While the wind speed gradients around these two periods (two hours before and after) approximate a normal distribution (p-value > 0.9 by Kalmogorov-Smirnov test) with a positive mean, the gradient at these two time junctions approximate a normal distribution with a negative mean and a relatively larger variance, thus indicating that the discontinuities are the result of a random process rather than a consistent drop in wind speed. It can also be clearly seen that the effect is more pronounced at the 0900-1000 UTC discontinuity than that at 2100-2200 UTC, though the larger-than-usual variance of wind speed gradients at the later junction is still a cause for concern. To investigate the spatial variation of these discontinuities, the mean difference between the gradient at each junction and the two adjacent time steps are shown in the

bottom row of Figure 2.11. It is apparent that the effect is more pronounced at the 0900-1000 UTC than at the 2100-2200 UTC discontinuity and, more importantly, that some locations are more susceptible to this effect, most visibly Southern Great Britain and the Southern North Sea. It should be noted that these discrepancies are consistent throughout all seasons.

There are two major implications of this modelling error. First, ERA5's representation of wind speed diurnal variation will not be representative of reality. Second, and more importantly, this error could lead to a misrepresentation of low wind speed events. Unlike a natural diurnal pattern where the likelihood of a low wind speed event starting at 1000 UTC is moderately low, ERA5's diurnal pattern exhibits a spike in likelihood at this hour of the day. Similarly, a significant drop in the likelihood of a low wind speed event ending at 1000 UTC was also observed. The likelihood of low wind speed events starting or ending at adjacent hours of the day remains comparable to the natural diurnal pattern. Hence, this implies that, for shorter events, this error will only increase the percentage frequency of one-hour low wind speed events and that for longer events, it will only extend the duration of low wind speed events by one hour.

To address this assimilation window error, researchers in the wind energy community have adopted the use of the ERA5 forecast field instead of the analysis field, as the forecast field is not influenced by the assimilation window. This approach helps to mitigate the impacts of such artificial patterns in the diurnal cycle. On balance, while such model error is undesirable, it is also unavoidable, and given that the impacts are limited, the utilisation of the fourth dimension in a 4D-VAR system still offers more advantages than disadvantages.

2.4 Conclusion

Prolonged low wind speed events, such as that in March 2021 in the United Kingdom, represent one of the biggest challenges in fully de-carbonising the electricity system, hence the need to quantify these occurrences. While their superior temporal and spatial coverage, compared to observation data, make reanalysis data useful in assessing these rare events,

their accuracy in predicting wind speed should be assessed prior to usage.

This paper evaluated ERA5 reanalysis wind speed data at 10 m against observation data from 205 weather stations, both onshore and offshore, around the UK from the year 1997 to 2020. ERA5 exhibits a positive mean wind speed bias in the onshore domain of 0.166 m/s and a negative mean wind speed bias of -0.136 m/s in the offshore domain. For both domains, ERA5 reanalysis under-predicts the hourly variability of wind speed by -0.365 m/s. Furthermore, it has been demonstrated that these errors are more pronounced in winter and autumn than in summer and spring. The spatial distribution of these errors indicates that the most extreme errors come from onshore validation sites that are situated in coastal or mountainous regions where ERA5's resolution is unable to resolve localised wind effects. While mountainous regions, which are not suitable for wind farms, may be less consequential, coastal regions do accommodate a number of wind farms and, hence, point out the need for higher-resolution models that can well capture this interface.

These errors, therefore, lead to an underestimation of the percentage frequency of low wind speed. However, a further investigation into the discrepancy between observed and ERA5 percentage frequency of low wind speed shows that this is mainly influenced by a large underestimation of short-term low wind speed events that persist for less than 12 hours, whereas longer events, which have higher significance on the electricity system, are shown to be markedly more accurately represented.

Reanalysis data are less than perfect and these findings show that, in agreement with evaluations of other reanalysis datasets, ERA5 is also subject to a significant level of bias, topography-induced errors, a misrepresentation of short-duration low wind speed events. However, the mean levels of mean wind speed bias and RMSE exhibited by the 205 validation sites demonstrate that despite these errors, ERA5 still outperforms its global reanalysis counterparts in the UK domain compared to results reported by previous studies. Hence, despite the shortcomings highlighted in this paper, ERA5 proves to be an important tool which can provide valuable information in the context of low wind speed events prediction.

References

[1] P. Potisomporn, T. A. A. Adcock, and C. R. Vogel. Evaluating ERA5 reanalysis predictions of low wind speed events around the UK. *Energy Reports*, 10:4781–4790,

2023.

[2] I. Staffell, R. Green, T. Green, and M. Jansen. Electric Insights Quarterly. Technical report, Drax Group, 2021. URL `https://reports.electricinsights.co.uk/wp-content/uploads/2021/05/Drax-Electric-Insights-Q1-2021-Report.pdf`.

[3] D. J. Cannon, D. J. Brayshaw, J. Methven, P. J. Coker, and D. Lenaghan. Using reanalysis data to quantify extreme wind power generation statistics: A 33 year case study in Great Britain. *Renewable Energy*, 75:767–778, 2015.

[4] H. C. Bloomfield, D. J. Brayshaw, and A. J. Charlton-Perez. Characterizing the winter meteorological drivers of the European electricity system using targeted circulation types. *Meteorological Applications*, 27:e1858, 1 2020.

[5] L. C. Dawkins. Weather and climate related sensitivities and risks in a highly renewable UK energy system: A literature review, 2019. URL `www.metoffice.gov.uk`.

[6] A. Das and S. B. Roy. Jra55 is the best reanalysis representing observed near-surface wind speeds over india. *Atmospheric Research*, 297:107111, 2024.

[7] H. Miao, D. Dong, G. Huang, K. Hu, Q. Tian, and Y. Gong. Evaluation of northern hemisphere surface wind speed and wind power density in multiple reanalysis datasets. *Energy*, 200:117382, 2020.

[8] D. Carvalho, A. Rocha, M. Gómez-Gesteira, and C. S. Santos. WRF wind simulation and wind energy production estimates forced by different reanalyses: Comparison with observed data for Portugal. *Applied Energy*, 117:116–126, 3 2014.

[9] M. S. Kumar and V. K. Anandan. Comparision of the NCEP/NCAR Reanalysis II winds with those observed over a complex terrain in lower atmospheric boundary layer. *Geophysical research letters*, 36, 2009.

[10] J. E. Stopa and K. F. Cheung. Intercomparison of wind and wave data from the ECMWF Reanalysis Interim and the NCEP Climate Forecast System Reanalysis. *Ocean Modelling*, 75:65–83, 2014.

[11] P. Kiss, L. Varga, and I. M. Jánosi. Comparison of wind power estimates from the ECMWF reanalyses with direct turbine measurements. *Journal of Renewable and Sustainable Energy*, 1:033105, 2009.

[12] S. Liléo and O. Petrik. Investigation on the use of NCEP/NCAR, MERRA and NCEP/CFSR reanalysis data in wind resource analysis. *Sigma*, 1, 2000.

[13] G. Gualtieri. Reliability of ERA5 reanalysis data for wind resource assessment: A comparison against tall towers. *Energies*, 14:4169, 7 2021.

[14] W. Fan, Y. Liu, A. Chappell, L. Dong, R. Xu, M. Ekström, T. M. Fu, and Z. Zeng. Evaluation of global reanalysis land surface wind speed trends to support wind energy development using in situ observations. *Journal of Applied Meteorology and Climatology*, 60:33–50, 2020.

[15] K. Kardakaris, I. Boufidi, and T. Soukissian. Offshore wind and wave energy complementarity in the Greek seas based on ERA5 data. *Atmosphere*, 12(10):1360, 2021.

[16] T. Soukissian and M.-A. Sotiriou. Long-Term Variability of Wind Speed and Direction in the Mediterranean Basin. *Wind*, 2(3):513–534, 2022.

[17] G. Gualtieri. Analysing the uncertainties of reanalysis data used for wind resource assessment: A critical review. *Renewable and Sustainable Energy Reviews*, 167:112741, 2022.

[18] E. Sharp, P. Dodds, M. Barrett, and C. Spataru. Evaluating the accuracy of CFSR reanalysis hourly wind speed forecasts for the UK, using in situ measurements and geographical information. *Renewable Energy*, 77:527–538, 2015.

[19] H. Hersbach, B. Bell, P. Berrisford, S. Hirahara, A. Horányi, J. Muñoz-Sabater, J. Nicolas, C. Peubey, R. Radu, D. Schepers, A. Simmons, C. Soci, S. Abdalla, X. Abellan, G. Balsamo, P. Bechtold, G. Biavati, J. Bidlot, M. Bonavita, G. D. Chiara, P. Dahlgren, D. Dee, M. Diamantakis, R. Dragani, J. Flemming, R. Forbes, M. Fuentes, A. Geer, L. Haimberger, S. Healy, R. J. Hogan, E. Hólm, M. Janisková, S. Keeley, P. Laloyaux, P. Lopez, C. Lupu, G. Radnoti, P. de Rosnay, I. Rozum, F. Vamborg, S. Villaume, and J. N. Thépaut. The ERA5 Global Reanalysis. *Quarterly Journal of the Royal Meteorological Society*, 146:1999–2049, 7 2020.

[20] C. Jamet and H. Loisel. *Data Assimilation Methods*. Wiley Blackwell, 3 2013. ISBN 9781118670330. doi: 10.1029/2008GM000763.

[21] S. Watson, P. Kritharas, and G. Hodgson. Wind speed variability across the UK between 1957 and 2011. *Wind Energy*, 18(1):21–42, 2015.

[22] Met Office. Met Office Integrated Data Archive System (MIDAS) Land and Marine Surface Stations Data (1853-Current), 2012. URL `http://catalogue.ceda.ac.uk/uuid/220a65615218d5c9cc9e4785a3234bd0`.

[23] C. Sloan and M. R. Clark. A comparison of three Met Office wind observing systems. *Atmospheric Science Letters*, 13:283–288, 2012.

[24] I. Staffell and R. Green. How does wind farm performance decline with age? *Renewable Energy*, 66:775–786, 2014.

[25] T. Burton, N. Jenkins, D. Sharpe, and E. Bossanyi. *Wind energy handbook*. John Wiley & Sons, 2011.

[26] J. A. Carta and P. Ramírez. Use of finite mixture distribution models in the analysis of wind energy in the Canarian Archipelago. *Energy Conversion and Management*, 48:281–291, 1 2007.

[27] J. V. Seguro and T. W. Lambert. Modern estimation of the parameters of the Weibull wind speed distribution for wind energy analysis. *Journal of wind engineering and industrial aerodynamics*, 85:75–84, 2000.

[28] J. P. Murcia, M. J. Koivisto, G. Luzia, B. T. Olsen, A. N. Hahmann, P. E. Sørensen, and M. Als. Validation of European-scale simulated wind speed and wind generation time series. *Applied Energy*, 305:117794, 1 2022.

[29] G. Sinden. Characteristics of the UK wind resource: Long-term patterns and relationship to electricity demand. *Energy Policy*, 35:112–127, 1 2007.

[30] R. W. Baker, S. N. Walker, and J. E. Wade. Annual and seasonal variations in mean wind speed and wind turbine energy production. *Solar Energy*, 45:285–289, 1990.

[31] R. J. Barthelmie. Prospects for offshore wind energy: The state of the art and future opportunities: Offshore wind climate and wind energy applications prospects for offshore wind energy: The state of the art and future opportunities offshore wind climate and wind energy applications. *Wind Engineering*, 17:86–99, 1993.

[32] P. Potisomporn and C. R. Vogel. Spatial and temporal variability characteristics of offshore wind energy in the United Kingdom. *Wind Energy*, 25(3):537–552, 2022.

[33] S. Mathew. *Wind energy: fundamentals, resource analysis and economics*, volume 1. Springer, 2006.

[34] P. Beaucage, A. Glazer, J. Choisnard, W. Yu, M. Bernier, R. Benoit, and G. Lafrance. Wind assessment in a coastal environment using synthetic aperture radar satellite imagery and a numerical weather prediction model. *Canadian Journal of Remote Sensing*, 33:368–377, 2007.

[35] M. Fujiwara, J. S. Wright, G. L. Manney, L. J. Gray, J. Anstey, T. Birner, S. Davis, E. P. Gerber, V. L. Harvey, M. I. Hegglin, C. R. Homeyer, J. A. Knox, K. Krüger, A. Lambert, C. S. Long, P. Martineau, A. Molod, B. M. Monge-Sanz, M. L. Santee, S. Tegtmeier, S. Chabrillat, D. G. Tan, D. R. Jackson, S. Polavarapu, G. P. Compo, R. Dragani, W. Ebisuzaki, Y. Harada, C. Kobayashi, W. McCarty, K. Onogi, S. Pawson, A. Simmons, K. Wargan, J. S. Whitaker, and C. Z. Zou. Introduction to the SPARC Reanalysis Intercomparison Project (S-Rip) and Overview of the Reanalysis Systems. *Atmospheric Chemistry and Physics*, 17:1417–1452, 1 2017.

[36] European Centre for Medium-range Weather Forecasts. ERA5 Data Documentation, 2018. URL {https://confluence.ecmwf.int/display/CKB/ERA5\%3A+data+documentation#ERA5:datadocumentation-Knownissues}.

Statement of Authorship

Publication details	
Title of paper	Evaluating ERA5 reanalysis predictions of low wind speed events around the UK
Publication status	Published
Publication reference	P. Potisomporn, T. A. A. Adcock, and C. R. Vogel. Evaluating ERA5 reanalysis predictions of low wind speed events around the UK. Energy Reports, 10:4781–4790, 2023

Student confirmation	
Student name	Panit Potisomporn
Contribution	The analysis and text were primarily developed and written by PP, with the input of co-authors. All sections were written by PP and edited by TAAA and CRV.

Student signature: _____ **Date**: _____

Supervisor confirmation	
Supervisor name	Dr. Christopher Vogel
Comments	I confirm that Panit has made a substantial contribution to the publication, and that the description above in the Statement of Authorship is accurate.

Supervisor signature: _____ **Date**: _____

CHAPTER 3

Modelling Great Britain wind power output and electricity demand

This chapter presents the modelling of GB-aggregated wind power output, as well as its relationship with electricity demand. It has been adapted from the supplementary information section of the article accepted and published in Renewable Energy *journal on 15th December 2023 [1].*

Modelling GB-aggregated wind power output is a necessary prerequisite for investigating extreme low wind power events and their impacts on the electricity system. A model that takes 10-m ERA5 wind speed data and a wind farms database and outputs GB-aggregated wind power output is presented, where each constituent procedure represents an improvement over conventionally used approaches and contributes valuable insights into the modelling of wind power output. The mean-variance scaling method was identified as a computationally efficient yet effective bias correction technique. The extrapolation of wind speed using a machine-learning-based technique outperformed the conventional log-law. Empirical calibration of the manufacturer's power curve at a farm level enhances flexibility in modelling aggregated wind power output. Furthermore, an hourly weather-dependent electricity demand model is presented and has been shown to have comparable performance to a daily model, providing a simple means of modelling the interaction between wind power and the electricity system. The validation of the model shows a high level of agreement between modelled GB-aggregated wind power output and measured wind power output, particularly concerning the representation of low wind power events.

3.1 Introduction

Given the scarcity of publicly available wind farms' power output data, the accurate modelling of wind power output and its relationship with the electricity system is an essential procedure for understanding low wind power events. The key objective of the process is to use the more readily available wind speed data and to transform such data into power output. Scale and scope are key factors in conceptualizing such a model. This importance arises from the rapidly increasing reliance of GB's and Europe's electricity systems on renewable energy, which has led to a substantial body of research focused on modelling the integration of renewable energy into the electricity system. As a result, the granularity and scope of the modelling approaches taken by these studies are highly varied.

On one end of the spectrum, many studies can be characterised as those that place great focus on the dynamics of an electricity system that is reliant on renewable energy [2–4]. As wind energy is merely one of the inputs of such studies, its modelling often takes the form of a conversion from wind speed to power output using a simple manufacturer's turbine power curve, while greater emphasis is placed on electricity system modelling. On the other end of the spectrum, several studies concentrate on modelling the effects of turbine wakes and farm-scale resistance and their impacts on farm power output [5–7]. In such studies, the methods used are highly physics-based but are often sophisticated, computationally expensive, and data-intensive and so, can only be applied to a limited number of wind farms. Between these ends of the spectrum are studies focused on wind power generation on a national scale [8–11]. As a result, the power output modelling approaches adopted in these studies involve methods that are elaborate but not overly granular so as to lead to inefficiencies when applied to a large number of wind farms.

In this study, given that the focus is placed on wind energy supply from the GB wind farms fleet and associated extreme events, the approach adopted here is more closely aligned with that of the latter body of research. The procedure in the majority of these studies can be summarised as follows. First, although some studies often regard modelled wind speed, especially reanalyses, as the ground truth, numerous studies apply bias correction to the input wind speed data as an initial step [12, 13]. Second, for those studies that use

wind speed at low altitudes, the extrapolation of wind speed to an altitude representative of wind turbine hub height is required. In most studies, this process is often carried out by the conventional logarithmic wind profile or the power law [11]. Last, wind speed at hub height is then converted to power output. Similarly, most of these studies often use simple manufacturer's turbine power curves for this conversion [14]. Recently, however, greater accuracy has been achieved by calibrating the power curve or tailoring the power curve to a distinct wind speed condition. Furthermore, in studies where the electricity system is concerned, it is simplistically represented by a demand-net-wind time series, i.e., the level of electricity demand net of wind energy or, in other words, the level of electricity demand not met by wind power generation [9].

Therefore, the objectives of the study outlined in this chapter are: first, to develop a model that takes reanalysis wind speed as an input and returns GB-aggregated wind power output, and second, to model the relationship of GB wind power with electricity demand as a representation of the electricity system. Given that previously the importance of these processes has often been overlooked, the insights derived from each process discussed in this chapter can provide valuable contributions to future models.

3.2 GB-aggregated power output model

The GB-aggregated power output model used in this study can be summarised as follows. First, for a given wind farm, ERA5 10-m wind speed was interpolated to its location. Second, the interpolated wind speed was bias-corrected as per the information obtained in Chapter 2. Third, the corrected wind speed was extrapolated to hub height using a machine-learning-based technique. Lastly, the hub height wind speed was converted to power output using a farm-representative power curve. This process was then repeated for all wind farms in the dataset, and power outputs from all wind farms were aggregated to obtain the GB-aggregated power output, which could then be converted to capacity factor. Although 100-m wind speed data is available as an ERA5 variable, the decision was made to base the model on 10-m wind speed data. This decision was made because the evaluation of ERA5 and bias identification in Chapter 2 was conducted at this altitude due

to the significantly greater availability of observed wind speed data at 10 m. Consequently, using ERA5 10-m wind speed data allows a more thorough and robust understanding of the associated uncertainties.

3.2.1 Bias correction

Several bias correction techniques have been developed in climatology, mostly for precipitation and temperature data, as part of climate change impact studies in recent decades [15–17]. Although these techniques are transferable among climate variables, it is only in the past few years that the bias correction of simulated wind speed has gathered the attention of the climate science community [12, 17]. The central principle of bias correction is to identify systematic errors present in simulated data and use such information to develop a transfer function that accurately adjusts the statistics of the biased data to align more closely with those of the reference data.

The Mean-Variance Scaling technique combines the adjustments for both the mean and variance of the modeled wind speed time series to align it with the reference data. First, the mean difference between the modeled and reference time series is corrected by removing the mean wind speed of the modeled time series in the calibration period, $\mu_{m,c}$, and adding the mean wind speed of the reference time series in the calibration period, $\mu_{r,c}$. Additionally, the variance is adjusted by scaling the modeled time series using the ratio of the standard deviation of the reference time series, $\sigma_{r,c}$, to that of the modeled time series, $\sigma_{m,c}$. The resulting corrected time series in the test period, $u^*_{m,t}$, is expressed as:

$$u^*_{m,t}(t) = [u_{m,t}(t) - \mu_{m,c}] \cdot \frac{\sigma_{r,c}}{\sigma_{m,c}} + \mu_{r,c}. \tag{3.1}$$

While these techniques involve simple adjustments of the time series' first two moments of statistics, Quantile Mapping and CDF Transform are another school of bias correction methods which adjusts the probability distribution of the modelled time series. Quantile Mapping [18] involves using the quantile-quantile relation to match the modelled time series' distribution in the calibration period $F_{m,c}(u)$ to that of the reference time series

$F_{r,c}(u)$, thus resulting in a transfer function that is employed in the test period:

$$u^*_{m,t}(t) = F^{-1}_{r,c}[F_{m,c}(u_{m,t}(t))], \tag{3.2}$$

One disadvantage of Quantile Mapping is that it only takes into account the cumulative distributions in the calibration period and therefore, values outside this range in the test period will not be incorporated. The CDF Transform overcomes this by also including the cumulative distribution function of the modelled time series in the test period $F_{m,t}(u)$ into the transfer function to yield the corrected CDF $F^*_{m,t}(u)$ as:

$$F^*_{m,t}(u_{m,t}) = F_{r,c}\left[F^{-1}_{m,c}\left(F_{m,t}(u_{m,t}(t))\right)\right], \tag{3.3}$$

before performing Quantile Mapping on $F^*_{m,t}(u_{m,t})$ to obtain $u^*_{m,t}(t)$.

These bias correction methods were evaluated in the temporal domain at five randomly selected observation sites. The 10-year data from 2010 to 2019 was split into an eight-year calibration period, where the transfer function was inferred, and a test period, where the inferred transfer function was applied to the two-year-long test data. The results from a validation site, which are representative of other locations and presented in Figure 3.1, demonstrate that all bias correction methods significantly increase wind speed prediction accuracy. Most noticeably, the mean error was reduced from 1.58 m/s to within -0.02 to 0.03 m/s, and the RMSE was reduced from 2.3 m/s to below 1.6 m/s for all methods. The equally significant decrease in the Weibull scale and shape factor errors also points to an increased agreement between the observed and ERA5 probability distributions, as confirmed visually by the probability density function (PDF) and cumulative density function (CDF) plots. Toward the lower tails of the PDF and CDF plots in Figure 3.1, all bias correction methods exhibit noticeable improvement in capturing low wind speeds compared to uncorrected ERA5 data. However, slight differences remain: the lowest wind speeds are overestimated by QM and CDF-t and are underestimated by mean-variance-corrected data. These trends vary from location to location but the overall improvement in agreement across the entire distribution leads to a subsequent improvement in ERA5's ability to estimate the frequency of low wind speeds, where the absolute error is now below

2.4%. Hence, it can be concluded that in the temporal domain, all bias correction methods significantly improve ERA5's performance and are approximately equally effective.

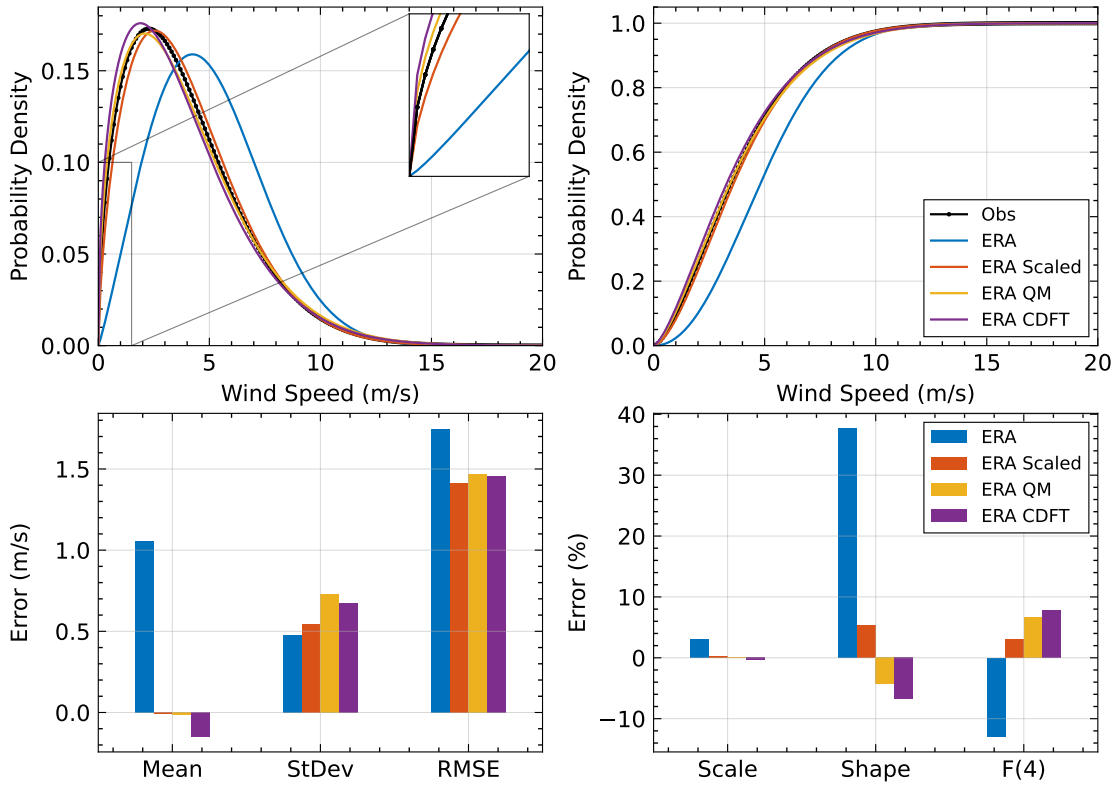


Figure 3.1: Validation of bias correction techniques performed at validation site located at 51.57,0.73 (Top left) Fitted Weibull probability distributions of observed, ERA5, and bias-corrected wind speed. (Top right) Fitted Weibull cumulative probability distributions of observed, ERA5, and bias-corrected wind speed. (Bottom) Error metrics comparison of ERA5 and bias-corrected wind speed time series.

Mean-variance scaling was selected as the preferred method for bias correction due to its straightforward implementation and its ability to avoid overfitting to historical distributions. This makes it a reliable choice in scenarios where future changes in variability or distributional shifts are anticipated. Additionally, since this study focuses on low wind speed events, an empirical investigation revealed that removing the mean wind speed bias effectively eliminates the $F(4)$ error. This relationship arises because, for the observed range of wind speed distributions in this dataset, the Gamma function is approximately flat. Consequently, the scale parameter of the Weibull distribution, which is strongly tied to the mean, primarily determines the wind speed distribution. Thus, correcting the mean directly leads to a corrected distribution. And although a widely known drawback of mean-

variance scaling is the possibility negative wind speeds, it was found that for this study's dataset, there were very few occurrences of negative corrected wind speeds and so, these were hard-truncated to 0 with minimal implications.

Following the evaluation of ERA5, 10-m wind carried out in Chapter 2, the values of bias reported were used to obtain the bias-corrected wind speed $u^*_{ERA}(t)$ from the uncorrected ERA wind speed $u_{ERA}(t)$, as summarised by:

$$u^*_{ERA}(t) = [u_{ERA}(t) - \overline{u}_{ERA}] \cdot \frac{\sigma_e}{\sigma_{ERA}} + \mu_e. \tag{3.4}$$

where $\overline{u}_{ERA}$ and σ_{ERA} are the mean and standard deviation of the uncorrected wind speed respectively, and μ_e and σ_e are the target mean and standard deviation of wind speed as informed by the bias identification process respectively.

3.2.2 Extrapolation of wind speed to hub height

Although the logarithmic wind profile has been extensively used in studies on wind power and meteorology to extrapolate wind speed to wind turbines' hub height, several studies have highlighted its limitations and inaccuracies. First, as pointed out by Optis et al. [19], the logarithmic profile tends to become increasingly inaccurate with increasing height and stratification stability as turbulent fluxes decrease in magnitude, causing decoupling from near-surface wind and is, therefore, less representative of hub height. Second, Dawkins and Rushby [9] noted that the logarithmic law is not appropriate for the study of extreme wind speeds, as it is not well-suited for lower wind speeds, which are the focus of this study. Third, extrapolating from 10 m to hub height using the log or power law is problematic because it oversimplifies complex, non-local, and location-dependent impacts of land use change on wind profiles, leading to overestimation of hub height winds and masking critical dynamical changes [20].

Recently, methods based on machine learning have emerged as a promising approach to vertically extrapolate wind speed, attracting a growing body of research. For example, Bodini and Optis [21] showed that a simple Random Forest Regression model, trained on four observation sites in Chicago, significantly outperformed both the power law and the

log-law when validated against a site 100 km away. Similarly, in a study more focused on low wind speed events, Dawkins and Rushby [9] also opted for a machine-learning-based vertical extrapolation of wind speed, using the Generalised Additive Model on ERA5 reanalysis and found good agreement between actual and modelled extrapolated wind speed.

In this study, a *Multi-layer Perceptron Regression* (MLPR) model, a feed-forward subset of the Deep Neural Network algorithm, was used to vertically extrapolate 10-m wind speed to 100 m at each wind farm. Multi-layer Perceptron Regression comprises neurons that act as logistic units, summing up weighted input signals and passing the resultant signal through an activation function [22]. These neurons are arranged into a network that always consists of an input layer representing the input features, followed by a variable number of hidden layers of neurons, before concluding at an output layer where the desired signal format is returned.

The model's inputs are all available within the ERA5 model and ERA5 grid points in the UK domain at regular spatial intervals and hourly time steps. Features included can be classified into three categories: physical, geographical, and temporal. The selection of physical features was largely influenced by Monin-Obukhov's similarity theory so that the model reflects the physical processes associated with the vertical profile of wind speed. These features include 10-m wind speed, 10-m wind direction, friction velocity, 2-m temperature, surface roughness, and boundary layer height. Geographical features include distance to the coast and elevation. Lastly, temporal features include the time of day and day of the year to capture the seasonal and diurnal variations. The target variable is ERA5 100-m wind speed and therefore, the model comprises ten inputs and one output. A summary of these features and their correlations (Pearson R) is presented in Figure 3.2.

Note that the MLPR model was trained on uncorrected ERA5 10-m wind speed data and validated on uncorrected ERA5 100-m wind speed data. This approach was designed to capture the underlying physical relationship between wind speeds at these heights without introducing bias from corrections. Once this relationship was established, it was applied to bias-corrected 10-m wind speed data to produce corresponding 100-m wind speed estimates, ensuring the extrapolation remains consistent with the corrected inputs. The training

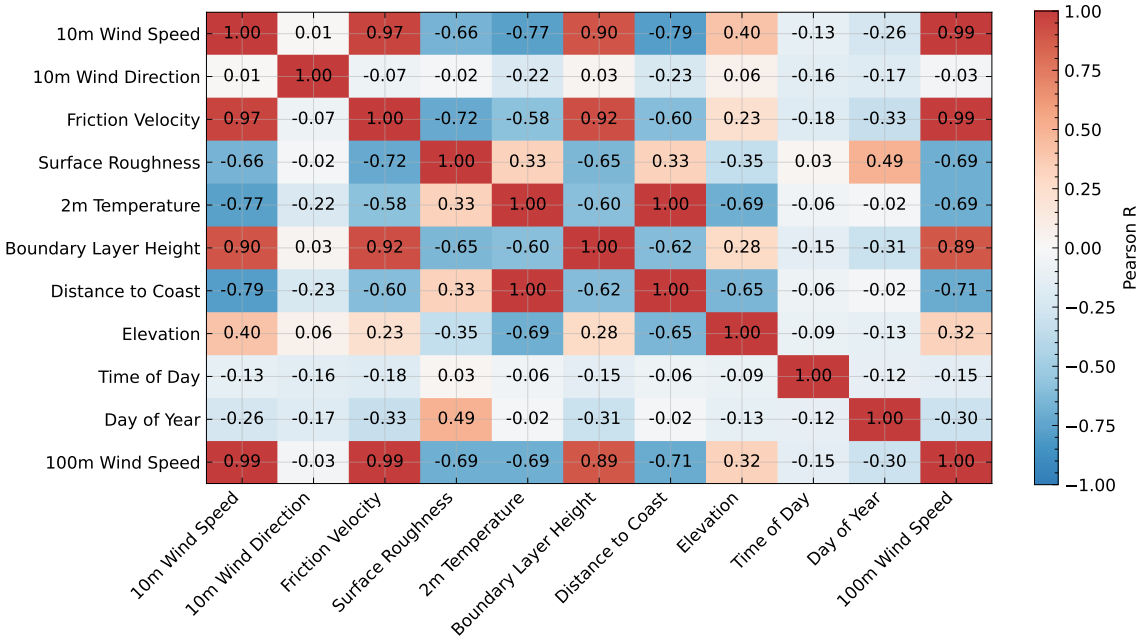


Figure 3.2: Matrix of Pearson R correlation between each feature used in training the model as well as the target variable.

occurs on one out of every 16 ERA5 grid points, sampled from randomly selected years, representing approximately 14 million data points. The trained neural network model was validated against ERA5 100 m wind speed data drawn from 169 random grid points that were not included in the training of the model, sampled from a randomly selected two-year period not included in the training, thus representing 25% of the training set size. The results presented in Figure 3.3 show MLPR's superiority in performance over a simple logarithmic profile. First, the mean RMSE of these test locations was reduced significantly from 0.91 m/s to 0.49 m/s when log-law extrapolation was replaced by the neural network approach. While the averages of mean error, standard deviation error, scale parameter error, and shape parameter error do not differ significantly, the ranges of these errors are much smaller under the neural network approach. For example, the ranges of mean error and standard deviation error were reduced from 1.29 m/s to 0.72 m/s and from 0.85 m/s to 0.28 m/s, respectively. Furthermore, mean Pearson R values also increased moderately when MLPR was used to extrapolate wind speed to 100 m.

Permutation Variable Importance and Dropped Variable Importance metrics were used to quantify the contribution of each variable to the predictive performance of the model. Permutation Variable Importance assesses the drop in performance when a variable's val-

ues are randomly shuffled, while Dropped Variable Importance measures the performance change when a variable is completely removed and the model retrained. Both metrics consistently highlight the physical features, particularly friction velocity and surface roughness, as the most important inputs to the model. Elevation, while less critical than physical features, was found to be significantly more important than other geographical features. Temporal features, in contrast, were shown to have minimal importance, reinforcing the dominance of physical inputs over time dependence in the vertical extrapolation of wind speed.

It should be noted that although the approach adopted here aims to capture the underlying physical relationship between wind speeds at 10 m and 100 m by leveraging the flexibility of MLPR to model non-linear dependencies and interactions reflective of atmospheric stability and boundary layer dynamics, one limitation is that 10-m and 100-m ERA5 wind speeds were obtained separately using distinct methodologies. Specifically, 10-m wind speeds are derived from near-surface parameterisations that incorporate observational data from the lowest model level in conjunction with Monin-Obukhov's similarity theory, while 100-m wind speeds are model-derived outputs based on atmospheric dynamics computed and interpolated between corresponding vertical levels [23]. This methodological disparity, therefore, poses a challenge when modelling the relationship between 10-m and 100-m wind speeds, as the variables being modelled are inherently derived using different processes that may not capture the same physical dependencies.

3.2.3 Wind farm power curve modelling

The ideal power curve of a wind turbine is produced by manufacturers based on empirical data and provides a simple means to convert wind speed to a turbine's power output. However, ideal power curves assume perfect wind availability and are established with respect to a single wind turbine at a single moment. There are several issues with this assumption. First, wind turbines are subjected to wear and tear, as noted by Staffell and Green [24], where turbine performance declines with age. Second, power production at cut-in and cut-off wind speeds is not necessarily as exact as ideal power curves portray. Non-zero power outputs below cut-in speed have been observed due to shutdown occurring at speeds below

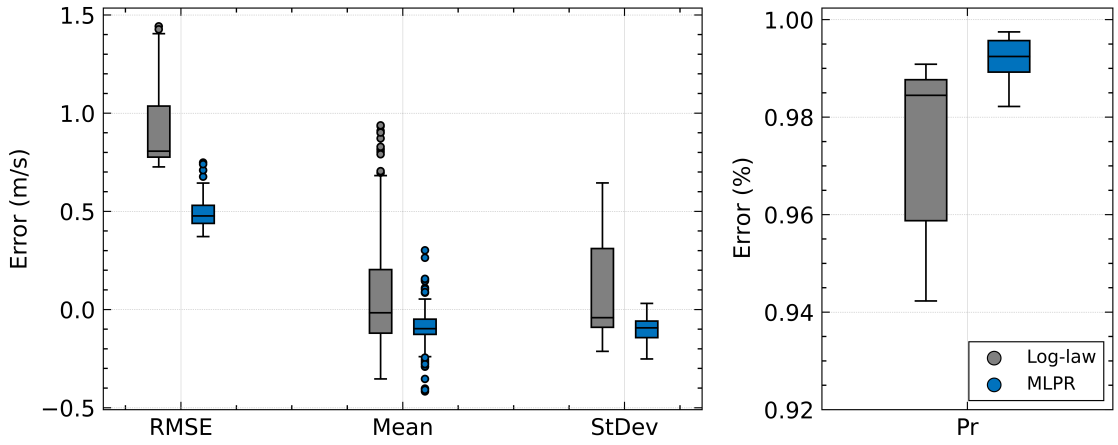


Figure 3.3: Comparison of error metrics (RMSE, mean bias, and standard deviation) and Pearson R (Pr) between the Log-law and MLPR methods. Each box plot is based on 169 randomly selected ERA5 test grid boxes.

the cut-in wind speed as well as for speeds above the cut-off limit due to the hysteresis effect [25]. Moreover, other physical factors also influence turbine performance, such as wind conditions and air density [26]. Hence, on a turbine level, the actual turbine power curve may differ significantly from the ideal power curve. However, the more important issue is that an ideal power curve only represents one turbine, whereas the scope of this study requires that power production is considered at a farm level. An ideal, single-turbine power curve cannot capture farm-scale effects, the most important of which are the spatial variation of wind speed and wake effects, both on a turbine and farm level. Hence, in this study, a *wind farm power curve model* was developed to model the relationship between wind speed and power output at a farm level, as opposed to employing a manufacturer's power curve. The process of constructing such a power curve can be summarised as follows.

First, following the approach taken by Bloomfield et al. [13], each wind farm was assigned one of the following three representative manufacturer's turbine power curves as per their International Electrotechnical Commission (IEC) classification, which is based on the farm's mean wind speed: Siemens SWT-3.6-107 (Class I), General Electric GE 1.5SL (Class II), and ENO Energy 100 2.2 MW (Class III). Note that this is a classification system published by the IEC [27], which captures the variation of the shape of power curves with the wind speed at which they are designed to operate and hence, provides greater specificity to the model.

Second, graphical data of the representative manufacturer's power curve were used to formulate a five-parameter logistic (5PL) curve, as given by:

$$P_{5PL} = f(u, \theta) = D + \frac{A - D}{(1 + (u/C)^B)^G}, \tag{3.5}$$

where A is the upper asymptote, D the lower asymptote, C the inflection point, B the slope at inflection point, and G the asymmetry factor. This provides a parametric, continuous transfer function for determining power output P_{5PL} from wind speed u. The use of the 5PL curve to represent the shape of the manufacturer's curve is based on findings that such a function demonstrates good accuracy in estimating power output from a turbine when validated against measured power output data [28]. Note that due to limited data availability near the cut-off speed, this section was fitted by inspection, as is commonly practised in parametric power curve modelling [29].

The third process aims to simulate losses at a wind farm level and calibrate the 5PL curve accordingly. A large body of research is dedicated to modelling wind farm power curves that take these losses into consideration [30–32]. However, these approaches are often computationally intensive, sophisticated, and require data specific to each farm. For a large-scale study such as this one, such granularity is not appropriate and may be unnecessary. Therefore, studies where wind farm power output is needed from several individual wind farms rely on the application of an empirical calibration to the aggregated power output [8, 33]. The approach taken by this study seeks a compromise between the two extremes by developing a wind farm power curve model whose shape is calibrated according to the expected losses as a function of wind farm size and domain.

Due to the scarcity of power output data from wind farms, only two low-capacity wind farms, namely Penmanshiel and Kelmarsh wind farms [34], were used to inform this process. For each wind farm, a 5PL curve was first fitted to the power output of the wind farm with respect to farm-averaged wind speed and compared to the manufacturer-curve-fitted 5PL curve. This process provides information on how the parameters of a 5PL curve for each wind farm vary from the manufacturer curve with farm energetic output. Next, this variation of the farm power curve was extrapolated to yield a continuous range of power curve shapes as a function of expected energetic output reduction, which is subsequently a

function of wind farm size, i.e., the number of turbines at a wind farm. Lastly, wind farm energetic availabilities obtained from Cevasco et al. [35] of 99.2% and 88.1% were applied to onshore and offshore wind farms, respectively, to take farm downtime into consideration.

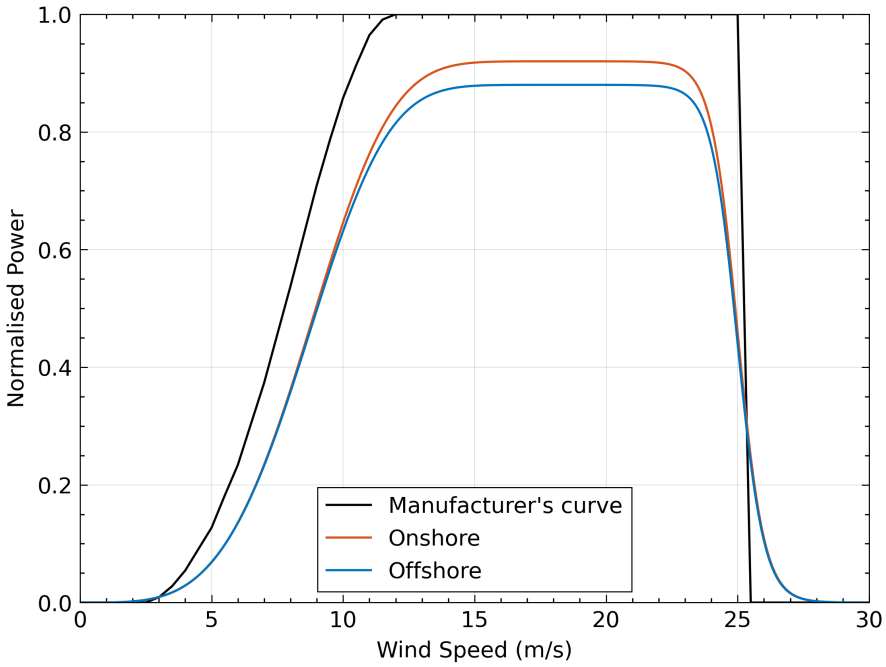


Figure 3.4: Effective normalised power curves for onshore and offshore farms compared against the original manufacturer's curve for a class-III wind farm.

The resultant Class III power curves for both onshore and offshore are compared to the original manufacturer's power curve and presented in Figure 3.4 as an example. Two features of such curves are of interest. First, it is evident that the inflection points of both curves are significantly shifted to higher wind speeds. This shift is due to the empirical calibration that takes wake effects into account. While such a change is substantial, measured power output from the wind farm datasets shows that this behaviour of a wind farm power curve can be expected. Second, it can be observed that the normalised rated powers of both curves are not equal to 1. This discrepancy is due to the energetic availability factors applied to the curve as a constant. Note that while the normalised rated power of the offshore curve is lower than that of the onshore curve, it does not necessarily mean that the resultant power is lower for the offshore domain than onshore.

3.2.4 Validation

The GB-aggregated CF model comprises three major procedures, namely the bias-correction of ERA5 wind speed, the vertical extrapolation of wind speed by MLPR, and the conversion to power output by a wind farm power curve. Each of these steps represents an improvement to what is considered the *baseline* scenario where a standard approach is taken i.e., using uncorrected ERA5 wind speed data, vertical extrapolation of wind speed by a logarithmic profile, and conversion to power output by a manufacturer's power curve. An evaluation was carried on the resultant power output in terms of hourly capacity factor at the end of each process against scaled actual wind power generation data from National Grid [36] (2010-2021) and the incremental changes in error metrics with respect to the implementation of each major component of the GB-aggregated CF model are presented in Table 3.1. It is evident that the approach taken in this study for each major process resulted in an incremental reduction in error. The most significant improvement of the model stems from the application of the wind farm power curve model. However, it also means that the resultant CF time series is highly sensitive to this process. All in all, compared to the baseline condition, the approach taken by this study to model the GB-aggregated CF time series resulted in an increase in accuracy by over 60%.

	RMSE	**MAE**	**Bias**	**Pr**
Baseline	0.201	0.169	0.168	0.916
+ **Bias correction**	0.191	0.155	0.152	0.917
+ **MLPR**	0.167	0.131	0.125	0.923
+ **Farm power curve**	0.092	0.065	0.025	0.923

Table 3.1: Validation of the modelled GB-aggregated CF against CF based on measured power output from National Grid [36]. Each row corresponds to the addition of each step of the model as opposed to the baseline case i.e., bias correction against no bias correction, MPLR against log-law, and a wind farm power curve against a manufacturer's power curve.

Density scatter plots of the baseline model CF and the final model CF against actual CF are also presented in Figure 3.5. Although a high level of RMSE still remains, the agreement between the final model CF and the actual CF is a significant improvement over the baseline model. This improvement is also observed for CF in the lower range, which is of particular importance for this study. The error metrics of the final model CF

also exhibit seasonality, as shown in Table 3.2. While the correlations in autumn and winter fall within the range observed in summer and spring, the former seasons exhibit 10–20% higher RMSE and MAE compared to the latter. These observations are consistent with the evaluation results in Chapter 2 where errors are higher during winter and autumn months. Furthermore, frequency-duration curves obtained by applying runs analysis on the CF time series for a number of different thresholds, as per [8], are presented in Figure 3.6. For all CF thresholds, it can be observed that the agreement between the final model's curve and the actual curve is strong, implying an accurate representation of low wind power events.

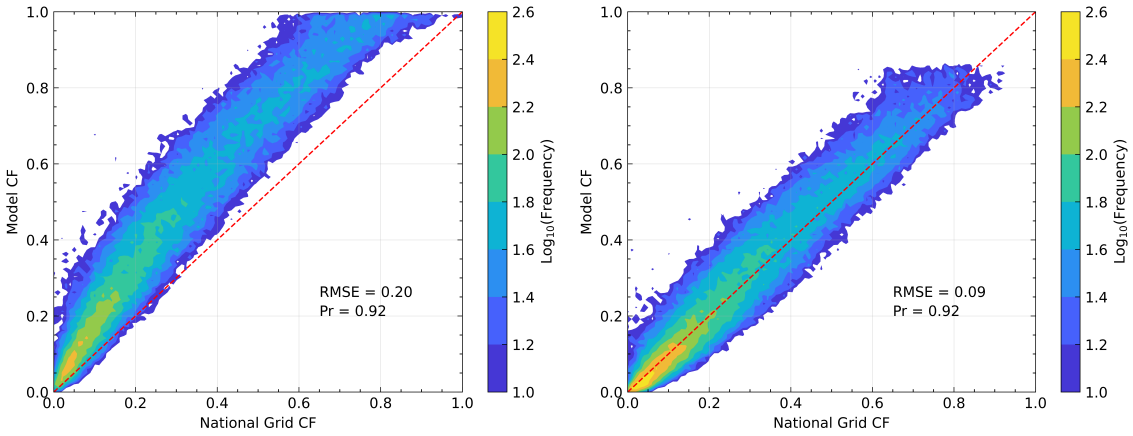


Figure 3.5: Validation of the modelled GB-aggregated CF against CF based on measured power output from Elexon [36] for the baseline model (left) and the final model (right).

	RMSE	MAE	Bias	Pr
Spring	0.084	0.060	0.009	0.925
Summer	0.084	0.059	0.029	0.901
Autumn	0.098	0.069	0.037	0.913
Winter	0.101	0.072	0.020	0.915

Table 3.2: Validation of the modelled GB-aggregated CF against CF based on measured power output from National Grid [36] for each season.

3.3 Electricity demand model

Electricity demand data is required to formulate a demand-net-wind (DNW) time series, which is used to identify extreme energy system stress events in this study. But as previ-

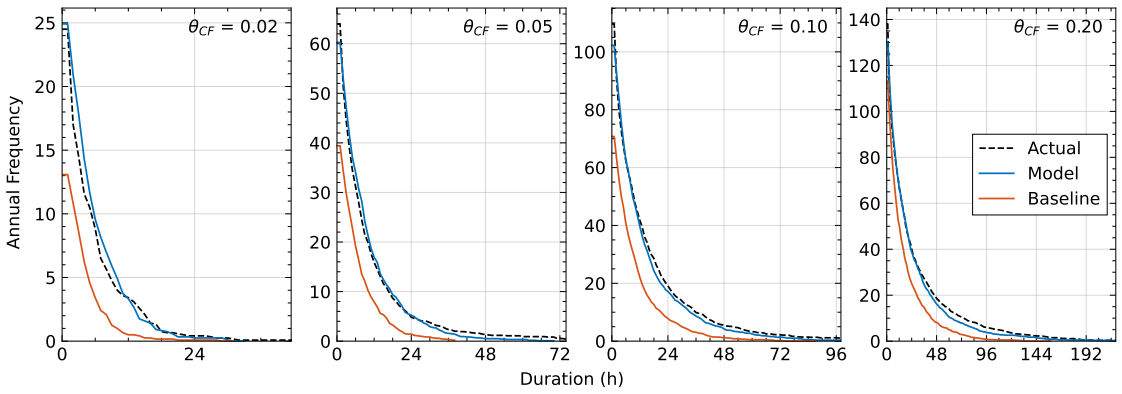


Figure 3.6: Low wind speed events were identified using a simple runs analysis at various capacity factor thresholds (θ_{CF}). The figure illustrates frequency-duration curves for these events, comparing the baseline model, the final model, and actual generation data.

ously mentioned, the limited temporal coverage of electricity demand data is not sufficient to obtain an adequate sample size of extreme events. However, it is well established that in GB, near-surface temperature is the most influential meteorological variable affecting electricity demand [13, 37, 38]. Therefore, given that near-surface temperature is available from ERA5, which has much higher temporal coverage than electricity data, electricity demand data was modelled from the reanalysis dataset instead.

The approach taken in this study is based on Bloomfield et al.'s [13] weather-dependent multiple linear regression model, which relates electricity demand to temporal variables and climate variables that are provided by ERA5. Although the original model was developed at a daily time step, the multiple linear regression model in this study was constructed on an hourly time step and is given by:

$$D(t) = \alpha_0 + \alpha_1 t + \alpha_2 HDH(t) + \alpha_3 CDH(t) + \sum_{i=4}^{10} \alpha_i \cdot dayofweek(i,t) + \sum_{j=11}^{34} \alpha_j \cdot hourofday(j,t) + \sum_{k=35}^{38} \alpha_k \cdot season(k,t). \tag{3.6}$$

In this model, $D(t)$ refers to electricity demand at an hourly time step t. α_i's are the coefficients of regression where $\alpha_0 + \alpha_1 t$ represent the background trend of electricity demand to allow the gradual change over time due to socio-techno-economical factors. α_4 to α_{10}, α_{11} to α_{34}, and α_{35} to α_{38}, correspond to the functions $dayofweek(i,t)$, $hourofday(j,t)$, and $season(k,t)$ respectively, each of which is equal to 1 if time step t corresponds to a

temporal characterisation of type i, j or k, and is equal to 0 otherwise. The remaining terms α_2 and α_3, represent the dependence of demand on weather with $HDH(t)$ (heating degree hours) and $CDH(t)$ (cooling degree hours) respectively. These two functions take the form:

$$HDH(t) = max[15.5°C - T(t), 0], \tag{3.7}$$

$$CDH(t) = max[T(t) - 22.0°C, 0]. \tag{3.8}$$

where $T(t)$ is hourly temperature at 2 m. In this study, HDH and CDH were obtained by spatially averaging the 2-m temperature and subsequently calculating their values. This approach was compared against another approach where HDH and CDH time series were obtained separately on ERA5 individual ERA5 grid boxes. Then, at each time step, the HDH and CDH values from all grid boxes were then aggregated into national HDH and CDH values by summing their population-weighted values. However, minimal differences in performance between the two approaches were observed and hence, the first approach was employed in this study.

The described multiple linear regression model was trained on ERA5 2-m temperature data against observed electricity demand data from National Grid [36] from 2010-2018 and validated from 2019-2021. The regression coefficients and the validation results are presented in Figures 3.8 and 3.7 respectively. First, it can be seen in Figure 3.8 that the regression coefficients expectedly represent the variation of demand with each of the three temporal functions, where demand is higher during weekdays, daytime, and winter and autumn. It should also be noted that α_1 is relatively small but non-zero, as it reflects the gradual long-term trend of electricity demand. Furthermore, as evidenced from the scatter-plot, the general agreement between modelled and actual electricity demand is adequate, while the Pearson R and RMSE values of 0.93 and 2.76 GW are within the ranges of those found by Bloomfield et al. [13]. However, it should be noted that the underestimation of demand in the upper range represents a significant limitation of the model.

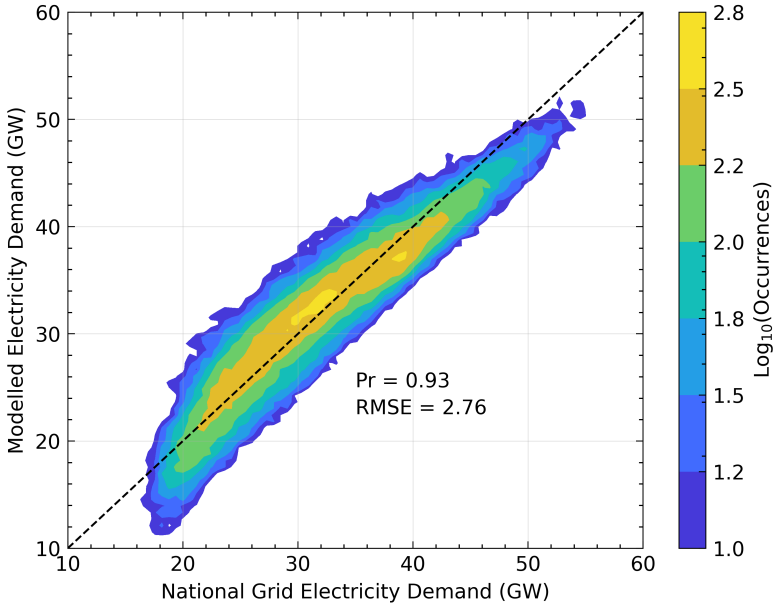


Figure 3.7: Modelled electricity demand plotted against measured electricity demand from National Grid [36]

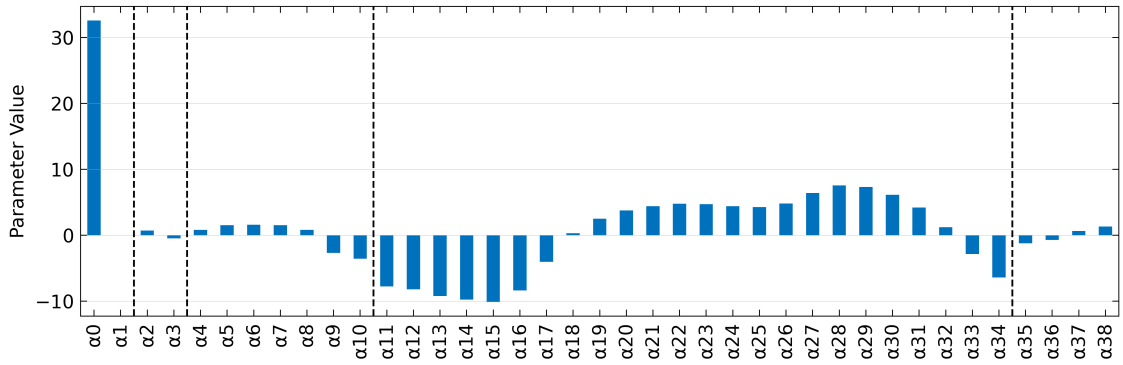


Figure 3.8: Regression coefficients of the weather-dependent multiple linear regression model. α_0 - α_1 correspond to the long-term trend of demand, α_2 - α_3 correspond to the weather-sensitivity of demand, α_4 - α_{10} correspond to Monday to Sunday, α_{11} - α_{34} correspond to 0000 - 2300 hours, and α_{35} - α_{38} correspond to spring (MAM), summer (JJA), autumn (SON), and winter (DJF) respectively.

3.4 Conclusions

This chapter outlines the modelling of Great Britain's wind power output and electricity demand based on climate variables, encompassing four main procedures: bias correction, extrapolation of wind speed to hub height, conversion to power output, and electricity demand modelling. The investigation of each procedure yields valuable insights, contributing

to a comprehensive understanding of the overall process. First, mean-variance scaling was found to be a computationally inexpensive bias correction method that also achieved a comparable level of effectiveness as distribution-based methods. Second, although the logarithmic wind profile has been extensively used for the vertical extrapolation of wind speed, an MLPR-based method has been shown to offer significant improvements. Third, an empirical calibration of the manufacturer's curve to obtain wind power output at a farm level has been shown to offer greater flexibility in modelling nationally aggregated wind power output, achieving high accuracy in the process. Fourth, an hourly weather-dependent electricity demand model was shown to achieve an accuracy comparable to a daily model.

Each of these processes represents an improvement to power output modelling methods that are conventionally used in studies of equivalent scope and scale. As a result, a validation of the resultant GB-aggregated power output has shown that the model was able to achieve a high level of agreement with measured national power output data in terms of the time series and, more crucially, with respect to the representation of low wind power events.

References

[1] P. Potisomporn, T. A. A. Adcock, and C. R. Vogel. Extreme value analysis of wind droughts in Great Britain. *Renewable Energy*, 221:119847, 2024.

[2] D. Raynaud, B. Hingray, B. François, and J. D. Creutin. Energy droughts from variable renewable energy sources in European climates. *Renewable Energy*, 125:578–589, 2018.

[3] F. Kaspar, M. Borsche, U. Pfeifroth, J. Trentmann, J. Drücke, and P. Becker. A climatological assessment of balancing effects and shortfall risks of photovoltaics and wind energy in Germany and Europe. *Advances in Science and Research*, 16:119–128, 2019.

[4] O. Ruhnau and S. Qvist. Storage requirements in a 100% renewable electricity system: Extreme events and inter-annual variability. *Environmental Research Letters*, 17(4): 044018, 2022.

[5] R. J. Barthelmie, S. C. Pryor, S. T. Frandsen, K. S. Hansen, J. Schepers, K. Rados, W. Schlez, A. Neubert, L. Jensen, and S. Neckelmann. Quantifying the impact of wind turbine wakes on power output at offshore wind farms. *Journal of Atmospheric and Oceanic Technology*, 27(8):1302–1317, 2010.

[6] A. Kirby, F.-X. Briol, T. D. Dunstan, and T. Nishino. Data-driven modelling of turbine wake interactions and flow resistance in large wind farms. *Wind Energy*, 26 (9):968–984, 2023.

[7] A. Niayifar and F. Porté-Agel. Analytical modeling of wind farms: A new approach for power prediction. *Energies*, 9(9), 2016.

[8] D. J. Cannon, D. J. Brayshaw, J. Methven, P. J. Coker, and D. Lenaghan. Using reanalysis data to quantify extreme wind power generation statistics: A 33 year case study in Great Britain. *Renewable Energy*, 75:767–778, 2015.

[9] L. Dawkins and I. Rushby. Characterising adverse weather for the UK electricity system, including addendum for surplus generation events, 2020. URL `www.metoffice.gov.uk`.

[10] P. Potisomporn and C. R. Vogel. Spatial and temporal variability characteristics of offshore wind energy in the United Kingdom. *Wind Energy*, 25(3):537–552, 2022.

[11] N. Ohlendorf and W.-P. Schill. Frequency and duration of low-wind-power events in Germany. *Environmental Research Letters*, 15(8):084045, 2020.

[12] I. Staffell and S. Pfenninger. Using bias-corrected reanalysis to simulate current and future wind power output. *Energy*, 114:1224–1239, 11 2016.

[13] H. C. Bloomfield, D. J. Brayshaw, and A. J. Charlton-Perez. Characterizing the winter meteorological drivers of the European electricity system using targeted circulation types. *Meteorological Applications*, 27(1):e1858, 2020.

[14] B. Kruyt, M. Lehning, and A. Kahl. Potential contributions of wind power to a stable and highly renewable Swiss power supply. *Applied Energy*, 192:1–11, 2017.

[15] J. Chen, F. P. Brissette, D. Chaumont, and M. Braun. Finding appropriate bias correction methods in downscaling precipitation for hydrologic impact studies over North America. *Water Resources Research*, 49:4187–4205, 2013.

[16] A. Dosio, P. Paruolo, and R. Rojas. Bias correction of the ENSEMBLES high resolution climate change projections for use by impact models: Analysis of the climate change signal. *Journal of Geophysical Research: Atmospheres*, 117, 2012.

[17] C. Teutschbein and J. Seibert. Bias correction of regional climate model simulations for hydrological climate-change impact studies: Review and evaluation of different methods. *Journal of Hydrology*, 456-457:12–29, 2012.

[18] R. Haas, J. G. Pinto, and K. Born. Can Dynamically Downscaled Windstorm Footprints Be Improved by Observations Through a Probabilistic Approach? 119, 2014.

[19] M. Optis, N. Bodini, M. Debnath, and P. Doubrawa. New methods to improve the vertical extrapolation of near-surface offshore wind speeds. *Wind Energy Science*, 6: 935–948, 6 2021.

[20] J. Wohland, P. Hoffmann, D. C. Lima, M. Breil, O. Asselin, and D. Rechid. Extrapolation is not enough: impacts of extreme land use change on wind profiles and wind energy according to regional climate models. *Earth System Dynamics*, 15(6): 1385–1400, 2024.

[21] N. Bodini and M. Optis. How accurate is a machine learning-based wind speed extrapolation under a round-robin approach? volume 1618. IOP Publishing Ltd, 9 2020.

[22] Y. S. Turkan, H. Y. Aydoğmuş, and H. Erdal. The prediction of the wind speed at different heights by machine learning methods. *An International Journal of Optimization and Control: Theories & Applications (IJOCTA)*, 6:179–187, 2016.

[23] J. Ramon, L. Lledó, V. Torralba, A. Soret, and F. J. Doblas-Reyes. What global reanalysis best represents near-surface winds? *Quarterly Journal of the Royal Meteorological Society*, 145(724):3236–3251, 2019.

[24] I. Staffell and R. Green. How does wind farm performance decline with age? *Renewable Energy*, 66:775–786, 2014.

[25] T. Üstüntaş and A. D. Şahin. Wind turbine power curve estimation based on Cluster Center Fuzzy Logic Modeling. *Journal of Wind Engineering and Industrial Aerodynamics*, 96:611–620, 2008.

[26] V. Sohoni, S. C. Gupta, and R. K. Nema. A critical review on wind turbine power curve modelling techniques and their applications in wind based energy systems. *Journal of Energy*, 2016:1–18, 2016.

[27] I. E. Commission et al. Wind turbines-part 1: design requirements. *IEC 61400-1-Ed. 3.0*, 2005.

[28] M. Lydia, S. S. Kumar, A. I. Selvakumar, and G. E. P. Kumar. A comprehensive review on wind turbine power curve modeling techniques. 30:452–460, 2014.

[29] OFGEM. Electricity capacity assessment report 2013. Technical report, 2013.

[30] S. Tao, Q. Xu, A. Feijóo, S. Kuenzel, and N. Bokde. Integrated wind farm power curve and power curve distribution function considering the wake effect and terrain gradient. *Energies*, 12(13):2482, 2019.

[31] B. P. Hayes, I.-S. Ilie, A. Porpodas, S. Z. Djokic, and G. Chicco. Equivalent power curve model of a wind farm based on field measurement data. In *2011 IEEE Trondheim PowerTech*, pages 1–7. IEEE, 2011.

[32] M. Vahidzadeh and C. D. Markfort. Modified power curves for prediction of power output of wind farms. *Energies*, 12(9):1805, 2019.

[33] D. R. Drew, D. J. Cannon, D. J. Brayshaw, J. F. Barlow, and P. J. Coker. The impact of future offshore wind farms on wind power generation in Great Britain. *Resources*, 4(1):155–171, 2015.

[34] C. Plumley. Kelmarsh and Penmanshiel Wind Farm Data (0.0.2), 2022. URL `https://data.niaid.nih.gov/resources?id=zenodo_5841833`.

[35] D. Cevasco, S. Koukoura, and A. Kolios. Reliability, availability, maintainability data review for the identification of trends in offshore wind energy applications. *Renewable and Sustainable Energy Reviews*, 136, 2021.

[36] Elexon. Elexon generation data. URL `https://www.elexonportal.co.uk/`.

[37] H. E. Thornton, A. A. Scaife, B. J. Hoskins, and D. J. Brayshaw. The relationship between wind power, electricity demand and winter weather patterns in Great Britain. *Environmental Research Letters*, 12:064017, 6 2017.

[38] J. W. Taylor and R. Buizza. Using weather ensemble predictions in electricity demand forecasting. *International Journal of Forecasting*, 19(1):57–70, 2003.

Statement of Authorship

Publication details	
Title of paper	Extreme value analysis of wind droughts in Great Britain - Supplementary information
Publication status	Published
Publication reference	P. Potisomporn, T. A. A. Adcock, and C. R. Vogel. Extreme value analysis of wind droughts in Great Britain - Supplementary information. Renewable Energy, 221:119847, 2024

Student confirmation	
Student name	Panit Potisomporn
Contribution	The analysis and text were primarily developed and written by PP, with the input of co-authors. All sections were written by PP and edited by TAAA and CRV.

Student signature: _____ **Date**: _____

Supervisor confirmation	
Supervisor name	Dr. Christopher Vogel
Comments	I confirm that Panit has made a substantial contribution to the publication, and that the description above in the Statement of Authorship is accurate.

Supervisor signature: _____ **Date**: _____

CHAPTER 4

Extreme value analysis of low wind power events in Great Britain

This chapter presents a frequency analysis and an extreme value analysis of low wind power events in GB. The article has been accepted and published Renewable Energy *journal on 15th December 2023 [1].*

Due to the growing proportion of wind energy in Great Britain's energy mix, prolonged periods of low wind power generation have become one of the biggest challenges in fully de-carbonising the electricity system. As such, the characterisation of their frequency and risk is of vital importance to the reliability of the electricity system. Employing concepts derived from hydrology, an extreme value analysis was carried out on low wind power events in Great Britain based on 72 years of ERA5 reanalysis data. The application of pooling procedures was found to be beneficial in identifying low wind power events whose capacity factor is not constantly below a threshold, while also being effective in ensuring the independence of such events. The Pearson-III distribution was identified as a suitable model to represent extreme low wind power events, while the Lognormal and Generalised Pareto distributions are also viable alternatives. Sustained periods of low wind power generation with a duration of 14 days were estimated to have a return period of five years and the longest event on record of approximately 26 days is expected to occur once every 100 years. The investigation of these low wind power events from a hydrological perspective has thus shown that prolonged periods of wind power generation that significantly impact the electricity system may not be such rare occurrences. A significant increase in energy storage capacity is, therefore, required to adequately address these low wind power events and minimise their impacts.

4.1 Introduction

In March 2021, Great Britain (GB) experienced one of the longest cold calm spells in over a decade; the national wind farm fleet operated at 11% of its rated capacity for 11 consecutive days during a period where low temperatures drove up heating and electricity demand [2]. In response, dispatchable fossil-fuelled generation was increased to compensate for the reduction in wind power generation. Although such low wind power events, which stem from extensive high-pressure systems [3], are uncommon, they are regarded as one of the biggest challenges in fully decarbonising the GB electricity system. Therefore, as the proportion of wind energy in the GB energy mix increases, so does the need to characterise the risk of low wind power events and their implications for the future and resilience of the GB electricity system.

Defining the low wind power event period is an important first step in characterising drought frequency and duration. Fig. 4.1 illustrates a time series of capacity factor CF, with events indicated in colour as periods below the CF threshold, θ_{CF}. One approach is to define a low wind power event as a period where the instantaneous power output is continuously below a specified threshold [4, 5]. Alternatively, low wind power events can be defined in terms of being below a specified threshold of the moving average of the wind energy time series, which can result in the identification of longer drought periods [6]. However, this approach is highly reliant on the choice of the averaging interval and may also introduce dependency between low wind power events.

As illustrated in Fig. 4.1, both approaches can be sensitive to the choice of wind speed or power threshold, in particular for small values, which may affect statistical descriptions of low wind power event likelihood and severity. While both methods identify event 1 as a single event, a short period γ_3 where $CF > \theta_{CF}$ separates events 2 and 3. Whether these are usefully characterised as separate events or as part of one longer event depends on the objectives of the analysis. Periods where instantaneous generation is below a threshold may be useful to characterise individually when dispatchable generation is used to compensate for low wind power, whereas grouping nearby events to calculate overall wind power deficits may be more appropriate when describing the need for energy storage technologies.

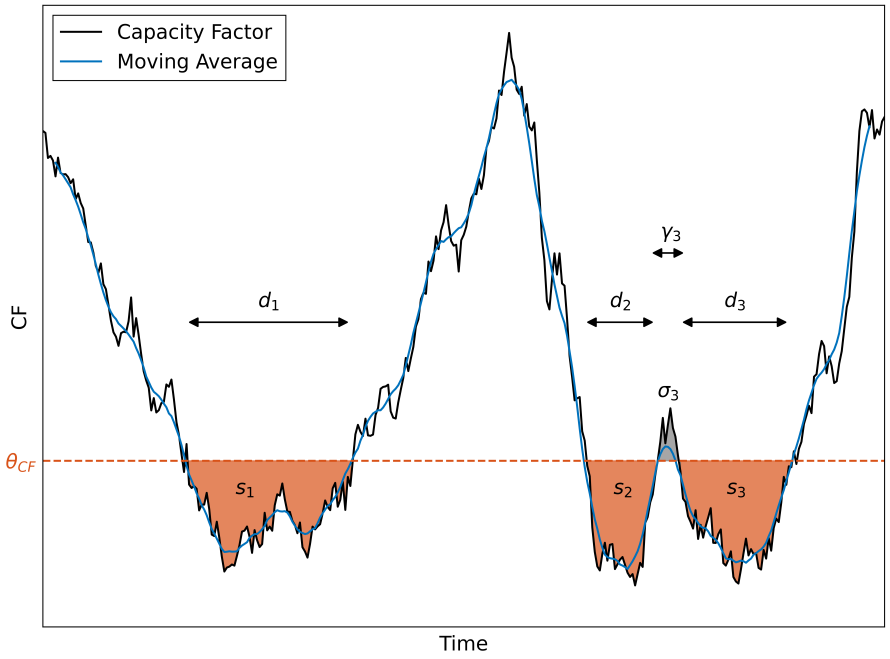


Figure 4.1: Illustrations of low wind power events (coloured in orange), as defined by the threshold level and their event characteristics: duration d_i, severity s_i, excess time γ_i, and excess severity σ_i.

Hydrology offers valuable insights for event characterisation. Analogous to low wind power events, hydrological droughts are prolonged periods of low streamflows that may have significant impacts on water supply. The analogy further extends in that streamflow and wind resource time series are both zero-limited, non-normally-distributed, and at particular time scales, non-stationary [7, 8]. By leveraging these conceptual and statistical similarities, several well-researched tools and techniques, which have been applied in a multitude of hydrological droughts studies, can be employed in the investigation of low wind power events.

Statistical descriptions of rare drought events have been made using extreme value analysis, a well-developed statistical methodology that focuses on modelling probabilities associated with rare events that display a substantial deviation from the median of a population [9]. Extreme values are extracted from the sample data, modelled with a distribution, and the return period is calculated from the distribution. An advantage of associating the sampled data with an extreme value distribution is that it allows inferences to be drawn extending beyond those observed in the sampled events themselves. This

process has been applied to the investigation of hydrological droughts; see e.g., Zelenhasić and Salvai [10], Tallaksen et al. [11], and Shiau [12]. Hydrological extreme value analyses are often complemented with other hydrology-based techniques. For example, runs analysis [13] is commonly used to identify periods of droughts from a streamflow time series and pooling procedures [11, 14, 15] are regularly employed to address the issues of minor and mutually dependent drought events [16].

Extreme value analyses have been conducted on low wind power events in the North Sea and Ireland by Patlakas et al. [17] and Leahy and McKeogh [18] respectively, who similarly found low wind speed events lasting over four days to have a return period of around ten years. To incorporate electricity demand and the influence of climate change into the analysis, Dawkins and Rushby [19] conducted an extreme value analysis on historical, simulated, and projected electricity demand net of wind generation (demand-net-wind) time series and found that periods of low wind power generation during peak demand with a duration of eleven days in winter are estimated to have a return period of ten years.

This study focuses on how the robustness of low wind power event analysis can be improved. Pooling procedures to group related low wind power event periods are compared with reference to the derived event severity and duration statistics. Fitted theoretical distributions are used for extreme value analysis in order to allow extrapolation of results to longer return periods than can be achieved empirically from observations alone. These are used to conduct a case study on the frequency and risk of low wind power events in GB.

4.2 Data sources and processing

In this study, an extreme value analysis of low wind power events was carried out on the simulated GB-aggregated capacity factor time series based on wind speed data from the European Centre for Medium-Range Weather Forecasts' Reanalysis-5 (ERA5) data for 1950-2022, assuming the 2022 distribution and capacity of wind farms in Great Britain. The steps to derive the aggregated CF series are summarised below, as per Chapter 3.

4.2.1 Reanalysis data description and evaluation

Released in 2019, ERA5 [20] is the latest generation reanalysis model produced by ECMWF using a four-dimensional variational (4D-VAR) assimilation scheme. With a spatial resolution of 0.25° latitude-longitude (approximately 27.5 km) and a maximum temporal resolution of 1-hourly time steps, ERA5 offers the highest spatiotemporal resolution out of all global reanalyses. Furthermore, ERA5's extension back to 1940 means it also provides one of the longest temporal coverages relative to other global reanalyses of comparable spatiotemporal resolution. This is of particular importance within the context of this study as the rarity of extreme low wind power events necessitates a long dataset that captures inter-decadal variability in wind speeds. For example, the average wind speed in GB during 1960-1980 was significantly lower than that in the following two decades [21].

Potisomporn et al. [22] evaluated ERA5 10 m wind speed against in-situ surface wind speed measurements from 205 onshore and offshore observation stations around GB from the period 1997-2021. It was found that ERA5 10 m wind speed exhibits biases in mean wind speed of 0.166 m/s and -0.136 m/s for the onshore and offshore domains respectively, while also underestimating wind speed standard deviation by over 0.35 m/s. The study also reported that the frequency of short-duration low wind speed events (defined as periods where the wind speed is below a typical wind turbine cut-in speed, 4 m/s, for less than 12 hours) is significantly underestimated in ERA5. This was attributed to ERA5 not adequately capturing hourly wind variability arising from small-scale atmospheric fluctuations, hence its inability to capture small, frequent drops in wind speed that give rise to short-duration events. However, longer low wind speed events, which are the focus of the present study, were found to be more accurately represented by ERA5 and corroborated by Cannon et al. [4] for the Modern-Era Retrospective analysis for Research and Applications 2 dataset.

In this study, ERA5 wind speed data were bias-corrected through mean-variance scaling using the bias levels reported by Potisomporn et al. [22], taking into account ERA5's inherent limitations in capturing short-duration low wind speed events.

4.2.2 GB wind farms and spatial interpolation

GB wind farms in this study are based on the 2022 distribution of wind farms, assumed to be constant throughout the study period. The distribution was sourced from National Grid's Transmission Entry Capacity register [23], National Grid's Embedded register [24], and Elexon [25]. Together, these datasets comprise 222 onshore and offshore non-embedded wind farms (metered and connected to the transmission network), as well as embedded wind farms (unmetered and directly connected to the distribution network), which represent 86% of installed wind power capacity in GB, and are illustrated in Figure 4.2. The gridded ERA5 10 m wind speed was bi-linearly interpolated to the location of each wind farm.

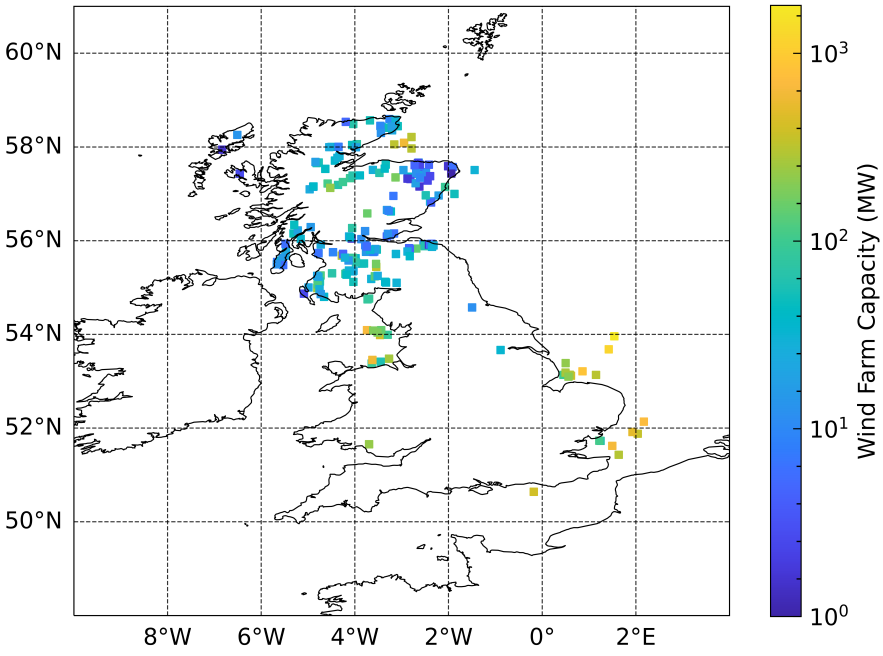


Figure 4.2: 2022 wind farm distribution and installed capacity in Great Britain based on National Grid and Elexon datasets [23–25].

4.2.3 Extrapolation of wind speed to hub height

Due to the widely-recognised limitations of the conventional logarithmic wind profile at low wind speeds [19, 26], in this study a Multi-layer Perceptron Regression (MLPR) model was used to vertically extrapolate 10 m wind speed data to 100 m at each wind farm. The model was designed to use meteorological variables relevant to Monin-Obukhov's similarity

theory that are available in ERA5 as input features, such as boundary layer height and friction velocity, as well as geographical and temporal features. The MLPR model was trained on 364 regularly sampled ERA5 grid points within the study domain and two randomly selected years, at hourly time steps, representing a training set of over 14 million data points. It should be acknowledged that 100 m is not the actual hub-height for most wind turbines; current onshore hub-heights are closer to 70 m, while offshore hub-heights are approximately 90 m [27]. However, the wind profile ensures that wind speeds at these heights are acceptably similar, making 100 m a commonly adopted reference height for hub-height wind speed analysis.

4.2.4 Power output modelling

Power curves provided by turbine manufacturers are a simple means to convert wind speed to power output. However, they do not capture the complexities of the relationship between wind speed and farm power output which is influenced by factors at a turbine level (e.g., hysteresis effects, decline in turbine performance with age) and at a farm level (e.g., wake effects, maintenance, spatial variability). Hence, a farm power curve model was developed and employed in this study to take these effects into account. The farm power curve was derived from representative turbine power curves using a five-parameter logistic function, which has been found to show substantial accuracy in estimating power output from a turbine [28]. Farm-level effects, namely wake losses and farm availability, were then estimated from measured wind farm power output data [29]. Finally, wind farm energetic availabilities obtained from Cevasco et al. [30] were applied to the power curve.

4.2.5 GB-aggregated CF and validation

The GB-aggregated and capacity-weighted CF was calculated for all $N = 222$ wind farms through:

$$CF(t) = \frac{1}{C} \sum_{i}^{N} cf_i(t) c_i, \tag{4.1}$$

where $C = \sum_i c_i$ is the total installed capacity of GB wind farms, cf_i the capacity factor of a single farm, and c_i the farm's installed capacity. The resultant GB-aggregated CF

was then validated against CF calculated from wind power generation data from National Grid [25], and is presented in Figure 4.3. While the CF RMSE value of 0.09 is not insignificant, the two time series are highly correlated and visually display reasonable agreement. Moreover, a sensitivity analysis conducted with respect to the distribution of wind farms (not presented) showed that the CF time series is very weakly sensitive to modest changes to the wind farm distribution, thereby providing greater confidence in using the resultant time series.

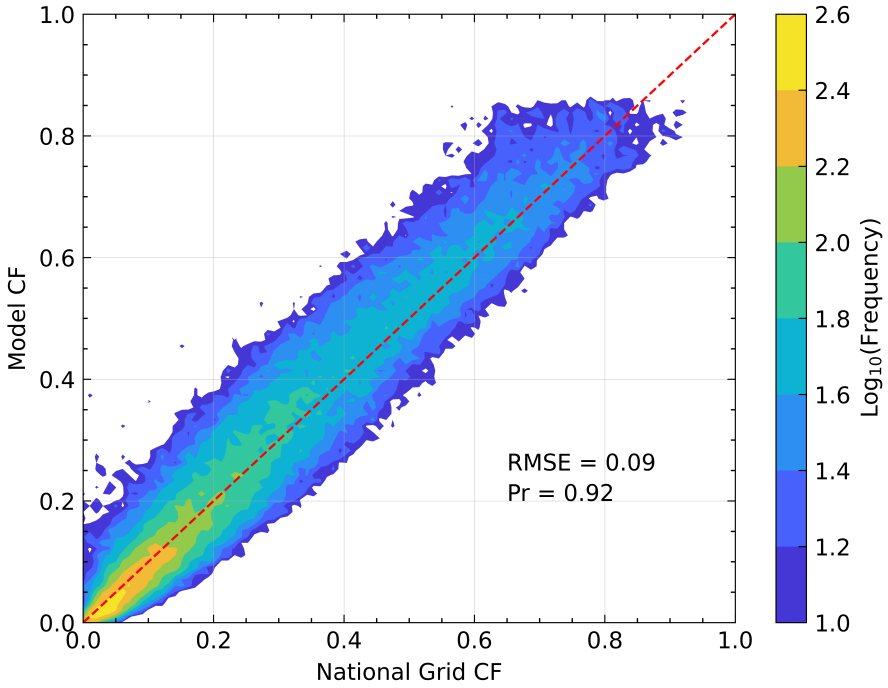


Figure 4.3: Modelled GB-aggregated capacity factor plotted against recorded capacity factor from National Grid ESO [25].

4.3 Application of pooling procedures to low wind power events

4.3.1 Runs analysis

Runs analysis was applied to identify low wind power events from the GB-aggregated CF time series. Runs analysis originates from the theory of runs [13], initially developed to identify hydrological droughts. The method allows a sequence of events to be identified

from the time series by assigning a value of one to the time steps where the data satisfy a specified threshold. In the present study, this becomes:

$$\delta(t) = \begin{cases} 1, & \text{if } CF(t) \leq \theta_{CF} \\ 0, & \text{if } CF(t) > \theta_{CF} \end{cases}, \tag{4.2}$$

where δ is a binary variable defined by whether the CF at time t is below a CF threshold θ_{CF} [31]. In this study, θ_{CF} values of 0.05, 0.10, and 0.20 were considered. Event characteristics of interest are the event duration d, defined as the length of time δ is consecutively equal to 1, and event severity s, the energy deficit represented by the area between the CF time series and the CF threshold, as shown in Figure 4.1.

4.3.2 Pooling procedures

High time resolution data series tend to identify many minor low wind power events, i.e., events of small duration and severity. The high frequency of these minor events may influence extreme value analysis conducted on the obtained low wind power events series.

A second and more significant issue that can arise is the occurrence of mutually dependent events. These are defined as instances when a low wind power event of long duration and high severity is interrupted by excess periods of relatively small duration and severity, thus dividing the single prolonged event into several events. Figure 4.1 provides an example where events 2 and 3 are separated by an excess period of relatively small duration γ_3 and severity σ_3. In the context of wind power production, such excess periods may occur due to short periods of higher wind speed localised to a limited number of wind farms with a high capacity within a longer period of generally low wind speeds. Mutually dependent events may therefore introduce errors into extreme value analysis by violating the assumption that the analysed events are independent.

Pooling procedures can be used to address the issues of minor and mutually dependent events as systematic processes that are performed alongside runs analysis to determine whether multiple events should be considered as separate events or as a single event. For example, events 2 and 3 in Figure 4.1 may be considered to be mutually dependent and therefore pooled into one event. Therefore, pooling only allows the clustering of relatively

minor events. However, it is important to note that while pooling can provide greater confidence that the resultant event series comprises independent events, it does not fully guarantee such independence. Correlations between low wind power events, which arise from mesoscale weather systems, may still be present. Nonetheless, the application of extreme value analysis on a time series of pooled events is a generally accepted practice, which provides a reasonable approximation [16].

The duration of a pooled event d_{pool} is defined as the sum of the durations of the pooled events including the excess period:

$$d_{pool,i} = d_i + \sum_{j}^{n} (d_j + \gamma_j), \tag{4.3}$$

where d_i is the duration of the primary event i, d_j the duration of the j-th excess event contributing to the pooled event, γ_j the excess period associated with the j-th excess event and, n the total number of excess events included in the pooling process.

The pooled event severity $s_{pool,i}$, is defined as the sum of pooled event severity net of excess severity:

$$s_{pool,i} = s_i + \sum_{j}^{n} (s_j - \sigma_j) \tag{4.4}$$

where s_i is the severity of the primary event i, s_j the severity of the j-th excess event contributing to the pooled event, σ_j the excess severity associated with the j-th excess event, and n the total number of excess events included in the pooling process. Note that this computation reflects the net energy deficit presented to the electricity system.

Three pooling procedures have been applied to the CF time series in this study in order to evaluate event duration and severity: Inter-event Time (IET); Moving Average (MA); and the Sequent Peak Algorithm (SPA) method.

Inter-event time method

The IET method, introduced by Zelenhasić and Salvai [10], considers droughts to be mutually dependent and thus pooled if the time between them is less than or equal to a predefined period γ_t. While the conventional IET method only considers the absolute value of the inter-event time, we adapt the IET method to also consider events to be mu-

tually dependent if the ratio of the excess period to the total duration of the events is less than or equal to a predefined ratio γ_r, i.e. $\gamma_i/(d_i + d_{i+1}) \leq \gamma_r$. This ensures that mutually dependent events are identified proportionately to their duration. For example, while events lasting 8 hours separated by an excess period of 4 hours may be considered as separate events, events lasting 100 hours separated by an excess period of the same duration may be more suitably considered to be parts of the same drought event. As such, IET pooling metrics in this study are defined by both the inter-event time γ_t and the inter-event time ratio γ_r. IET pooling is evaluated iteratively, so events that are initially separate may eventually be pooled together on subsequent passes as an event gets longer.

Moving average method

The MA method [11] involves applying a moving filter with an n-hour interval to average the CF time series. As a result, short excess periods are filtered out and mutually dependent events are pooled. The degree of pooling is controlled by the length of the averaging interval n.

There are two caveats which arise from the smoothing of the CF time series. First, the pooled event may start after the first time step the series is below the threshold and may end before the last time step the series is below the threshold. Second, while it is standard to compute event duration and severity from the modified time series, these will be different than those computed from the original CF time series due to averaging. Thus, here the moving-average-filtered time series was used only to identify the start and end of events, whereas the event characteristics were computed with respect to the original time series.

Sequent peak algorithm

The SPA method [15] is based on the energetic content of the underlying time series, and unlike the previous procedures, does not require user-specified parameters. A deficit time series $w(t)$ is formulated by summing the hourly CF deficit (the difference between θ_{CF} and the CF time series below θ_{CF}) and subtracting the excess CF (the difference between

θ_{CF} and the CF time series above θ_{CF}) until $w(t)$ returns to zero. $w(t)$ cannot be negative:

$$w(t) = \begin{cases} w(t-1) + \theta_{CF} - CF(t), & \text{if } w(t-1) + \theta_{CF} - CF(t) > 0 \\ 0, & \text{if } w(t-1) + \theta_{CF} - CF(t) \leq 0 \end{cases}. \tag{4.5}$$

$w(t)$ is therefore a time series of m uninterrupted periods of deficit. For each period i, the start of the event is defined when $w_i(t) > 0$, and the end of the event is defined as the time step where $w_i(t)$ reaches its maximum. The severity of the event is computed based on the original CF time series per Equation 4.4 by using the time steps obtained from $w_i(t)$. As such, events that are separated by an excess period whose excess energy is not sufficiently high to offset the severity of the events, i.e., $w(t)$ remains above zero, will be considered to be mutually dependent and hence pooled. However, a well-recognised limitation of such an approach is that relatively minor events that follow a major event are not identified because a local peak of $w(t)$ is reached before the minor event occurs. Therefore, a modified SPA pooling procedure is employed in this paper whereby $w(t)$ is set to 0 at the time step that immediately succeeds a local peak in order to detect events that would otherwise be missed.

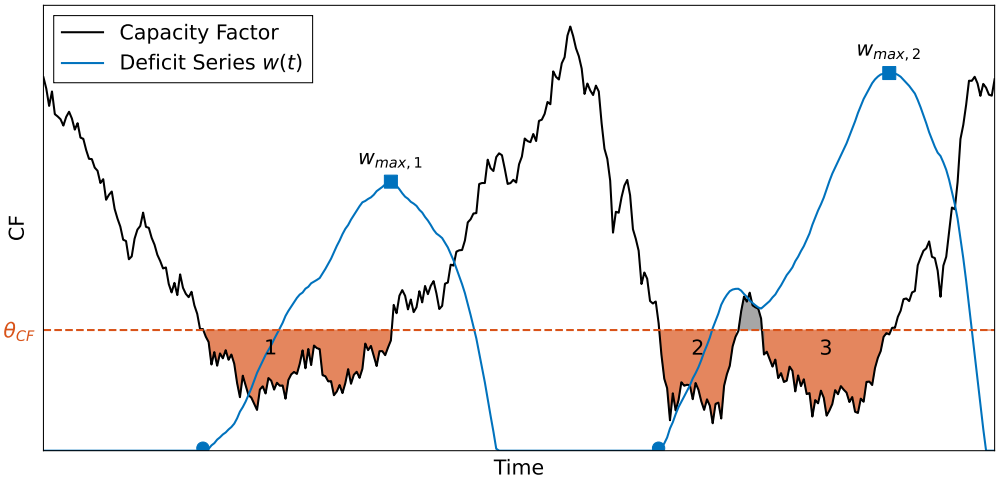


Figure 4.4: Illustration of the deficit series $w(t)$ used in the Sequent Peak Algorithm. Circles mark the starts of events (the first time steps $w(t)$ is locally above 0) and squares mark the ends of events (the local peaks of $w(t)$).

4.3.3 Sensitivity to pooling procedure

Figure 4.5 shows the sensitivity of low wind power event metrics to the parameters of each pooling procedure with a capacity factor threshold $\theta_{CF} = 0.1$. Sensitivity is assessed relative to the annual frequency, duration, and severity, of all identified low wind power events, normalised with respect to the base case where no pooling procedure is applied. As the SPA method is parameterless, its normalised metrics do not change as a function of inter-event threshold or moving-average interval.

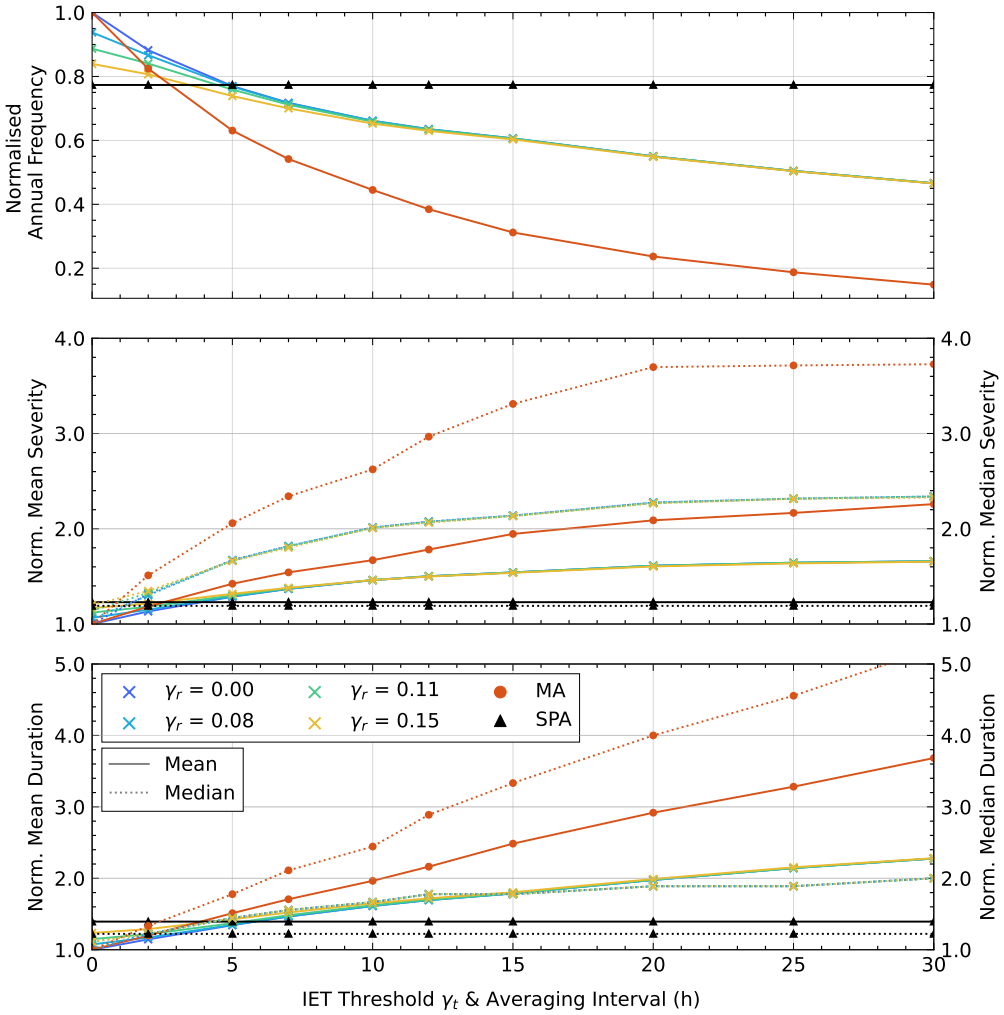


Figure 4.5: Low wind events metrics annual frequency (top), severity (middle), duration (bottom), normalised with respect to no applied pooling procedure, as functions of the inter-event threshold period γ_t (IET) and averaging interval (MA). Inter-event ratios $0 \leq \gamma_r \leq 0.18$ are shown for the modified IET method. The capacity factor threshold $\theta_{CF} = 0.1$. Note that the SPA method is parameterless so its events metrics are constant.

Increasing the MA method averaging interval results in the smoothing of the capacity factor time series which has the effect of eliminating shorter-duration events. Consequently, the normalised annual frequency drops with an increase in averaging interval as fewer events are identified. Similarly, event severity and duration increase as the shorter events are excluded and longer events are pooled together. The rate of increase of mean and median normalised severity reduces with averaging period due to the finite energy deficit of the pooled events (limited by θ_{CF}), whereas duration continues to increase as the averaging interval tends to spread the events out in time.

For the IET method, the normalised event metrics are presented as functions of the time threshold γ_t and the time ratio threshold γ_r. All events are pooled into a single event for values of γ_r exceeding 0.18, providing an upper limit. Similar to the MA method, larger inter-event threshold times γ_t result in more events being pooled together, hence the normalised annual frequency reduces, albeit not as dramatically as the MA method where averaging of the CF time series can remove some shorter events. Similarly, event duration and severity increase with γ_t as more events are pooled together although preserving shorter events means that the mean and median statistics do not change as significantly as for the MA method.

Hence, it is clear that SPA serves as a stable benchmark since it is unaffected by parameter selection. The SPA method produces metrics that are generally consistent with moderate parameter values for the MA and IET methods, especially in terms of annual frequency. In contrast, the MA and IET methods exhibit significant sensitivity to parameter choices, which is a major drawback. For the MA method, small changes in the averaging interval can drastically alter the identified event frequency by smoothing out shorter events, while simultaneously inflating event severity and duration. Similarly, for the IET method, minor adjustments to the inter-event thresholds (γ_t and γ_r) can lead to abrupt changes in event pooling, sometimes grouping independent events and leading to multiple negative severity events. This high sensitivity makes the MA and IET methods less robust and highlights the potential for misrepresentation of low wind power event metrics if parameter values are not carefully calibrated.

4.3.4 Frequency, duration, and severity of low wind power events

To enable cross-comparison between the MA, IET, and SPA methods, intervals have been chosen that balance pooling events together and the minimisation the modification of the underlying time series through averaging [16], as well as the minimisation of negative-severity events. For the MA method, an averaging interval of 12 h was adopted, and for the IET method, $\gamma_t = 12$ h and $\gamma_r = 0.08$ were selected. Annualised frequency-duration and frequency-severity curves for $\theta_{CF} = 0.1$ are presented in Figure 4.6 alongside summary statistics in Table 4.1 to illustrate the differences in the low wind power events identified by the different pooling procedures. The shallower gradients of their frequency-duration and -severity curves with respect to the baseline show that pooling allows longer events to be identified while also filtering out minor events. This is reflected in the decreased annual frequency of events and the increase in mean, median, and maximum duration and severity.

The MA method results in the largest decrease in the annual frequency as low wind power events of less than the averaging period are filtered out, seen as the plateau in the MA frequency-duration curve. There is an associated large increase in mean and median duration and severity as relatively small events are neglected. While the maximum event duration increases from the baseline case, it is not as significant as for the IET or SPA methods.

Compared to the MA method, the IET frequency-duration and -severity curves display a higher frequency of longer duration and more severe events. Consequently, the maximum event duration and severity with the IET method is greater than that identified by the MA method. However, the changes in mean and median event duration and severity from the no-pooling baseline case are smaller than those with the MA method as the IET method also preserves the frequent short duration and low-severity events.

The SPA method demonstrates the greatest increase in the frequency of long and severe low wind power events compared to the no-pooling baseline. While the maximum severity of SPA-identified events is comparable to the other methods, the maximum event duration reaches up to 616 hours, more than a threefold increase compared to the baseline case.

Pooling Procedure	Annual Frequency	Duration (h)			Severity (GWh)		
		Mean	Median	Max	Mean	Median	Max
Base	99.6	15.5	9	187	14.8	5.0	278.5
IET-12h-0.08	63.1	26.4	16	356	22.2	10.5	314.7
MA-12h	38.3	33.5	26	256	26.3	15.0	304.0
SPA	77.0	21.6	11	616	18.2	6.0	314.8

Table 4.1: Low wind power events statistics for IET, MA, and SPA pooling procedures with a capacity factor threshold $\theta_{CF} = 0.1$.

Hence, it is evident that the SPA's distinct approach that considers the CF time series' energetic content leads to the identification of much longer and more severe events.

However, compared to the baseline, the SPA-identified event series demonstrates the smallest decrease in annual frequency as well as the lowest increase in mean and median duration and severity. This is because the SPA method preserves the most minor events out of all three pooling procedures. While the SPA is able to pool many events over a long period, it does not pool minor events that precede a major one, hence more minor events are preserved in the pooled series.

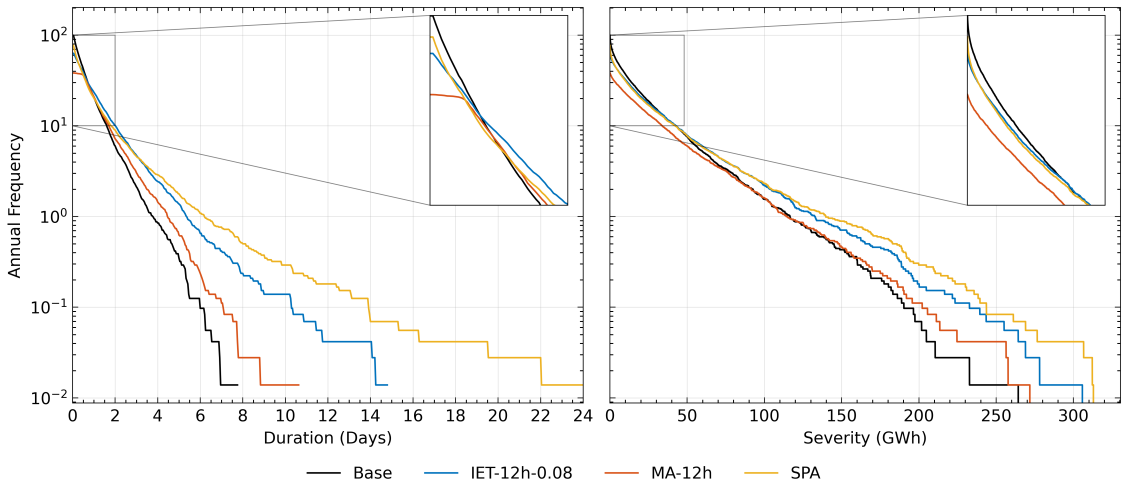


Figure 4.6: Frequency-duration (left) and frequency-severity (right) curves of low wind power events as determined by the IET (blue), MA (red), and SPA (yellow) pooling procedures presented on a logarithmic y-axis. The no-pooling baseline is presented in black. Events are defined with respect to a capacity factor threshold $\theta_{CF} = 0.1$.

4.4 Extreme value analysis: a 72-year case study of low wind power events in Great Britain

4.4.1 Extreme value models

Two commonly used approaches to define extreme values of severity and duration from the event time series were considered: the Annual Maximum Series (AMS) model and the Partial Duration Series (PDS) model. Their differences are summarised below and in Figure 4.7.

In the AMS framework, the event with the highest magnitude within each year is extracted for extreme value analysis. Events spanning multiple years are assigned to the year they begin. While the main advantage of using the AMS model is its simplicity, there are a number of caveats. First, if the chosen θ_{CF} is too low so that there are years without any events, the extreme event sample size may be small, impacting the derived statistics. The CF threshold values used in this study are sufficiently high to avoid such occurrences. Second, extracting the highest magnitude event of each year does not guarantee that the extracted sample contains events with the highest magnitudes from the population, i.e., two events with the highest magnitudes in the population may occur in the same year and hence, the event with the second highest magnitude is omitted from the sample. In this study, the AMS extreme value series contains 72 events.

The PDS model includes low wind power events that exceed a certain truncation level α. The truncation level α is different from the CF threshold θ_{CF} as α is defined with respect to the discrete event duration and severity series, not the CF series. The main advantage of the PDS model is that all events with the highest magnitude are included, providing a more robust definition of the extreme events than the AMS model. However, it is sensitive to the truncation level α. While systematic methods exist to select α, in practice, this process is determined based on subjective judgement and often relies on values adopted by existing studies [16]. In this study, the 0.95 quantile for each event variable was selected as the truncation level.

In this study, both models were used to define the extreme value region for both low

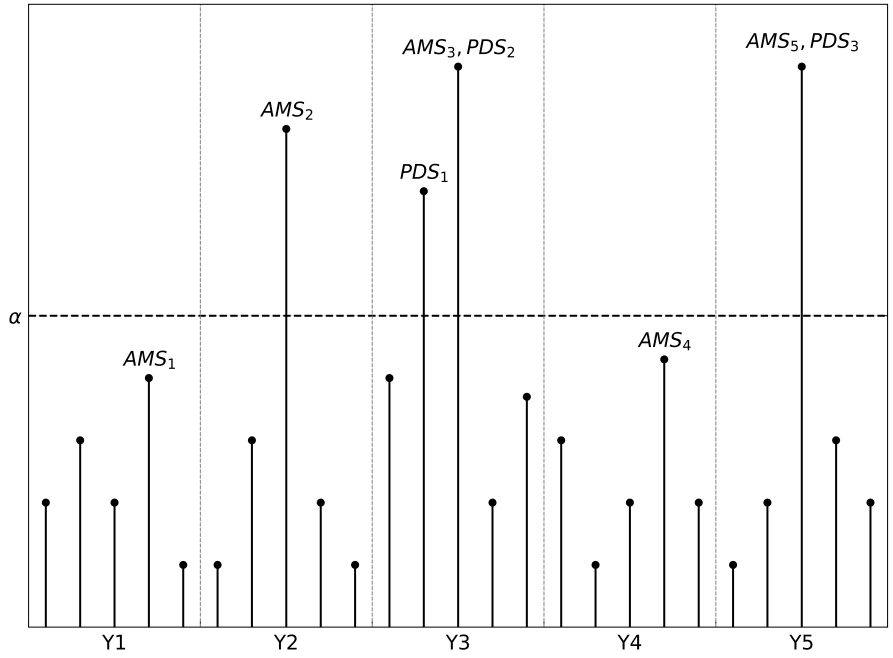


Figure 4.7: An illustration of a hypothetical discrete low wind power series where each stem corresponds to an event of a certain magnitude and grey dashed lines mark the end of each year. Suppose such a series is five years long and contains five events each year. Events with the annually highest magnitude are included in the AMS series, while those whose magnitudes are greater than a truncation level α are included in the PDS.

wind power event duration and severity series, and the results from both models are compared. Hence, for each θ_{CF}, four extreme value series were analysed as per Table 4.2.

	AMS	**PDS**
Duration	AMS Duration (D_{AMS})	PDS Duration (D_{PDS})
Severity	AMS Severity (S_{AMS})	PDS Severity (S_{PDS})

Table 4.2: Extreme value series analysed in this study.

Distribution fitting and evaluation

Theoretical extreme value distributions can provide a means to robustly extrapolate from a limited extreme value sample and describe the sample's statistical properties. Five distributions commonly used to represent extreme hydrological drought events were investigated: Lognormal, Generalised Extreme Value (GEV), Pearson Type III (Pearson-III), Generalised Pareto (Gen. Pareto), and Generalised Logistic (Gen. Logistic) distributions [16, 11]. The GEV distribution conventionally has three parameters, and other distribu-

tions were also considered in their three-parameter form where the third parameter is the location parameter. The distributions were fitted to each of the four extreme value series using maximum likelihood estimation.

The suitability of the distributions was evaluated based on the Cramér-von Mises (CvM) test and Akaike Information Criterion (AIC). The CvM test was chosen due to its approach to evaluating goodness-of-fit across the entire distribution, while the AIC statistic was selected for its effectiveness in assessing the parsimony of different distributions. The distribution which passes the CvM test and achieves the lowest AIC was chosen as the representative theoretical distribution for a given extreme value series. Additionally, an L-moment ratios diagram was used to compare the L-skewness and L-kurtosis to the L-moment ratio loci of each candidate theoretical distribution.

Return periods and confidence intervals

Following Shiau [12], the return period for a univariate extreme value series can be calculated assuming that the events are independently and identically distributed. Defining X to be an independent drought event of magnitude x, L the time period between any two successive events, and T the time period between two successive events with magnitudes greater than or equal to x, i.e., the recurrence interval. The recurrence interval for event $X \geq x$ is then:

$$E[T] = \frac{E[L]}{1 - F(x)}, \tag{4.6}$$

where $E[L]$ is the expected inter-arrival time between successive extreme events and $F(x)$ is the cumulative density function of the drought variable. For the AMS series, since events are sampled annually, $E[L] = 1$, whereas for the PDS series, $E[L]$ is the mean inter-arrival rate in years.

The return period of each extreme value series was calculated according to Eq. 4.6, using the fitted distributions selected as described in Section 4.4.1. Next, the associated uncertainty was obtained using non-parametric bootstrapping. The underlying extreme value series was randomly sampled with replacement so that the bootstrapped sample size matched that of the extreme value series. The selected theoretical distribution was fitted to the bootstrapped sample, and the return period was calculated as per Equation 4.6.

This process was repeated to generate 500 bootstrapped samples and at each x, the 95% confidence interval is presented.

4.4.2 Extreme value distribution evaluation

The SPA method was chosen as the low wind power events pooling procedure due to the favourable performance noted in Section 4.3.3. Hence, D_{AMS}, D_{PDS}, S_{AMS}, and S_{PDS} are modelled on the low wind power events identified by the SPA procedure. Capacity factor thresholds of $\theta_{CF} = (0.05, 0.10, 0.20)$ are investigated.

Figure 4.8 illustrates the loci of L-skewness/L-kurtosis for all candidate distributions as well as for the extreme value series data. The upward curvature of the L-moment ratios reflects the heavy tails of the extreme value distributions. Higher values of θ_{CF} tend to result in heavier-tailed and more asymmetric distributions than lower values of θ_{CF}. Similarly, the PDS data tend to be heavier-tailed and more asymmetric than their AMS counterparts for the same θ_{CF}. This is driven by the greater number of extreme events identified for higher θ_{CF} or with the PDS method.

It is observed in Figure 4.8 that the extreme value series are fairly well modelled by the Pearson-III distribution for lower θ_{CF} values, whereas the Gen. Pareto distribution and lognormal distributions better model the data at higher θ_{CF}. Additionally, the Gen. Pareto distribution models all the PDS series well, consistent with extreme value theory which posits that excess values over a certain threshold are Gen. Pareto distributed. The Gen. Logistic distribution does not appear to model the extreme value series well.

These findings are supported by the CvM test and AIC as presented in Table 4.3. For $\theta_{CF} = 0.05$, the CvM test failed to reject the null hypothesis that the extreme value series are drawn from any of the candidate distributions except for the Gen. Logistic distribution for the D_{PDS} case. The Pearson-III distribution achieved the lowest CvM test statistic as well as the lowest AIC score across all extreme value series. Note that the CvM test statistic measures the discrepancy between the observed data and the fitted distribution, while the presented p-value indicates the probability of rejecting the null hypothesis that the data come from the specified distribution. This further implies that the Pearson-III distribution adequately captures extreme value series for lower values of θ_{CF}, with the

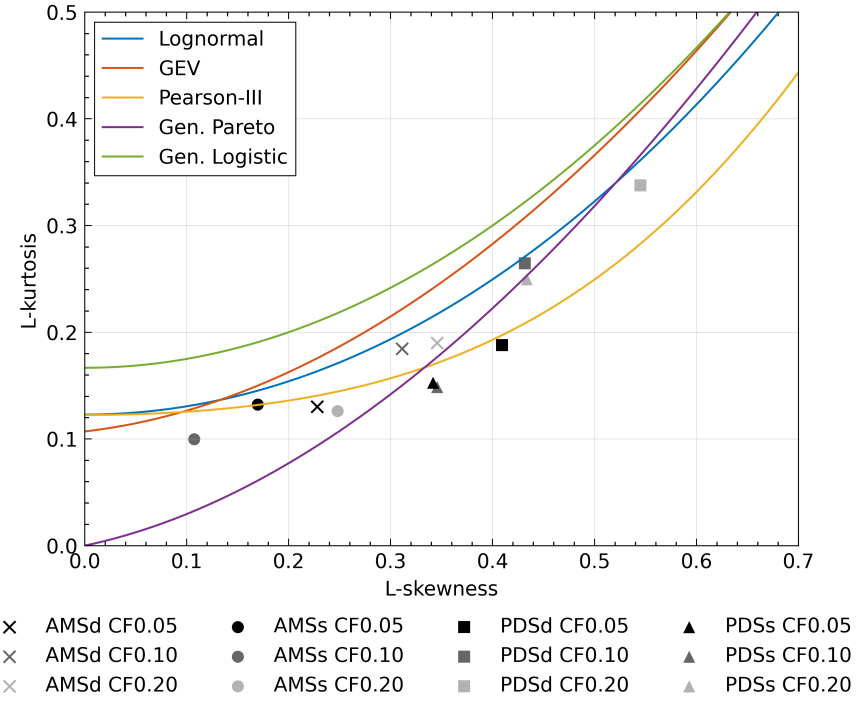


Figure 4.8: L-skewness vs. L-kurtosis of candidate theoretical extreme value distributions compared to the AMS and PDS duration and severity series for three capacity factor thresholds $\theta_{CF} = (0.05, 0.10, 0.20)$.

GEV and Lognormal distributions as suitable alternatives.

For the extreme value series corresponding to $\theta_{CF} = 0.10$, the CvM test and AIC results are less conclusive. While the Pearson-III distribution was chosen for the severity cases S_{AMS} and S_{PDS}, the Lognormal and Gen. Pareto distributions were the most suitable distributions for the duration cases D_{AMS} and D_{PDS} respectively. In most cases, these distributions offer suitable alternatives to each other as well.

For $\theta_{CF} = 0.20$, the Pearson-III distribution remains the best-fit distribution for all series except for D_{PDS}, which is best represented by the Gen. Pareto distribution. The Lognormal and Gen. Pareto distributions are suitable alternatives for the D_{AMS} and S_{PDS} series, while for S_{AMS}, the Gen. Logistic distribution is the second best-fit distribution.

In general, the Pearson-III distribution performs best at modelling most of the extreme value series, with the Lognormal and Gen. Pareto distributions offering adequate alternatives, especially for PDS series for the Gen. Pareto distribution.

$\grave{}_{CF}$	Distribution	D_{AMS} p-value	D_{AMS} AIC	D_{PDS} p-value	D_{PDS} AIC	S_{AMS} p-value	S_{AMS} AIC	S_{PDS} p-value	S_{PDS} AIC
0.05	**Lognormal**	0.814	711.2	0.622	1626.4	0.368	605.7	0.344	1387.8
	GEV	0.708	712.9	0.325	1641.2	0.338	606.5	0.260	1404.2
	Pearson-III	0.947	**709.3**	0.569	**1524.9**	0.444	**604.8**	0.849	**1358.3**
	Gen. Pareto	0.501	710.7	0.437	1632.7	0.112	611.5	0.647	1396.6
	Gen. Logistic	0.638	715.4	0.001	1730.7	0.362	606.9	0.010	1454.1
0.1	**Lognormal**	0.983	**835.0**	0.537	2770.8	0.860	787.9	0.386	2733.8
	GEV	0.920	836.4	0.477	2785.8	0.000	1051.1	0.219	2755.3
	Pearson-III	0.966	835.4	0.244	2796.6	0.869	**787.0**	0.683	**2710.2**
	Gen. Pareto	0.398	839.9	0.675	**2765.2**	0.259	789.9	0.637	2723.4
	Gen. Logistic	0.555	844.9	0.001	2898.9	0.784	788.6	0.002	2829.1
0.2	**Lognormal**	0.942	1081.0	0.864	3674.0	0.000	1273.7	0.676	3767.7
	GEV	0.835	1083.9	0.738	3689.4	0.000	1325.3	0.482	3784.7
	Pearson-III	0.952	**1080.3**	0.002	3661.9	0.752	**1056.7**	0.113	**3745.0**
	Gen. Pareto	0.815	1081.1	0.728	**3672.6**	0.001	1070.5	0.909	3753.7
	Gen. Logistic	0.282	1098.4	0.000	3949.0	0.460	1063.1	0.000	3911.7

Table 4.3: Results from the CvM test and AIC presented for AMS duration (D_{AMS}), PDS duration (D_{PDS}), AMS severity (S_{AMS}), and PDS severity (S_{PDS}) at $\theta_{CF} = (0.05, 0.10, 0.20)$. Low wind power events were pooled using the SPA procedure. The theoretical distribution for each extreme value series whose AIC value is highlighted in bold was selected as the representative distribution.

4.4.3 Return periods and confidence intervals

Using the best-fit theoretical distribution for each $\theta_{CF} = 0.10$ extreme value series, the corresponding return period curves and their 95% confidence intervals, as well as empirically computed return periods are presented in Figure 4.9. The return levels for selected periods for all extreme values series at $\theta_{CF} = (0.05, 0.10, 0.20)$ are summarised in Table 4.4. All curves are concave, reflecting a diminishing probability of more extreme, rarer events. The return period curve shows good agreement with empirically calculated return periods up to a return period of 20 years. The uncertainty around the rarest events is captured by the widening confidence interval, increasing from ±12% for a 5 year return period compared to ±22% at 50 years. This is due to rarity and thus limited sample size of the most extreme events. Nevertheless, the observed return periods are within the 95% confidence intervals at these higher return periods.

Furthermore, the return levels associated with the AMS and the PDS approaches for event severity and duration at a given return period are in reasonable agreement, differing by 15% and 4% respectively. This suggests that both approaches are able to capture the characteristics of extreme events, providing confidence in the reliability and robustness of the estimated return periods and levels. Similarly, by repeating the fitting and bootstrapping processes for other suboptimal distribution and comparing how varying the underlying distributions affects these confidence intervals, it was noted that the AMS estimates show limited sensitivity to the chosen distribution, while the PDS estimates exhibit greater vulnerability to modelling decisions. These findings highlight the importance of carefully evaluating and justifying assumptions within PDS analyses to ensure that the resulting return levels remain robust and reliable.

A low wind power event defined by $\theta_{CF} = 0.10$ lasting approximately 1 week is expected to occur once every 2 years, and once every 10 years for a circa 2-week event. The longest low wind power event in the 72-year record, which began in July 1955, is 616 hours long (approximately 26 days) and has a return period of 100 years. The second and third longest events are observed in 2018 and 2014 respectively. A low wind power event lasting at least 1 week occurs 53 times over the 72-year study period whereas a 1-week period

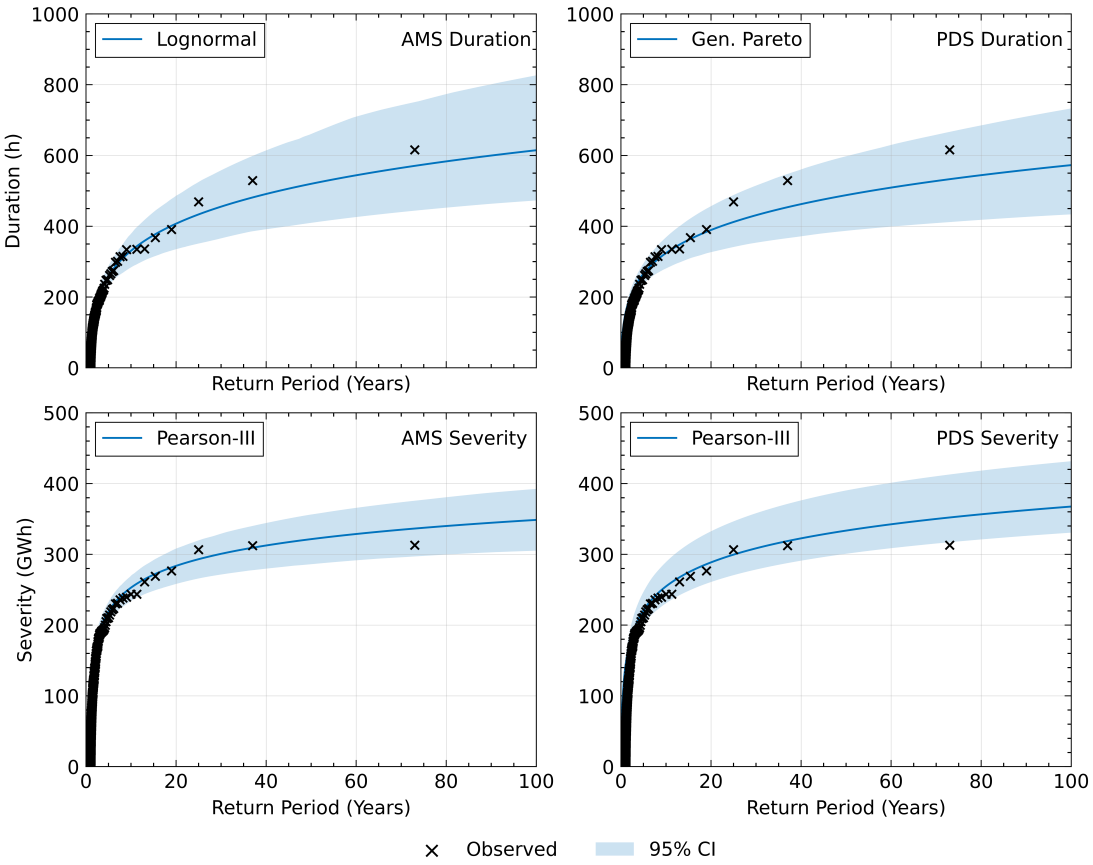


Figure 4.9: Return levels and the 95% confidence interval plotted against return periods calculated from the best-fit theoretical distribution for D_{AMS}, D_{PDS}, S_{AMS}, and S_{PDS} corresponding to $\theta_{CF} = 0.10$. Black crosses show return periods empirically computed from the observed extreme low wind power event series.

where the CF time series never exceeds θ_{CF} occurs only 3 times over the same 72-year period. As the events are identified by the SPA procedure, it is important to note that the return duration does not necessarily indicate that the CF time series never exceeds θ_{CF} during the period, but rather signifies that the energetic content of the CF time series is in deficit with respect to the θ_{CF} throughout the period. In comparison, the longest event identified by the baseline (constantly-below-threshold) approach began in September 1966 and lasted 167 hours (approximately 1 week), with the second and third longest events observed in 1984 and 2010, thus highlighting the inherent differences between SPA-defined and baseline-defined events.

Event severity refers to the energy deficit with respect to constant production at the level of θ_{CF}. For example, relative to $\theta_{CF} = 0.10$ using the S_{AMS} estimates, a low wind

power event with a deficit of 165 GWh is expected to occur once every 2 years, while the most severe event in the 72 year record of 315 GWh is expected to occur slightly under once every 50 years. Similar to event duration, the SPA method identifies some low wind power events with relatively modest severity due to pooling mutually dependent events together and thus also capturing intermediate periods where the instantaneous $CF > \theta_{CF}$, limiting event severity. Within the 72 years of data, an SPA-defined low wind power event corresponding to $\theta_{CF} = 0.10$ of at least 165 GWh occurs 53 times.

4.5 Discussion

4.5.1 Implications for the electricity system

To demonstrate the relationship between the severity of low wind power events and energy storage requirements, a basic energy storage model adapted from Ruhnau and Qvist [32] was employed. In this model, the CF time series of length T is segmented into $n_L = T-L+1$ overlapping windows of length L. Event severity is calculated for each of these windows and the maximum severity $S_{max,L}$ associated with the window length L is recorded. This process is then repeated for incrementally increasing values of L. The model was applied on the GB-aggregated time series with respect to a capacity factor threshold of 0.1 and the results are plotted in Figure 4.10, against the most severe low wind power events at each duration as identified by SPA and the baseline runs analysis case. First, it can be observed more clearly that the relationship between extreme event duration and severity is non-linear i.e., the most severe event is not necessarily the longest. In this case, the peak of the curve, which, by Ruhnau and Qvist's [32] definition, corresponds to the energy storage requirement at 0.1 CF threshold, has a severity of 314.8 GWh. But more importantly, this peak, along with other prominent peaks, are also captured by the SPA method, but not by a simple runs analysis.

This result shows that using pooling procedures to assess low wind power events provides a novel perspective on estimates of the risks of events for the electricity system as well as an understanding on their implications for energy storage. This is because in this framework, prolonged low wind power events are considered not as periods where the *wind*

$\grave{}_{CF}$	E[T] (y)	D_{AMS} (h) Fit	0.025	0.975	D_{PDS} (h) Fit	0.025	0.975	S_{AMS} (GWh) Fit	0.025	0.975	S_{PDS} (GWh) Fit	0.025	0.975
0.05	**2**	79	62	88	89	83	96	39	35	43	44	39	51
	5	116	101	133	127	111	142	55	50	62	56	48	68
	10	142	122	163	167	139	194	66	58	76	65	56	80
	50	198	160	245	306	227	391	89	73	108	87	72	110
	100	221	161	281	391	278	520	98	79	121	96	79	123
0.1	**2**	173	154	195	198	183	214	165	149	181	176	157	199
	5	260	223	300	266	235	298	219	201	237	221	194	258
	10	331	273	391	324	277	379	253	227	274	255	223	303
	50	520	391	683	488	373	644	321	272	370	334	290	410
	100	615	445	854	573	418	809	349	291	409	368	319	457
0.2	**2**	699	421	819	684	605	777	870	736	964	926	734	1105
	5	1244	849	1615	1127	938	1365	1271	1099	1450	1224	948	1493
	10	1643	1190	2284	1616	1261	2093	1544	1331	1794	1452	1111	1805
	50	2551	1888	3766	3605	2394	5582	2137	1793	2641	1987	1483	2564
	100	2938	2164	4439	5050	3124	8480	2383	1974	3018	2218	1642	2889

Table 4.4: Return periods and confidence intervals for the AMS and PDS series of SPA-identified event duration and severity at different CF thresholds.

power never exceeds a specified threshold, but rather that *wind energy* generation falls below a threshold throughout the event. Hence, the use of SPA procedures offers a time-series-based tool to estimate energy storage requirements of an electricity system from a resource perspective. We note that the SPA analysis identifies similar maximum severity events as the energy storage model of Heide et al.'s [33] model, which was developed in the context of energy storage modelling from an electricity system perspective. However, identification of less severe events with SPA analysis allows statistical models of low wind power events to be developed as discussed in Section 4.4.

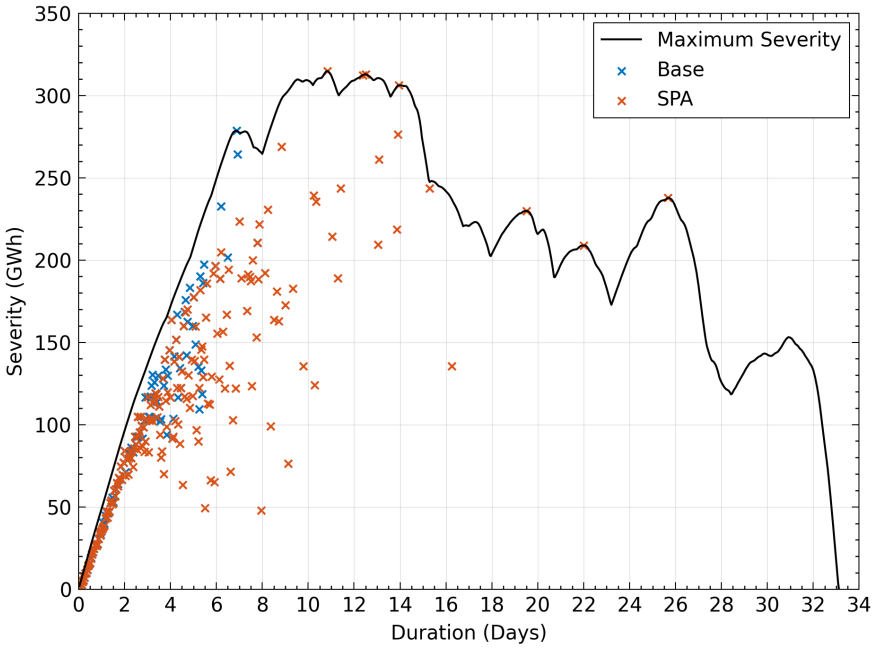


Figure 4.10: Maximum event severity adapted from Ruhnau and Qvist's energy storage model. Black curve shows the maximum event severity for a given overlapping time window. Points refer to the maximum event severity for each event duration as identified by a simple runs analysis and by the SPA method.

Return periods estimated from this definition of low wind power events suggest that the likelihood of prolonged periods of low wind energy may be higher than previously understood. While the severity of events, defined in terms of the energy deficit, does not necessarily increase as significantly as their duration due to pooling, these low wind power events still pose a challenge to the resilience of the electricity system. Additionally, we note that the current (2022) GB energy storage capacity was estimated to be approximately 115 GWh [34]. The estimated return period for severity suggests that GB's current energy

storage would satisfy events with a return period of 1.17 years in order to maintain a net energetic output corresponding to $CF = 0.10$.

As with findings from Cannon et al. [4] and Potisomporn and Vogel [5], the majority of the identified low wind power events occur in spring and summer, with the longest events also occurring in these seasons. Electricity demand in European countries however is generally higher in winter [35], so a low wind power event could have greater impact in winter even if it is not as severe as others. To gauge the impacts that these low wind power events have on the electricity system, the event pooling and extreme value analysis outlined in this paper was employed on a daily time series of electricity demand net of wind energy generation (demand-net-wind), as outlined in Chapter 3.

Such events are referred to as electricity system stress events and are defined to correspond to meeting or exceeding the 90^{th} percentile of demand-net-wind, with the resulting return periods presented in Table 4.5. The reader is reminded that SPA pooling means that electricity system stress events are not defined as periods where the 0.9 quantile threshold is exceeded continuously, but rather as periods where there is an energy deficit with respect to this threshold, ending only when the deficit peaks.

Unlike low wind power events, over 80% of the events identified from the demand-net-wind time series occur in winter and autumn, and none occur in summer. An electricity system stress event that lasts approximately 10 days is estimated to occur once every 2 years, while one that lasts approximately 1 month is expected to occur once every 10 years. The maximum event duration identified in the dataset is 68 days and is expected to occur once every approximately 80 years. An event with a severity of 755 GWh, or 6.5 times the current energetic capacity of the UK wind energy storage, is estimated to occur once every 2 years, while the most severe event that was observed in the 72-year simulation, with a severity of 4.8 TWh, is expected to occur once every 150 years. At present, a mix of dispatchable (generally fossil-fuelled) and baseload generation is used to satisfy the residual demand net of wind generation. However, as the generation portfolio changes in future, there may be a greater need for interconnection to neighbouring countries and energy storage technologies to satisfy the mismatch between wind generation and energy demand.

E[T] (y)		D_{AMS} (days)	D_{PDS} (days)	S_{AMS} (GWh)	S_{PDS} (GWh)
2	**Fit**	10.7	10.2	755	547
	0.025	9.2	9.7	706	525
	0.975	12.8	11.3	875	584
5	**Fit**	19.2	18.7	1325	1087
	0.025	16.0	16.2	1261	945
	0.975	23.2	21.9	1546	1292
10	**Fit**	27.3	26.5	1783	1520
	0.025	21.7	21.0	1689	1253
	0.975	35.3	31.8	2115	1814
50	**Fit**	57.4	52.3	3014	2744
	0.025	37.4	34.1	2785	1921
	0.975	92.6	63.1	3691	3715
100	**Fit**	77.6	67.6	3629	3400
	0.025	44.8	40.9	3250	2119
	0.975	139.1	81.9	4528	5001

Table 4.5: Return periods and confidence intervals for the AMS and PDS series of SPA-identified event duration and severity from demand-net-wind.

4.5.2 Model limitations

The extreme value analysis conducted in this study provides novel insights into the frequency of low wind power events. Using pooling procedures strengthens the assumption of event independence and an Augmented Dickey-Fuller (ADF) test validated that the CF time series can be considered to be stationary. This test is carried out by assessing the presence of a unit root, a condition where a time series is non-stationary because its value at any time is strongly dependent on its value in the previous time step. However, there are also limitations and uncertainties associated with the analysis. The appropriateness of event pooling, the choice of pooling procedure, and the identification of extreme events through annual maximum series or partial duration series are all intertwined with the structure of the electricity system and how it is affected by low wind power events.

The fact that GB-aggregated CF time series was synthesised from ERA5 reanalysis data has a number of advantages. First, the ability of macro-scale reanalysis models to reproduce periods of low wind energy has been reported previously [22]; while small, short-period events tend to be underestimated, it can reproduce longer-period events. Second, the usage of ERA5 reanalysis data provides the advantage of being based on historical

observations, ensuring that the dataset reflects realistic atmospheric conditions and variability. However, the main limitation with such an approach is that the underlying sample is limited in size and is inherently limited to the range of events that have occurred during the observation period. An alternative approach, as employed by Dawkins and Rushby [19] and Kay et al. [36], is to use large ensembles of climate model simulations, such as the UNSEEN framework (UNprecedented Simulated Extremes using ENsembles) or the DePrySys (Decadal Prediction System), to generate synthetic yet physically plausible extreme events that extend beyond the historical observational record. This approach enables the exploration of a broader range of extreme low-wind scenarios, providing additional insights into the potential frequency and severity of rare, high-impact events. By sampling from a much larger event space, such frameworks help overcome the limitations of reanalysis datasets constrained by historical observations.

The extreme value analysis in this study was conducted separately on event duration and severity. However, low wind power event is characterised by both of these variables simultaneously which are necessarily related. Thus, the traditional approach of using distinct univariate distributions to describe duration and severity may overlook the interdependence of the variables. An area of future work is to investigate bivariate distributions and joint return periods (see e.g. [12]) to better characterise prolonged low wind power events.

4.6 Conclusions

Low wind power events represent a major challenge in the decarbonisation of the GB electricity system. Using the 72-year ERA5 reanalysis dataset, this study has leveraged the similarities between low wind power events and hydrological droughts to apply well-established statistical techniques and methodologies to conduct an extreme value analysis of low wind power events in GB.

Pooling procedures in conjunction with runs analysis, are commonly employed hydrological techniques to identify and group drought periods. Application of the IET, MA, and SPA methods to the GB-aggregated capacity factor time series, allowed the identification

of longer low wind power event periods, during which wind power generation may not necessarily be below a given threshold at all times, but the energy deficit below a threshold may nevertheless have significant impacts on the electricity system. This approach to examining low wind power events may be particularly relevant to the evaluating the role and need for energy storage technologies.

While each pooling procedure has strengths and weaknesses, SPA was found to identify the longest events whilst also preserving more frequent short events, and does not require tuning of model parameters such as averaging periods. Using the SPA pooling procedure, it was found that low wind power events corresponding to a $\theta_{CF} = 0.10$ could persist for a duration of up to 26 days.

Extreme low wind power events were identified using the AMS and PDS methods, with the Pearson-III distribution modelling the extreme events well across a number of capacity factor thresholds. The Lognormal distribution was also found to work well for some extreme value series. Additionally, the Generalised Pareto distribution was particularly suitable for modelling PDS-extracted extreme value data, consistent with extreme value theory.

In the case study conducted on GB's wind farm fleet, a low wind power event defined below $\theta_{CF} = 0.10$ using SPA pooling with a duration of up to one week could be expected to occur as frequently as once every 2 years, while the longest event in the 72-year record, which persisted for 26 days, is expected to occur once every 100 years. A similar extreme value analysis was also carried out on the demand-net-wind time series to incorporate electricity demand into the analysis. It was found that the current estimated total energetic capacity of GB energy storage is equivalent to sustained periods where demand-net-wind is above 0.9 quantile with a 1-year return period.

These results suggest that the March 2021 event, with a duration of 11 days and an energetic deficit of 1 TWh with respect to demand-net-wind, was not a particularly rare event. In fact, a low wind power event with comparable duration and severity occurred in December of the same year. In light of this, it is clear that the growing reliance on wind energy necessitates the development of strategies to mitigate the impacts of these low wind power events on the electricity system.

References

[1] P. Potisomporn, T. A. A. Adcock, and C. R. Vogel. Extreme value analysis of wind droughts in Great Britain. *Renewable Energy*, 221:119847, 2024.

[2] I. Staffell, R. Green, T. Green, and M. Jansen. Electric Insights Quarterly. Technical report, Drax Group, 2021. URL `https://reports.electricinsights.co.uk/wp-content/uploads/2021/05/Drax-Electric-Insights-Q1-2021-Report.pdf`.

[3] B. Li, S. Basu, S. J. Watson, and H. W. Russchenberg. A brief climatology of dunkelflaute events over and surrounding the North and Baltic Sea areas. *Energies*, 14(20):6508, 2021.

[4] D. J. Cannon, D. J. Brayshaw, J. Methven, P. J. Coker, and D. Lenaghan. Using reanalysis data to quantify extreme wind power generation statistics: A 33 year case study in Great Britain. *Renewable Energy*, 75:767–778, 2015.

[5] P. Potisomporn and C. R. Vogel. Spatial and temporal variability characteristics of offshore wind energy in the United Kingdom. *Wind Energy*, 25(3):537–552, 2022.

[6] N. Ohlendorf and W.-P. Schill. Frequency and duration of low-wind-power events in Germany. *Environmental Research Letters*, 15(8):084045, 2020.

[7] Z. Liu, P. Jiang, L. Zhang, and X. Niu. A combined forecasting model for time series: Application to short-term wind speed forecasting. *Applied Energy*, 259:114137, 2020.

[8] S. Eslamian. *Handbook of engineering hydrology: Fundamentals and applications*. CRC Press, 2014.

[9] S. Coles, J. Bawa, L. Trenner, and P. Dorazio. *An introduction to statistical modeling of extreme values*, volume 208. Springer, 2001.

[10] E. Zelenhasić and A. Salvai. A method of streamflow drought analysis. *Water Resources Research*, 23(1):156–168, 1987.

[11] L. M. Tallaksen, H. Madsen, and B. Clausen. On the definition and modelling of streamflow drought duration and deficit volume. *Hydrological Sciences Journal*, 42 (1):15–33, 1997.

[12] J. Shiau. Return period of bivariate distributed extreme hydrological events. *Stochastic Environmental Research and Risk Assessment*, 17:42–57, 2003.

[13] V. M. Yevjevich. An objective approach to definitions and investigations of continental hydrologic droughts. *Hydrology Papers Colorado State University*, 1967.

[14] J. R. Stedinger. *Handbook of Hydrology*. McGraw–Hill, 2003.

[15] R. M. Vogel and J. R. Stedinger. Generalized storage-reliability-yield relationships. *Journal of Hydrology*, 89(3-4):303–327, 1987.

[16] A. K. Fleig, L. M. Tallaksen, H. Hisdal, and S. Demuth. A global evaluation of streamflow drought characteristics. *Hydrology and Earth System Sciences*, 10(4):535–552, 2006.

[17] P. Patlakas, G. Galanis, D. Diamantis, and G. Kallos. Low wind speed events: persistence and frequency. *Wind Energy*, 20(6):1033–1047, 2017.

[18] P. G. Leahy and E. J. McKeogh. Persistence of low wind speed conditions and implications for wind power variability. *Wind Energy*, 16(4):575–586, 2013.

[19] L. Dawkins and I. Rushby. Characterising adverse weather for the UK electricity system, including addendum for surplus generation events, 2020. URL `www.metoffice.gov.uk`.

[20] H. Hersbach, B. Bell, P. Berrisford, S. Hirahara, A. Horányi, J. Muñoz-Sabater, J. Nicolas, C. Peubey, R. Radu, D. Schepers, A. Simmons, C. Soci, S. Abdalla, X. Abellan, G. Balsamo, P. Bechtold, G. Biavati, J. Bidlot, M. Bonavita, G. D. Chiara, P. Dahlgren, D. Dee, M. Diamantakis, R. Dragani, J. Flemming, R. Forbes, M. Fuentes, A. Geer, L. Haimberger, S. Healy, R. J. Hogan, E. Hólm, M. Janisková, S. Keeley, P. Laloyaux, P. Lopez, C. Lupu, G. Radnoti, P. de Rosnay, I. Rozum, F. Vamborg, S. Villaume, and J. N. Thépaut. The ERA5 Global Reanalysis. *Quarterly Journal of the Royal Meteorological Society*, 146:1999–2049, 7 2020.

[21] S. Watson, P. Kritharas, and G. Hodgson. Wind speed variability across the UK between 1957 and 2011. *Wind Energy*, 18(1):21–42, 2015.

[22] P. Potisomporn, T. A. A. Adcock, and C. R. Vogel. Evaluating ERA5 reanalysis predictions of low wind speed events around the UK. *Energy Reports*, 10:4781–4790, 2023.

[23] National Grid Electricity System Operator. Transmission Entry Capacity Register, 2022.

[24] National Grid Electricity System Operator. Embedded Register, 2022.

[25] Elexon. Elexon generation data. URL `https://www.elexonportal.co.uk/`.

[26] M. Optis, N. Bodini, M. Debnath, and P. Doubrawa. New methods to improve the vertical extrapolation of near-surface offshore wind speeds. *Wind Energy Science*, 6: 935–948, 6 2021.

[27] H. C. Bloomfield, D. J. Brayshaw, M. Deakin, and D. Greenwood. Hourly historical and near-future weather and climate variables for energy system modelling. *Earth System Science Data*, 14(6):2749–2766, 2022.

[28] M. Lydia, S. S. Kumar, A. I. Selvakumar, and G. E. P. Kumar. A comprehensive review on wind turbine power curve modeling techniques. *Renewable and Sustainable Energy Reviews*, 30:452–460, 2014.

[29] C. Plumley. Kelmarsh and Penmanshiel Wind Farm Data (0.0.2), 2022. URL `https://data.niaid.nih.gov/resources?id=zenodo_5841833`.

[30] D. Cevasco, S. Koukoura, and A. Kolios. Reliability, availability, maintainability data review for the identification of trends in offshore wind energy applications. *Renewable and Sustainable Energy Reviews*, 136, 2021.

[31] D. Raynaud, B. Hingray, B. François, and J. D. Creutin. Energy droughts from variable renewable energy sources in European climates. *Renewable Energy*, 125:578–589, 2018.

[32] O. Ruhnau and S. Qvist. Storage requirements in a 100% renewable electricity system: Extreme events and inter-annual variability. *Environmental Research Letters*, 17(4): 044018, 2022.

[33] D. Heide, M. Greiner, L. Von Bremen, and C. Hoffmann. Reduced storage and balancing needs in a fully renewable European power system with excess wind and solar power generation. *Renewable Energy*, 36(9):2515–2523, 2011.

[34] International Electrotechnical Commission. Electrical energy storage: White paper, 2011.

[35] F. Mockert, C. M. Grams, T. Brown, and F. Neumann. Meteorological conditions during periods of low wind speed and insolation in Germany: The role of weather regimes. *Meteorological Applications*, 30(4):e2141, 2023.

[36] G. Kay, N. J. Dunstone, A. Maidens, A. A. Scaife, D. M. Smith, H. E. Thornton, L. Dawkins, and S. E. Belcher. Variability in north sea wind energy and the potential for prolonged winter wind drought. *Atmospheric Science Letters*, 24(6):e1158, 2023.

Statement of Authorship

Publication details	
Title of paper	Extreme value analysis of wind droughts in Great Britain
Publication status	Published
Publication reference	P. Potisomporn, T. A. A. Adcock, and C. R. Vogel. Extreme value analysis of wind droughts in Great Britain. Renewable Energy, 221:119847, 2024

Student confirmation	
Student name	Panit Potisomporn
Contribution	The analysis and text were primarily developed and written by PP, with the input of co-authors. All sections were written by PP and edited by TAAA and CRV.

Student signature: _____ **Date**: _____

Supervisor confirmation	
Supervisor name	Dr. Christopher Vogel
Comments	I confirm that Panit has made a substantial contribution to the publication, and that the description above in the Statement of Authorship is accurate.

Supervisor signature: _____ **Date**: _____

CHAPTER 5

Spatial variability of extreme wind events: Implications for the future electricity system

This chapter analyses how the spatial distribution of the GB wind farm fleet impacts its risk profile concerning extreme low wind events and the implications for the future electricity system. The article is under internal review for submission to a peer-reviewed journal.

A geographically diverse wind farm fleet can result in power output that is less variable and more reliable. The future deployment of wind farms in the spatial domain and its impacts on extreme low wind power events are, therefore, important and are the focus of this chapter. Using ERA5 reanalysis data from 1950-2021, a frequency analysis and an extreme value analysis were carried out on the planned GB wind farm fleet for 2030 and various scenarios for 2050. It was found that the 2030 farm distribution leads to a reduced risk of low wind power events lasting longer than 1 week due to greater spatial diversification of the fleet and the deployment of wind farms in regions with higher wind power output potential. However, the risk of shorter low wind power events remains relatively unchanged. Subsequently, an exploration of several scenarios of wind farm distribution in 2050 further highlights the significance of a spatially diversified wind farm fleet and yields important insights. Regions that are further offshore were found to possess higher wind power potential and stability but such advantages diminish with increasing distance. The less developed Western and Northern regions enhance the overall spatial diversity of the wind farms fleet and hence, can aid in achieving a more resilient fleet. The Northwestern and Southwestern regions also represent unexplored regions, which can significantly reduce the risk of extreme low wind power events. These findings underscore the critical importance of strategic spatial planning in the deployment of future wind farms.

5.1 Introduction

The previous chapter focused on the development of a statistically robust frequency analysis and extreme value analysis, and their application in quantifying the risk of extreme low wind power events for the current GB wind farms fleet. Given the ambitious targets of up to 38 GW of additional onshore and offshore wind capacity planned for 2030 [1], and a substantial expansion to 160 GW by 2050 [2], the immediate questions that arise are how this risk profile will change with the distribution of wind farms in the near future and what strategies can be employed to further mitigate low energy generation risks. Therefore, it is essential to evaluate the variation of the risk profile with the wind farms' spatial distributions to determine the viability and strategic deployment of wind farms, using the insights gained to inform future expansions.

A limited number of studies have carried out a risk quantification of extreme low wind power events on the current GB wind farm fleet. In addition to the study outlined in Chapter 4, Cannon et al. [3] conducted a frequency analysis on extreme wind power generation based on the 2012 wind farm distribution using reanalysis data. Projections of this risk in the future are also limited in number. For example, Drew et al. [4] quantified the frequency of low wind events for the 2025 GB wind farm fleet. Abdelaziz et al. [5] investigated the impacts of climate change on extreme low wind events using return periods calculated at individual grid points. Similarly, Giddings et al. [6] simulated a limited number of scenarios for GB's future wind farm fleet and compared the frequency of extreme events for each scenario.

A strategic approach to wind farm deployment is essential for mitigating the impacts of these extreme low wind events on the electricity system, with the spatial variability of wind being a critical guiding factor. It is well known that wind speed correlations decrease with distance; as a result, a spatially diverse wind farm fleet yields smoother, more reliable power output [7–9]. However, achieving a spatially balanced portfolio is economically and technically challenging, making it important to investigate the spatial variability of wind speed and particularly low wind power events. Previous studies focusing on the spatial distribution of wind farms often have a broad scope, are conducted on a continental scale

including both wind and solar [10, 11], focus on a limited number of scenarios [6, 5], or do not focus on extreme low wind power events [12].

Therefore, the goal of this study is to evaluate the impacts of spatial variability on the risk of extreme low wind power events through formal extreme value analyses. This will be achieved through two specific objectives. First, it aims to quantify the risk of extreme low wind power events for the expected wind farm distribution of the near future. Second, it aims to investigate the impacts of spatial variability on this risk profile, seeking to provide recommendations for future wind farm deployment. This chapter is organized into two distinct snapshots: the *Near-future* analysis and the *Far-future* analysis. This approach allows for the assessment of the wind farm fleet's progress in relation to the risk posed by extreme low wind power events to the electricity system. It also addresses the higher degree of uncertainty inherent in projections further into the future, which necessitates the use of varying sophistication in data processing methods. Additionally, this greater uncertainty permits a broader exploration of potential scenarios, enabling a thorough analysis of future developments and their potential implications, leading to varied focal points in each analysis.

For both analyses, the scope of the study is limited to using historical data from 1950-2021 to describe the risk of extreme low wind power events for future wind farm distributions. Therefore, the crucial assumption made throughout the study is that historical extreme statistics can describe future conditions. Nevertheless, the impacts of climate change on extreme statistics are not yet conclusive. Although Abdelaziz et al. [5] found a climate-change-induced increase in the risk of extreme low wind power events, other studies have noted that inter-annual and hourly variability of wind speed is more significant than climate-change-induced non-stationarity [6, 13]. Given that the main focus of this study is on spatial variability, priority was placed on an approach based on reliable, accurate, and bias-corrected reanalysis data that has been validated for such usage. Moreover, climate projections are often associated with significant uncertainties arising from model variability, scenario assumptions, and internal climate variability [14]. Therefore, relying on reanalysis data, which has assimilated real observational data, provides a more robust basis for assessing the risk of extreme low wind power events.

5.2 Near-future analysis

The Near-future analysis focuses on the GB wind farms fleet in 2030. The projection of this fleet is based on the Renewable Energy Planning Database (REPD) [1], a quarterly extract published by the Department for Energy Security and Net Zero, which tracks the progress of UK renewable electricity projects. These projects include onshore and offshore wind farms that are due to commence operation by 2030 and, therefore, represent a suitable forecast of the wind farm fleet in 2030. The main objective of this analysis is to describe changes in the production profile of wind energy and the risk profile of low wind events resulting from the planned addition of wind farms to the current fleet.

5.2.1 Data and Methods

The process of obtaining GB-aggregated power output follows the methods outlined in Section 4.2 and can be summarised as follows. First, ERA5 reanalysis 10-m wind speed data was bias-corrected based on the information presented in Chapter 2. The bias-corrected wind speed was then interpolated to the locations of wind farms in the fleet. The locations of the current fleet's wind farms are based on those from the REPD, which were operational as of the end of 2022. For the Near-future fleet, additional wind farms are included based on those that are either approved or in development but not yet operational. Second, for each wind farm, the 10-m wind speed was extrapolated to a representative hub height of 100 metres using a pre-trained Multi-layer Perceptron Regression model outlined in Section 3.2.2. Third, the hub height wind speed was converted to power output using an empirically calibrated wind farm power curve. Lastly, the individual wind farm power outputs were aggregated to obtain the GB-aggregated wind power output.

5.2.2 Fleet

As outlined in Table 5.1, the addition of 279 wind farms brings the total number of farms from 208 to 487 and the total capacity from 20.9 GW to 59.4 GW. For both onshore and offshore wind farms, the capacities of the additional farms are generally greater than those of the current fleet, resulting in an increase in the mean wind farm capacity from 100.3

MW to 122.1 MW. This change is particularly notable in the offshore fleet, where the mean farm capacity increases from 366.1 MW to 696.3 MW. These additions are illustrated in Figure 5.1. It can be seen that ongoing and future onshore wind farm developments are concentrated in Scotland, while offshore developments are predominantly located in the North Sea, with the exception of Gwynt y Môr wind farm in the Irish Sea.

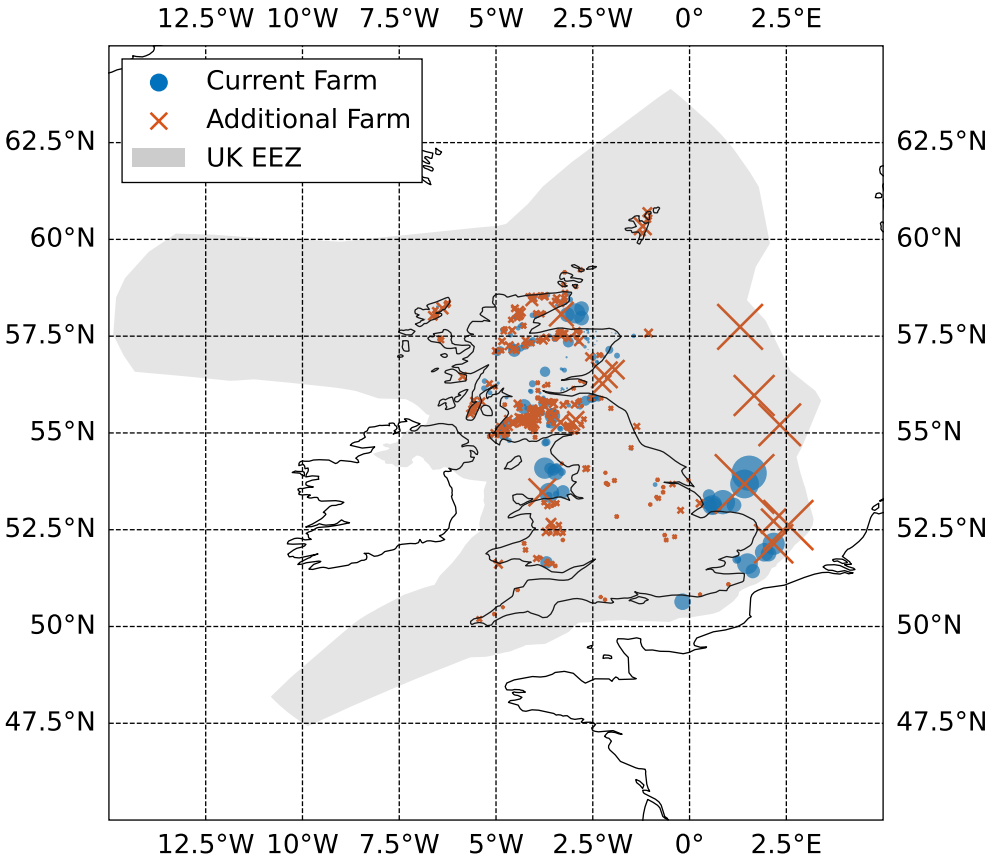


Figure 5.1: The locations of wind farms in the current (2022) and additional wind farms for the Near-future (2030) fleets. The sizes of the symbols reflect the capacities of the wind farms.

Figure 5.2 illustrates an inter-farm distance-correlation (Pearson R of capacity factor) plot where each data point corresponds to a farm-pair. A number of observations can be made. First, as corroborated by previous studies on the spatial variability of wind speed [7, 8], a decrease in correlation with distance that resembles an exponential decay can be observed. Second, within the 0-400 km range, a cluster of points undershoots the curvature. This behaviour is attributed to data points that correspond to onshore-onshore farm-pairs, which exhibit a higher rate of decrease in correlation than other types of farm-pairs do,

		Current	Additional	Near-future
Onshore	**Total capacity (MW)**	7323.2	14551.5	21874.7
	Number of farms	171	262	433
	Mean capacity (MW)	42.8	55.5	50.5
Offshore	**Total capacity (MW)**	13544.4	24053.4	37597.8
	Number of farms	37	17	54
	Mean capacity (MW)	366.1	1414.9	696.3
Total	**Total capacity (MW)**	20867.6	38604.9	59472.5
	Number of farms	208	279	487
	Mean capacity (MW)	100.3	138.4	122.1

Table 5.1: Fleet statistics for the Current (2022) and the Near-future (2030) fleets.

due to higher surface roughness and terrain impacts in the onshore domain. Third, plotted above the data points are the mean distance-correlations of the current and the Near-future fleet. Given that the majority of additional wind farms will be situated in approximately the same regions, except for a few large wind farms in the North Sea (Cerulean and Dogger Bank), the increase in mean inter-farm distance and hence, the decrease in mean inter-farm correlation, are limited.

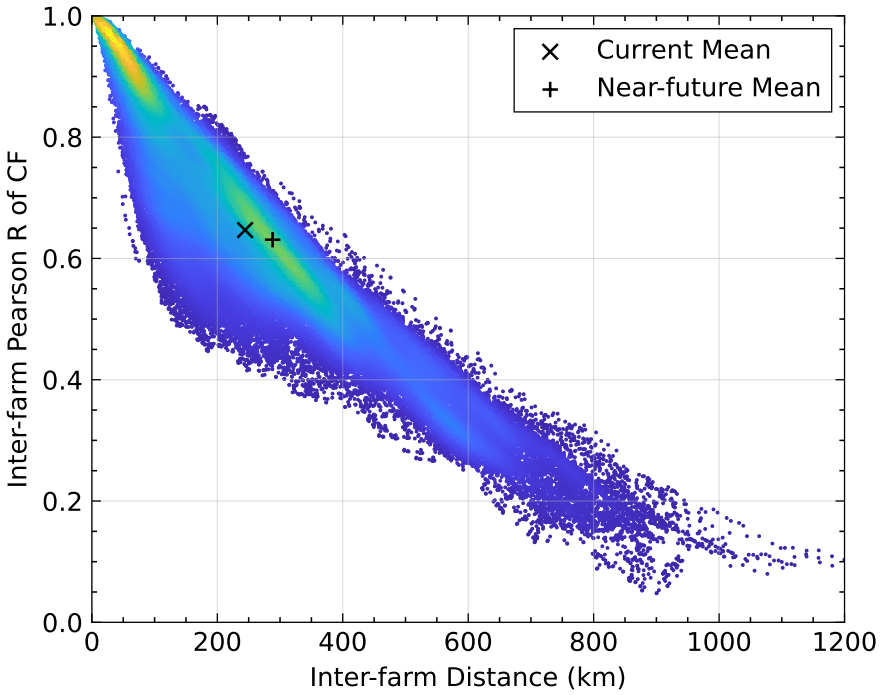
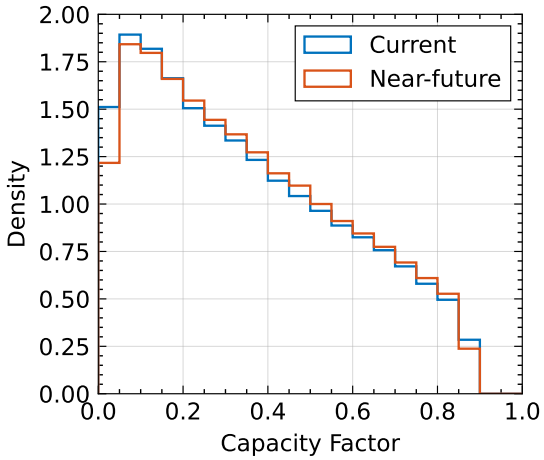


Figure 5.2: Scatter plot of inter-farm Pearson R against inter-farm distance where each data point corresponds to a farm-pair. A brighter color indicates a higher density of data points.

5.2.3 Capacity factor

The current and Near-future fleets' GB-aggregated capacity factor (CF) time series distributions and statistics are shown in Figure 5.3. Compared to the current fleet, the Near-future fleet's CF time series exhibits marginal improvements from a statistical point of view, with minimal increases in mean and median CF and minimal decreases in standard deviation and coefficient of variation (CoV). While their distributions are also approximately quite similar, it can be clearly seen that probability density of CF below 0.2 (the highest CF threshold employed in this study) of the future fleet is consistently below that of the current fleet. As such, the probability that the future fleet's CF is below 0.2 ($F(0.2)$) is 0.152 compared to the current fleet's 0.17. This difference equates to 158 fewer hours per year where the future fleet capacity factor falls below the 0.2 threshold compared to the current fleet.



Fleet	Current	Near-fut.
Mean	0.346	0.354
Median	0.307	0.318
StDev	0.235	0.232
CoV	0.678	0.656
F(0.2)	0.170	0.152

Figure 5.3: Capacity factor distributions and statistics for the Current (2022) and the Near-future (2030) fleets.

5.2.4 Low wind power events

As per the methods described in Section 4.3.2, the Sequent Peak Algorithm (SPA) was applied to both the current and the Near-future fleets' CF time series to identify low wind power events for CF thresholds of 0.05, 0.10, and 0.20. Due to the previously described trends in CF statistics and distribution, low wind power metrics have also shown significant improvements across all CF thresholds as shown in Table 5.2. Focusing on the 0.10 CF

threshold, the expected annual frequency decreases by approximately six events per year. Additionally, there is a reduction in both the mean event duration and the coefficient of variation. However, it can be observed from the frequency-duration curve shown in Figure 5.4 that the major improvement stems from the reduction in the annual frequency of extremely long low wind power events (as a fraction of the current fleet's frequency for an event of the same duration) i.e., those that are longer than a week. Furthermore, to quantify the risk of these events, an extreme value analysis as described in Section 4.4.1 was applied to the annual maxima series (AMS) of these low wind power events and the resultant return period curves are shown in Figure 5.4. Compared to the current fleet, the Near-future fleet's curve demonstrates a significant increase in return period for events longer than a week, and continues to diverge from the current curve. However, the Near-future fleet still demonstrates a comparable frequency of events shorter than a week.

CF Thresh.		**0.05**		**0.10**		**0.20**
Fleet	**Current**	**Near-fut.**	**Current**	**Near-fut.**	**Current**	**Near-fut.**
Annual Freq.	42.8	33.3	62.3	56.2	57.3	57.3
Mean (h)	15.8	15.8	25.0	24.7	55.4	51.2
Max (h)	204	185	618	391	3963	2821
Median (h)	10	10	13	14	18	18
IQR (h)	14	15	23	23	39	38
CoV	1.16	1.14	1.46	1.38	2.73	2.36

Table 5.2: Low wind power events statistics for the Current (2022) and the Near-future (2030) fleets.

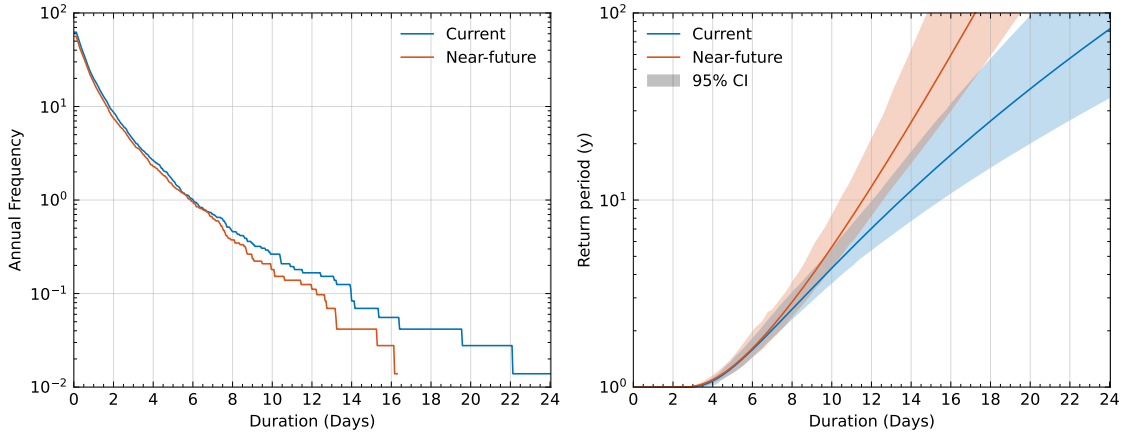


Figure 5.4: Frequency-duration curves (left) and return periods (right) of low wind power events from the Current (2022) and the Near-future (2030) fleets.

5.3 Far-future analysis

The Far-future analysis focuses on the possible GB wind farm fleet scenarios in 2050. The projection of this fleet is based on National Grid ESO's Future Energy Scenarios (FES) [2], an annual report that outlines a range of credible pathways for GB's electricity system to achieve net-zero carbon emissions. Among other projections, the report provides forecasts of wind energy capacity up to the year 2050, reflecting different scenarios that consider varying levels of policy ambition, technological advancements, and market conditions. Given the absence of concrete plans for such a distant future, the primary goal of this analysis is to explore various scenarios in which the GB wind farm fleet could be developed to achieve the highest level of resilience.

5.3.1 Data and methods

Unlike the Near-future analysis, where the REPD provides details on the locations of wind farms and the target capacity in 2030, the Far-future analysis, which focuses on the 2050 fleet, lacks definitive deployment plans. Therefore, this allows for the exploration of various scenarios that the 2050 fleet could take. These numerous scenarios are governed by two variables, namely the *Projected Value*s (PV) of the electricity system and the *Spatial Distribution* (SD) of wind farms.

The PV variable is based on FES projections under four scenarios: Falling Short (FS), Leading the Way (LW), System Transformation (ST), and Consumer Transformation (CT). (The reader is referred to Appendix A for a description of each scenario.) For each scenario, two quantities are relevant to the study: the projected capacities of the onshore and offshore fleets, and the projected annual electricity demand. As a simplification, it is assumed that each projected value in 2050 can only take on a value from each of the four scenarios. Therefore, the range of PV is limited to these four discrete sets of values, which are presented in Table 5.3.

While the PV variable is based on published projections, similar projections are not available for the locations of wind farms in 2050. This circumstance presents two implications. First, the range of possible scenarios is practically infinite. Second, it is no longer

FES 2050 Scenario	FS	LW	ST	CT
Onshore wind capacity (GW)	28.3	41.8	32.5	44.4
Offshore wind capacity (GW)	77.6	96.8	105.1	115.0
Annual electricity demand (TWh)	516.3	469.4	445.2	550.5

Table 5.3: Projected Values for the year 2050 taken from the FES report [2].

possible to apply the methods outlined in Section 5.2.1, which rely on the interpolation of reanalysis wind speed to wind farm locations. Therefore, in this Far-future analysis, GB-aggregated power output replaces wind farm power output with zone power output as the aggregating unit. The methods are as follows:

First, the UK Exclusive Economic Zone (EEZ) was divided into 20 zones, as shown in Figure 5.5. Second, for a given zone, wind speed from grid points contained within the boundary of that zone is aggregated by averaging to yield the representative wind speed time series of that zone. Third, the zone-representative wind speed time series is extrapolated to a representative hub height of 100 meters, then converted to power output as per the methods outlined in Section 4.2 to yield the zone-representative power output time series. Lastly, GB-aggregated power output is obtained from the zone-capacity-weighted averaging of these zone-representative power output time series. The zoning scheme is predominantly based on the onshore transmission systems, the inclusion of existing wind farms as of the Near-future analysis, and most importantly, the simultaneous minimisation of zone sizes and the number of zones (the reader is referred to Appendix B for more details on the zone-aggregated power output).

Hence, from the descriptions above, the influences of these two variables on the Far-future scenarios can be characterised as follows. SD governs the proportions of the total available capacity that the zones will receive and hence, is the major driver of wind CF. In contrast, PV governs the electricity demand and the wind farm fleet's total capacity. Therefore, it determines both the supply of electricity from wind energy in terms of power output and energy yield, as well as the relationship between wind power output and electricity demand. In summary, the SD variable is the main driver of the variation in the supply of wind energy and the PV variable is the main driver of the electricity system as a whole. Therefore, the Far-future analysis is further divided into two sub-analyses: the

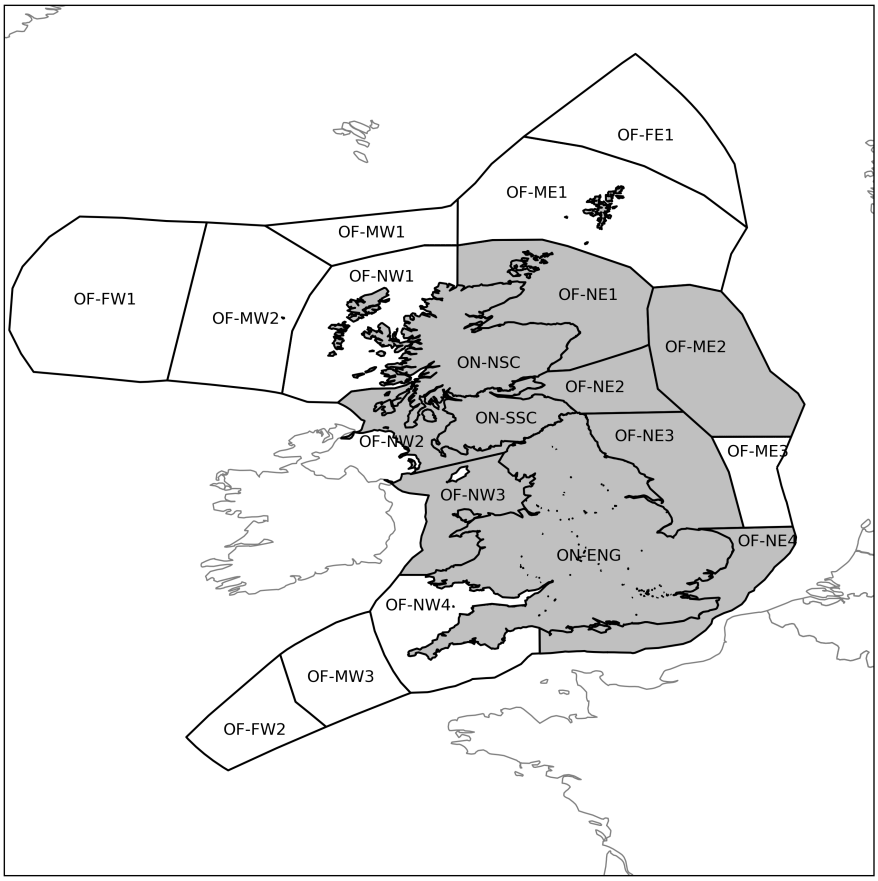


Figure 5.5: A map showing the division of the UK EEZ into 20 zones, consisting of 3 onshore and 17 offshore zones. Shaded zones represent regions that are occupied by wind farms as of the Near-future analysis.

first analysis concerns extreme events associated with the supply of wind energy, while the second analysis focuses on extreme events associated with the relationship between wind energy and the electricity system.

5.3.2 Wind energy supply

The statistics of the zone-representative CF time series are illustrated in Figure 5.6, showing notable spatial variations. The mean and median CFs are higher in zones further offshore, with the north having higher CFs than the South. The Northwest, in particular, shows notably higher mean and median CFs compared to other zones, highlighting its superior wind energy potential. And although the Southeast currently accommodates the majority of GB wind farms fleet due to the region's shallower seabed and proximity to

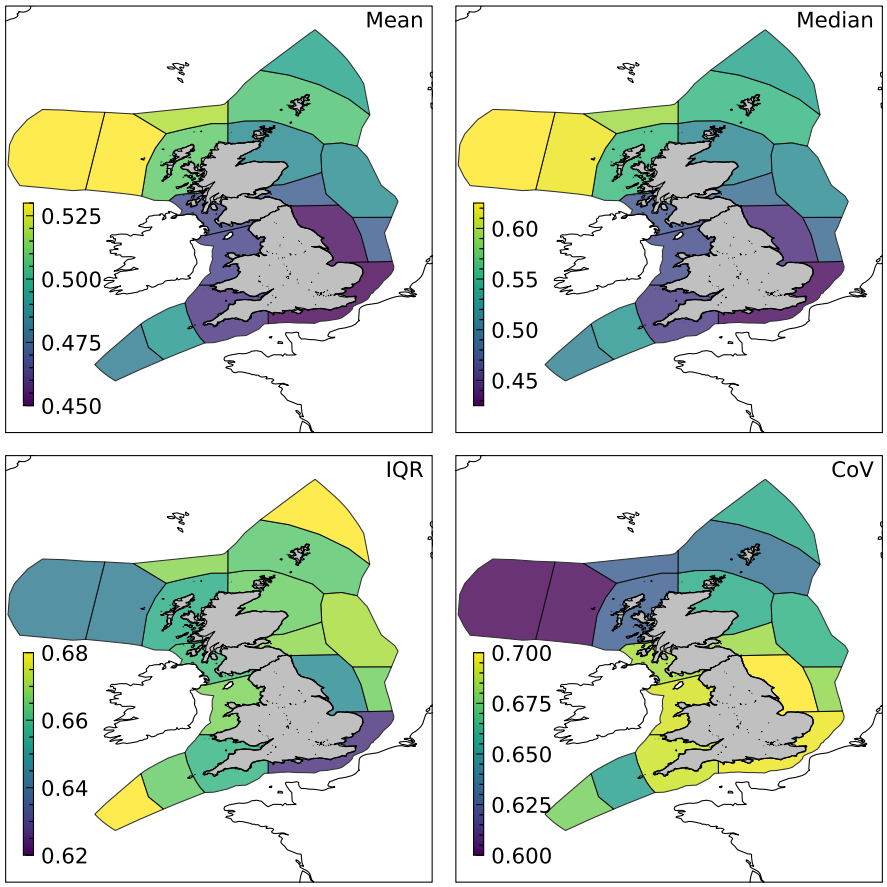


Figure 5.6: Capacity factor statistics for the 17 offshore zones.

shore, it has a lower mean CF relative to other offshore regions. The interquartile range (IQR) map indicates significant variability in the Northeastern and Southwestern zones, suggesting substantial fluctuations in CF within these areas. In contrast, the coefficient of variation (CoV) highlights higher relative variability in the central zones, which is not entirely consistent with the IQR patterns. This discrepancy suggests that while some regions have high absolute variability (IQR), their relative variability to the mean (CoV) differs, indicating diverse wind conditions across the zones.

The differences between the zones indicate that various combinations of capacity allocation will result in distinct risk profiles concerning extreme low wind power events. Therefore, the goal of this analysis is to explore the sensitivity of the wind farms fleet's risk profile to the different spatial distributions of wind farms. To allocate capacity among 20 wind farm zones efficiently, the SD variable is divided into different dimensions, each representing a specific way of clustering and comparing the zones, thereby simplifying the

allocation process. By clustering zones within each dimension, the focus is shifted to allocating capacity between these clusters, reducing the complexity associated with the vast number of possible combinations and making the process more structured and manageable.

Several potential dimensions can be considered based on geographical groupings, but four key dimensions concerning the future of GB's wind farm fleet are addressed in this study: 1. *Offshore distance*, 2. *East vs. West*, 3. *North vs. South*, and 4. *Northwest vs. Southwest*. For each dimension, various scenarios representing different combinations of capacity allocation among the zones are explored. Two scenarios are present throughout all dimensions: the *Unchanged* scenario, where the proportions of capacity allocation among the zones match those of the Near-future fleet (i.e., no new zones are used), and the *Zone-balanced* (Zone-bal.) scenario, where additional capacity is distributed in a manner that seeks to achieve uniform final capacities across all zones. These baseline scenarios remain constant throughout all dimensions.

To further simplify the investigation of these scenarios, the proportions of onshore zones' capacity with respect to total onshore capacity are assumed to remain constant until 2050, essentially limiting the onshore fleet's contribution to the differences between each scenario. Furthermore, given the focus of this study on low wind power events, the scope of this analysis excludes considerations of technical and economic constraints on turbine deployments, though their significance will be acknowledged. Results from each dimension are presented below.

Offshore distance

The first dimension of interest is offshore distance. It is well known that wind energy potential is higher further offshore, but at the same time, constructing wind farms further offshore and likely into deeper-water sites leads to increases in foundation, installation, and operational costs [15, 16]. Therefore, the main question this dimension aims to answer is what additional advantages regarding the reduction of risks associated with extreme low wind power events can be gained by allocating a higher level of capacity to zones that are further offshore.

An overview of the zone clusters and the different scenarios is presented in Figure

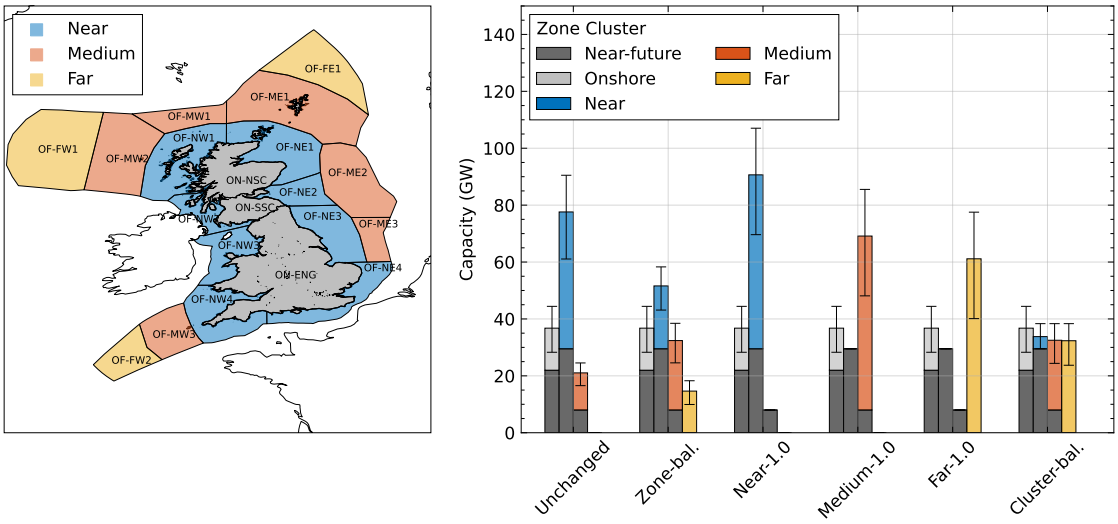


Figure 5.7: Overview of zone clusters and the capacity allocation for each scenario in the *offshore distance* dimension. The map (left) illustrates the different zone clusters by distinct colours. The bar chart (right) shows the different final capacities of the clusters in 2050 corresponding to the different scenarios where dark grey bars represent the existing capacity in a cluster as of 2030. Error bars show the variation of these 2050 capacities due to the different levels of available capacity for allocation as per the four PV scenarios.

5.7. Four scenarios are explored in this dimension: Near-1.0, where 100% of additional capacity is allocated to the Near cluster; Medium-1.0, where 100% of additional capacity is allocated to the Medium cluster; Far-1.0, where 100% of additional capacity is allocated to the Far cluster; and Cluster-balanced (Cluster-bal.), where capacity is distributed in a manner that seeks to achieve uniform final capacities across all zone clusters. For each cluster, its allocated capacity is then distributed to achieve uniform final capacities across all zones. This is different than the Zone-bal. scenario, which distributes capacity equally to all zones, of which there are not an equal number in each cluster.

Statistics of GB-aggregated CF under each scenario are presented in Figure 5.8. As expected, the Unchanged and Near-1.0 scenarios result in the lowest CF mean and the highest variability. This is because the majority of Near-future capacity is allocated to zones in the Near cluster, which have the lowest CF and highest variability. The Near-1.0 scenario achieves a slightly higher CF than the Unchanged scenario due to allocation to other zones in the Near cluster with higher CF and lower variability, as well as from greater spatial diversification. The remaining four scenarios, which allocate capacity to zones further offshore, show lower variability and equally high mean and median CFs, with

the Far-1.0 scenario demonstrating the notably higher median CF and lower variability than other scenarios. This is due to the allocation of capacity to zones with higher CF and lower variability, as well as greater spatial diversification of the wind farms fleet. Moreover, it is worth noting that the more significant differences between the scenarios are demonstrated by the variability, as represented by IQR and CoV, rather than by mean and median CF.

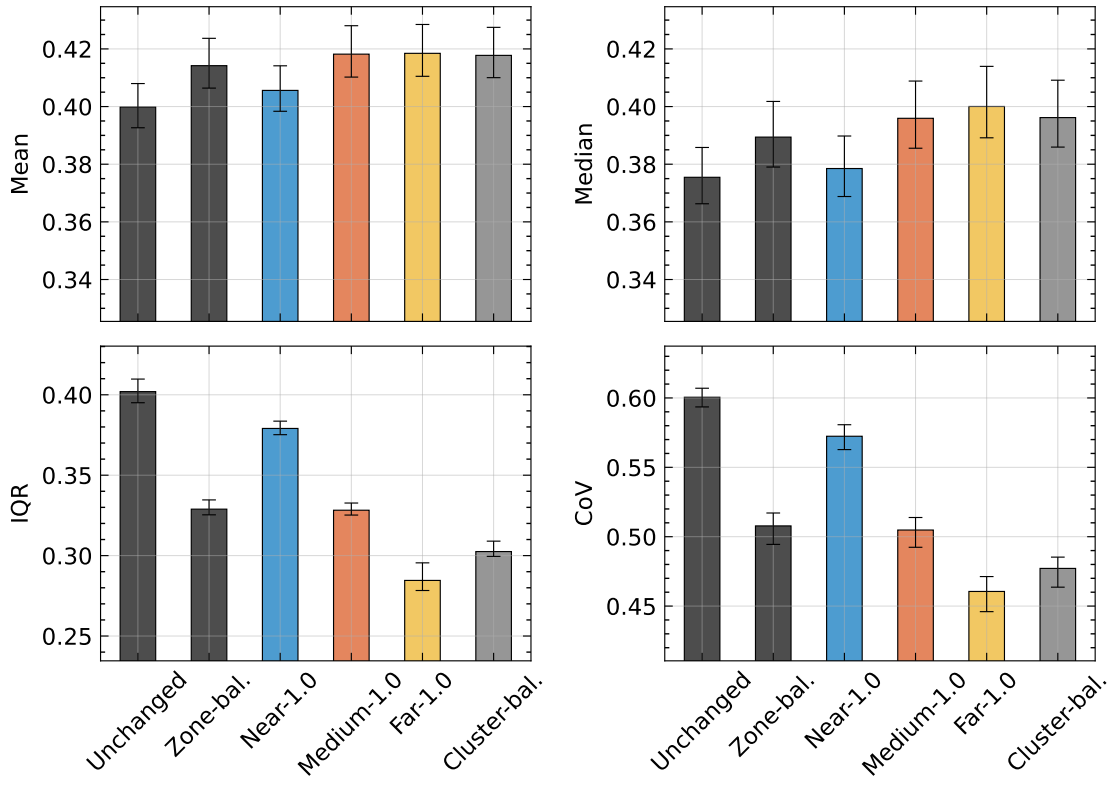


Figure 5.8: Capacity factor statistics for each scenario in the *offshore distance* dimension.

Low wind power events were identified from the GB-aggregated CF of each scenario using the SPA as per the methods outlined in Section 4.3.2, and an extreme value analysis as described in Section 4.4.1 was carried out on their AMS. Their frequency-duration curves and return period curves of the different scenarios are presented in Figure 5.9. Reflecting the CF statistics presented above, the annual frequency of low wind power events is substantially higher for events of all durations for the Unchanged and Near-1.0 scenarios. Consequently, the risk of extreme low wind power events is significantly higher for these two scenarios, as reflected by the associated return periods. Note that the Near-1.0

scenario only gives rise to a statistically significant (based on a 95% confidence interval) decrease in return periods for extreme low wind power events of duration lower than 5 days. On the other hand, the remaining four scenarios show a significant improvement from the Unchanged scenario in their frequency-duration and return period curves, with the Far-1.0 scenario showing the greatest improvement. Although this result is expected, it is important to highlight that for extreme low wind power events of duration greater than 4 days, these four scenarios show no statistically significant difference in terms of the return periods. Hence, a key finding from these results is that the reduction in risk from the Medium-1.0 to the Far-1.0 scenario, is less pronounced, particularly for longer extreme events, compared to the reduction in risk from the Near-1.0 to the Medium-1.0 scenario.

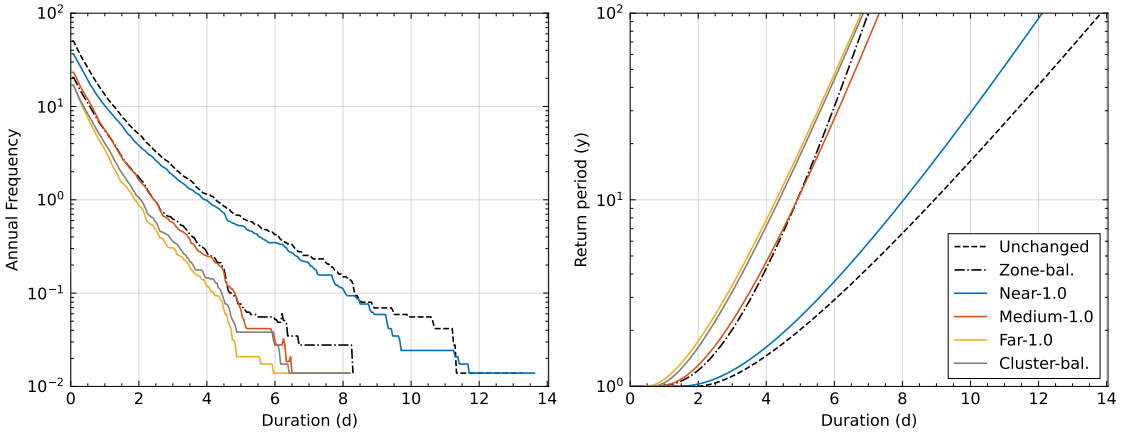


Figure 5.9: Frequency-duration curve (left) and return period (right) of low wind power events for each scenario in the *offshore distance* dimension. Confidence intervals are omitted to maintain clarity. 95% confidence intervals at certain low wind power event durations are tabulated in Appendix C.

In summary, allocating capacity to zones further offshore results in a wind farm fleet that is less susceptible to extreme low wind power events due to the utilization of zones with higher power output quality and greater spatial diversification. However, the reduction in risk is more significant when concentrating resources from the Near region to the Medium region than from the Medium region to the Far region, indicating diminishing returns with further offshore expansion. This can be attributed to the fact that mean and median CF of the Far region are not substantially higher than the Medium region, as well as the fact that the Far region has fewer zones than the Medium region, hence, offering only a marginal improvement in spatial diversity of the farms fleet. Although they were not presented in

terms of return periods, findings from [15] also suggest this diminishing benefits of exploring regions further offshore.

East vs West

Planned wind farm developments up until 2030 are concentrated in the North Sea, meaning that, according to the zoning scheme devised in this study, a large proportion of Near-future wind farms is located in the East. While this is largely due to the shallower seabed in the North Sea, the region, as previously discussed, does not possess the highest power output quality. Therefore, the main question associated with the *East vs West* dimension is how significantly the wind farm fleet can benefit from allocating resources to the West.

An overview of the zone clusters and the different scenarios is presented in Figure 5.10. In addition to the two baseline scenarios, the four dimension-specific scenarios are: East-1.0, where 100% of additional capacity is allocated to the East cluster; West-1.0, where 100% of additional capacity is allocated to the West cluster; Split, where additional capacity is divided equally among the two clusters; and Cluster-balanced (Cluster-bal.), where capacity is distributed in a manner that seeks to achieve uniform final capacities across all clusters.

Statistics of GB-aggregated CF under each scenario are presented in Figure 5.11. Apart from the Unchanged scenario, whose GB-aggregated CF displays a significantly lower mean, the other scenarios' mean and median CF are of comparable levels, with the West-1.0 scenario having the highest mean CF due to a slightly higher overall CF in the West. The main difference between the scenarios, however, is observed in the variability of the CF time series. Apart from the Unchanged and the East-1.0 scenarios, other scenarios allocate a considerable proportion of capacity to the West and see a significant decrease in CF variability due to greater spatial diversification of the wind farms fleet.

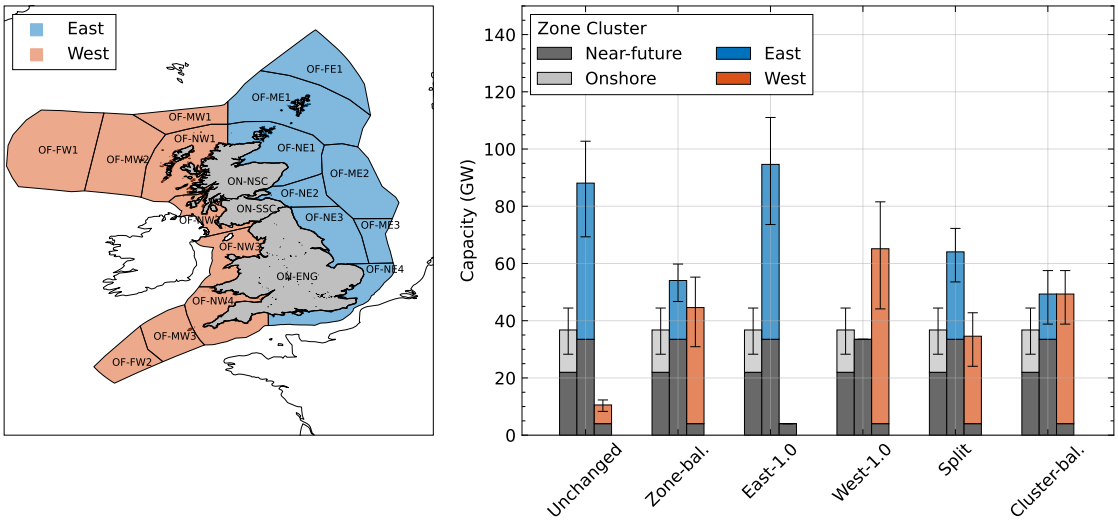


Figure 5.10: Overview of zone clusters and the capacity allocation for each scenario in the *East vs. West* dimension. The map (left) illustrates the different zone clusters by distinct colors. The bar chart (right) shows the different final capacities of the clusters in 2050 corresponding to the different scenarios, where dark grey bars represent the existing capacity in a cluster as of 2030. Error bars show the variation of these 2050 capacities due to the different levels of available capacity for allocation as per the four PV scenarios.

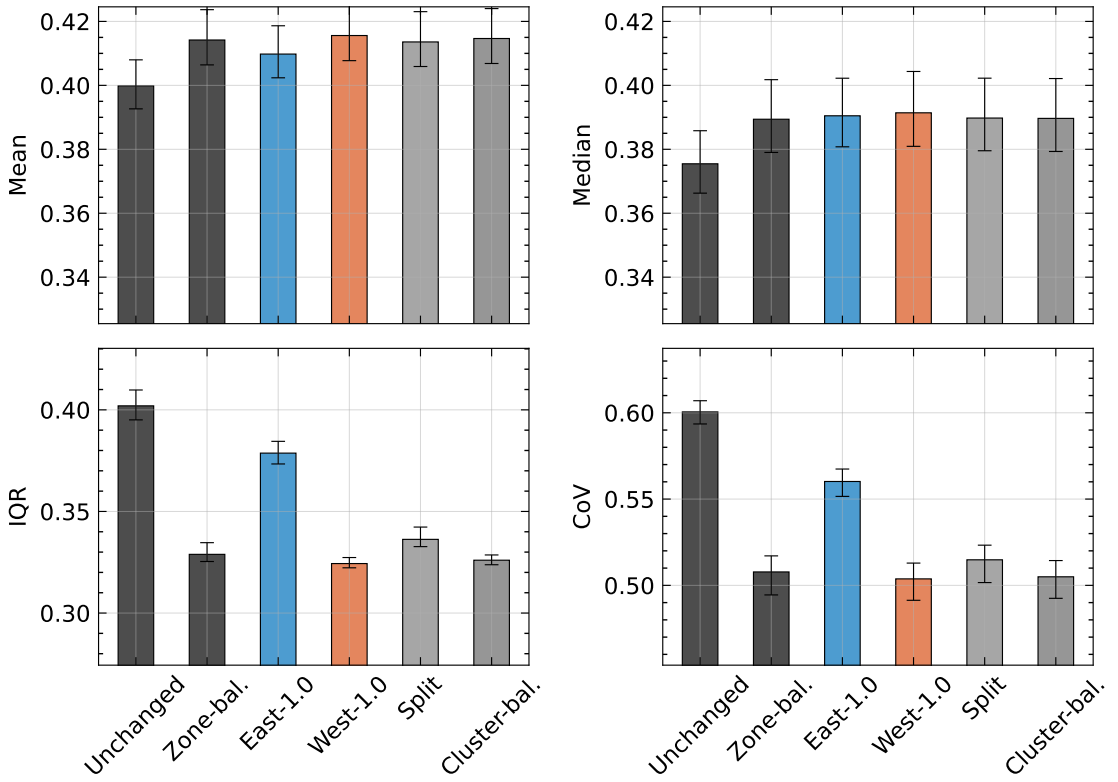


Figure 5.11: Capacity factor statistics for each scenario in the *East vs. West* dimension.

The frequency-duration curves and return period curves of the different scenarios are presented in Figure 5.12. It is shown that only concentrating future resources in the East can marginally reduce the risk of extreme low wind power events from the Unchanged scenario, but only if capacity is also allocated to unexplored zones in the East cluster to achieve greater spatial diversification and exploit zones with higher power output quality. For low wind power event durations, their return periods under the East-1.0 scenario show a statistically significant (based on 95% confidence intervals) increase compared to those under the Unchanged scenario. Furthermore, while the West-1.0 and the remaining scenarios show no significant statistical difference between their return period curves among themselves, all exhibit statistically significant increases in return periods, and hence lower risk, compared to the East-1.0 scenario. This finding suggests that allocating resources to the West gives rise to a wind farm fleet that is more resilient to the risk of extreme low wind power events. Such results also corroborate findings from Regen [12], which show that the average time per month offshore wind capacity factor is below 10% decreases with increasing allocation of capacity to the West.

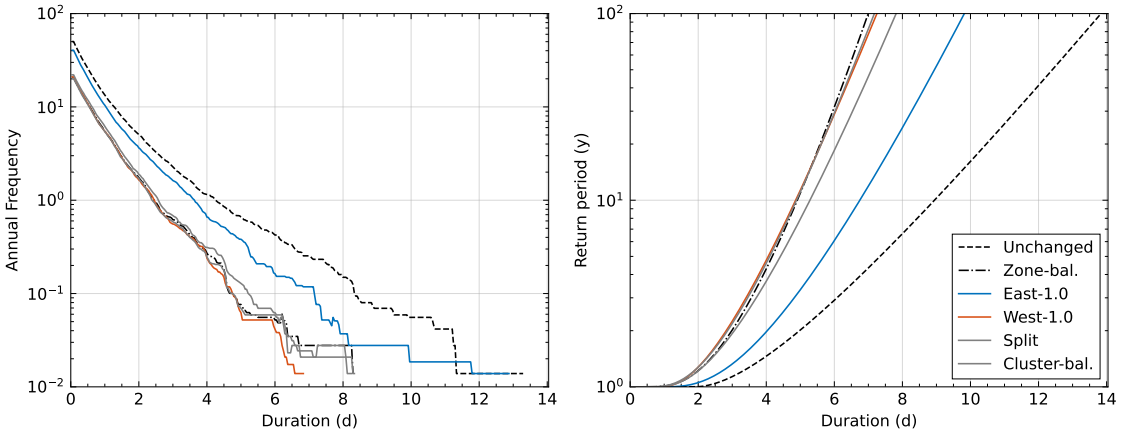


Figure 5.12: Frequency-duration curve (left) and return period (right) of low wind power events for each scenario in the *East vs. West* dimension. Confidence intervals are omitted to maintain clarity. 95% confidence intervals at certain low wind power event durations are tabulated in Appendix C.

Therefore, the consideration of the *East vs. West* dimension clearly shows the importance of spatial diversification. This significance is demonstrated by the substantial improvement in the risk profile of the Far-future fleet to extreme low wind power events. Although the Western zones exhibit a slightly higher overall power output, it is the signif-

icant reduction in CF variability that leads to a reduction in the frequency of extreme low wind power events. Hence, allocating substantial resources to the West is a key aspect in improving the resilience of the Far-future fleet, and evidence indicates that directing only a proportion of additional capacity there can achieve significant improvements.

North vs South

Advancements in offshore wind turbine foundation technology are expected to allow offshore wind farms to be built in regions with deeper seabeds located further north in the North Sea, such as the Dogger Bank wind farm, which utilizes monopiles with higher structural integrity, or the Cerulean wind farm, which utilizes floating foundations. As a result, the imbalance between the Northern and Southern cluster's capacity is not as pronounced as that between other dimensions' clusters. Given the continual development in offshore wind turbine foundations, the main question addressed here is whether one cluster offers benefits over the other.

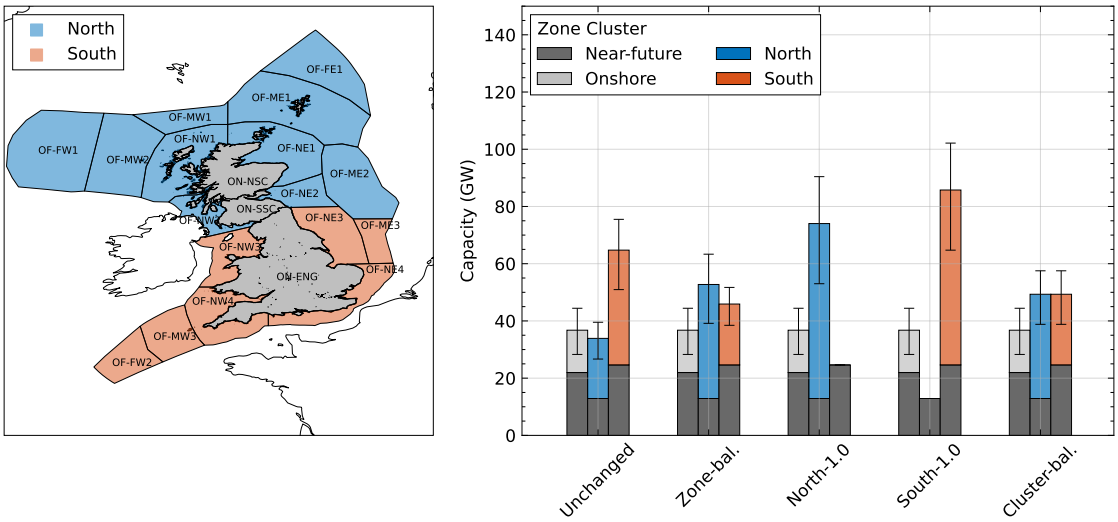


Figure 5.13: Overview of zone clusters and the capacity allocation for each scenario in the *North vs. South* dimension. The map (left) illustrates the different zone clusters by distinct colors. The bar chart (right) shows the different final capacities of the clusters in 2050 corresponding to the different scenarios, where dark grey bars represent the existing capacity in a cluster as of 2030. Error bars show the variation of these 2050 capacities due to the different levels of available capacity for allocation as per the four PV scenarios.

An overview of the zone clusters and the different scenarios is presented in Figure 5.13. In addition to the two baseline scenarios, the three dimension-specific scenarios are:

North-1.0, where 100% of additional capacity is allocated to the North cluster; South-1.0, where 100% of additional capacity is allocated to the South cluster; and Cluster-balanced (Cluster-bal.), where capacity is distributed in a manner that seeks to achieve uniform final capacities across all zone clusters.

Statistics of GB-aggregated CF under each scenario are presented in Figure 5.14. Excluding the baseline Unchanged scenario, the South-1.0 scenario, as expected, exhibits the worst performance, both in terms of mean and median CF levels as well as CF variability. This is due to the lower power output and the higher power output variability displayed by the Southern zones. On the other hand, the North-1.0 scenario gives rise to the GB-aggregated CF with the highest mean and median. However, more balanced capacity allocations, as in the Zone-bal. and the Cluster-bal. scenarios, lead to the lowest variability of the CF time series.

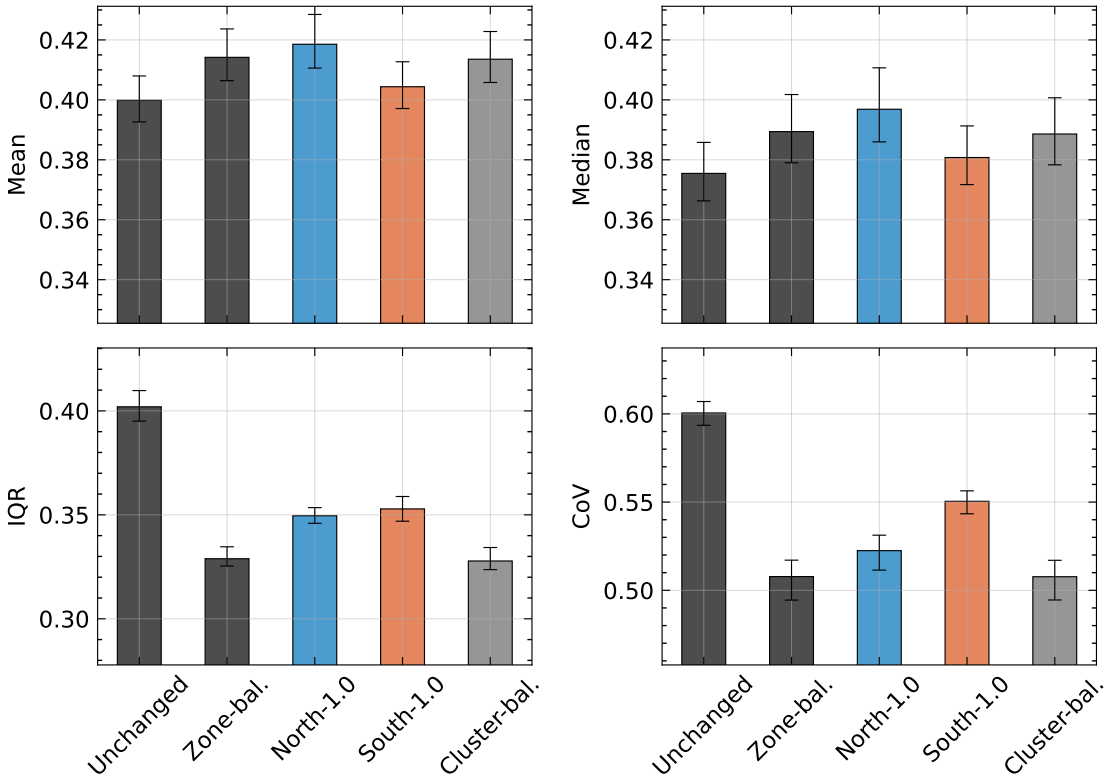


Figure 5.14: Capacity factor statistics for each scenario in the *North vs. South* dimension.

The frequency-duration curves and return period curves of the different scenarios are presented in Figure 5.15. Focusing on the return period curves of the Unchanged and South-

1.0 scenarios, there is sufficient evidence (based on 95% confidence intervals) to conclude that continuing to allocate resources to the shallower seabeds of the South, albeit in a spatially diversified manner, can achieve a wind farm fleet that gives rise to reduced risks to extreme low wind power events. But due to the high power output level and lower output variability, there is also sufficient evidence to conclude that the North-1.0 scenario results in lower risk of extreme low wind power events than the South-1.0 scenario for all extreme low wind power events. While both scenarios still fall short of the Balanced scenarios, their increased return periods compared to the North-1.0 scenario are only statistically significant for extreme low wind power events that last 3 days or shorter.

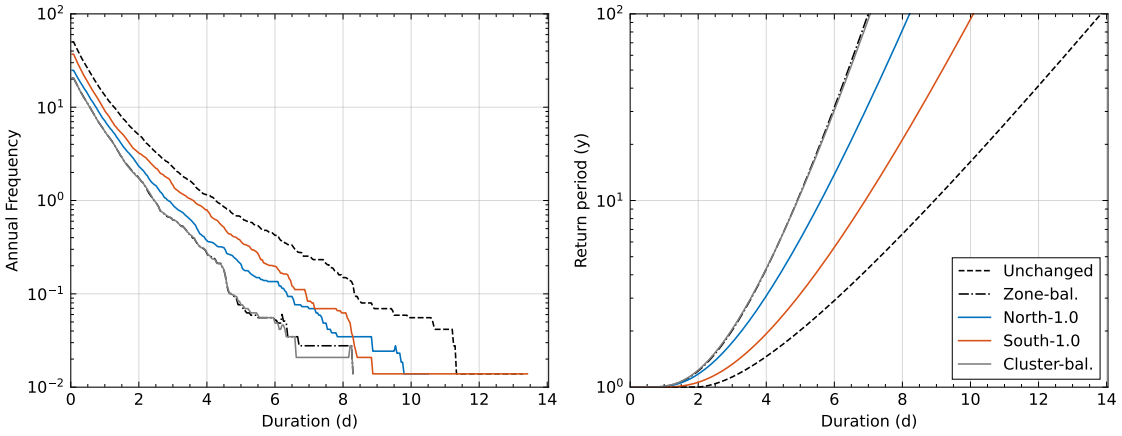


Figure 5.15: Frequency-duration curve (left) and return period (right) of low wind power events for each scenario in the *North vs. South* dimension. Confidence intervals are omitted to maintain clarity. 95% confidence intervals at certain low wind power event durations are tabulated in Appendix C.

These results highlight two key insights. First, the Northern offshore region's higher power output potential makes it more attractive than the Southern region in terms of reducing the risk of extreme low wind power events. Second, they illustrate the trade-off between focusing on zones with higher CF and seeking a balanced portfolio. This is because, although the North-1.0 scenario displays higher mean CF due to the higher CF of the Northern cluster's zones, allocating 100% of additional resources to such zones does not achieve the level of spatial diversification required for a more resilient wind farm fleet, as also noted by Giddings et al. [6].

Northwest vs Southwest

Technical constraints and the absence of established infrastructure as in the North Sea mean that the Southwest and Northwest offshore regions of the UK are largely unexplored for wind farm developments up to 2030. However, these areas have been identified as key zones for future projects, with early planning and initial stages of development already underway [17]. The main question associated with the *Northwest vs Southwest* dimension is how significantly the wind farm fleet can benefit from allocating resources to these areas of higher challenges.

An overview of the zone clusters and the different scenarios is presented in Figure 5.16. In addition to the two baseline scenarios, the three dimension-specific scenarios are: NW-1.0, where 100% of additional capacity is allocated to the Northwest cluster; SW-1.0, where 100% of additional capacity is allocated to the Southwest cluster; Other-1.0, where 100% of additional capacity is allocated to zones not in either the Northwest or the Southwest cluster; and Cluster-balanced (Cluster-bal.), where capacity is distributed in a manner that seeks to achieve uniform final capacities across all zone clusters.

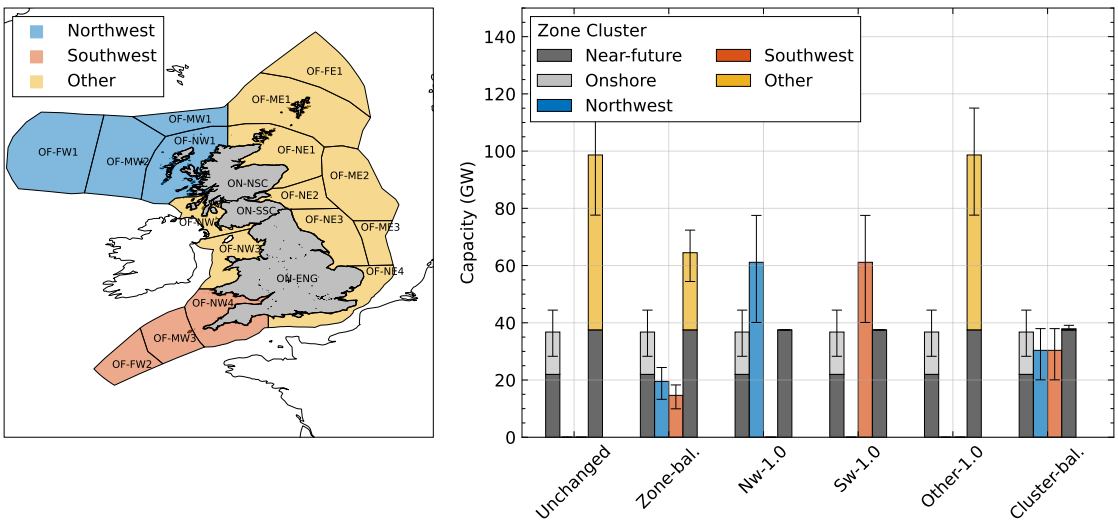


Figure 5.16: Overview of zone clusters and the capacity allocation for each scenario in the *Northwest vs Southwest* dimension. The map (left) illustrates the different zone clusters by distinct colors. The bar chart (right) shows the different final capacities of the clusters in 2050 corresponding to the different scenarios, where dark grey bars represent the existing capacity in a cluster as of 2030. Error bars show the variation of these 2050 capacities due to the different levels of available capacity for allocation as per the four PV scenarios.

Statistics of GB-aggregated CF under each scenario are presented in Figure 5.17. Focusing first on power output level, as represented by GB-aggregated CF mean and median, the Unchanged scenario is the least favourable outcome, while the SW-1.0 and the Other-1.0 scenarios both offer marginally higher median and mean CF levels. As anticipated, the NW-1.0 scenario yields the highest mean and median CF due to the fact that the Northwest cluster encompasses zones with the highest levels of power output potential. Subsequently, considering the variability of the CF time series, the Unchanged scenario consistently exhibits the highest variability of power output, while the Balanced scenarios show the lowest variability. One notable observation here is that although the Other cluster contains the highest number of zones, some of which are not occupied by the Near-future fleet, the Other-1.0 scenario does not lead to as significant an improvement in power output variability compared to scenarios that include the Northwest and Southwest zones. This finding suggests that both the Northwest and the Southwest clusters are situated substantially far from the centre of the Near-future fleet's capacity, meaning wind speed in these regions would be substantially less correlated to other zones.

The frequency-duration curves and return period curves of the different scenarios are presented in Figure 5.18. The SW-1.0 and Other scenarios give rise to statistically significant (based on 95% confidence intervals) higher levels of return periods for all extreme low wind power event durations compared to the Unchanged scenario. Although their return periods diverge at higher event durations, there is not sufficient evidence to suggest that their risk profiles differ from one another at any single duration. In comparison to these two scenarios, the NW-1.0 scenario gives rise to lower risk, but such a finding is only statistically significance for extreme low wind power events with duration lower than 7 days. NW-1.0 shows the highest performance, as expected, due to its higher power output potential, as also noted by Abdelaziz et al. [5]. However, the frequency-duration curve indicates a lower frequency of the longest low wind power events for the SW-1.0 scenario, leading to a faster increase in the return period and, hence, reduced risk for very long low wind power events. As seen in previous dimensions, the Balanced scenarios, which achieve greater spatial diversification, are found to give rise to the most improved risk profile, especially for events longer than 6 days.

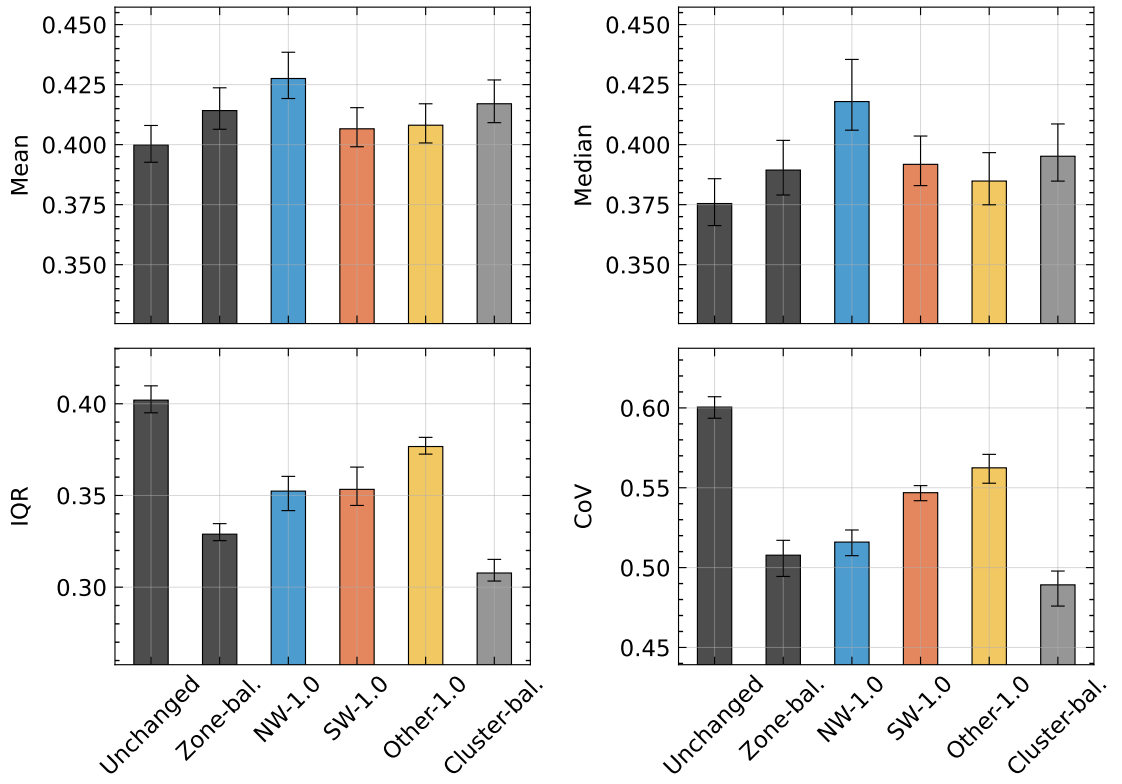


Figure 5.17: Capacity factor statistics for each scenario in the *Northwest vs Southwest* dimension.

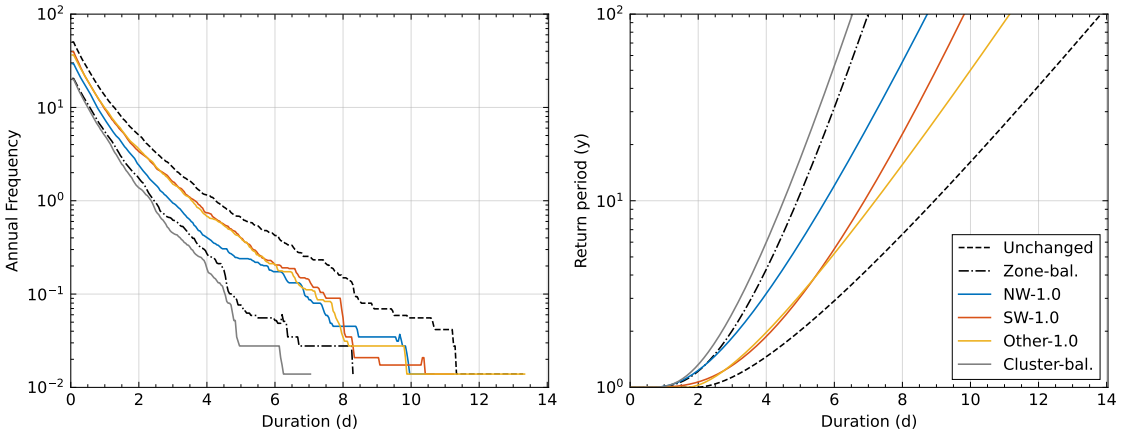


Figure 5.18: Frequency-duration curve (left) and return period (right) of low wind power events for each scenario in the *Northwest vs Southwest* dimension. Confidence intervals are omitted to maintain clarity. 95% confidence intervals at certain low wind power event durations are tabulated in Appendix C.

The important point to note in the results from this *Northwest vs Southwest* dimension is that the number of zones in either of the zone clusters of interest is smaller than the Other cluster. Therefore, the fact that both the NW-1.0 and SW-1.0 scenarios lead to

risk profiles that are at least comparable to the Other-1.0 scenario shows the potential of these two regions to make significant contributions to reducing the risk of low wind power events. Additionally, the fact that the risk profiles of these two zone clusters differ from one another further reinforces this observation. Therefore, these findings point to the significance of these two zone clusters for the resilience of the Far-future fleet.

5.3.3 Electricity system

An overview of wind energy supply and annual electricity demand is presented in Figure 5.19. In this electricity system analysis, wind energy supply is based on the baseline Zone-bal. scenario, which represents the most balanced SD pathway. The available capacity for allocation for each PV scenario, along with annual electricity demand, is given in Table 5.3. As shown, the FS scenario, which is the only FES scenario where the net zero target is not met by 2050, is the only one where annual electricity demand still exceeds annual wind energy supply, and by a significant amount. For the remaining scenarios, annual wind energy supply is projected to exceed electricity demand by varying amounts, with the LW scenario showing the lowest proportion of demand to supply, followed by ST and CT.

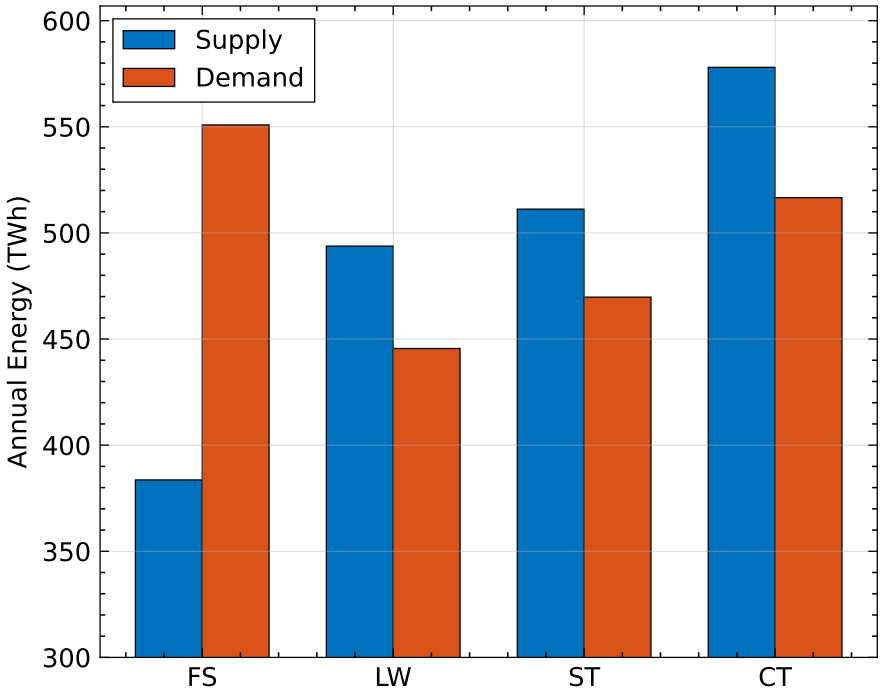


Figure 5.19: Overview of annual electricity demand and production for each FES scenario.

A daily demand-net-wind (DNW) time series was utilized instead of a CF time series to investigate the relationship between wind energy supply and the electricity system. The formulation of the DNW time series is summarized as follows. First, the wind power output time series was computed according to the methods outlined in Section 5.3.1 under the baseline Zone-bal. scenario, which represents the most balanced spatial distribution pathway. Second, a normalised, weather-dependent electricity demand time series was computed based on the methods detailed in Section 3.3 and was mean-scaled by the daily average electricity demand corresponding to the annual electricity demand. Next, similar to the wind energy supply analysis (Section 5.3.2), the SPA method was used to identify electricity system stress events, i.e., events of high DNW (using a 650 GWh threshold, which corresponds to the 0.9 quantile of LW's DNW series, representing the most stringent threshold), and an extreme value analysis was carried out on the AMS of these events.

The frequency-duration curves of these electricity system stress events and their return period curves are presented in Figure 5.20. Most noticeably, FS shows the highest frequency of stress events longer than 2 days as well as the highest maximum event duration at 190 days. The fact that the annual frequency of the FS scenario is within the levels of other scenarios suggests that a single stress event under the FS scenario encompasses what would constitute several shorter events in other scenarios. As a result, a 10-day stress event can be expected to occur once every year under the FS scenario. For the remaining scenarios, LW demonstrates the lowest risk, with the return period of a 10-day stress event at once every 6.4 years, followed by ST and CT.

A large range of outcomes is observed from these results, driven by the poor resilience of the electricity system under the FS scenario, where annual wind energy supply remains lower than annual electricity demand. On the other hand, the risk of system stress events is substantially reduced under the remaining scenarios, all of which feature a surplus of wind energy supply over electricity demand, advanced energy storage solutions, and effective demand-side management strategies to ensure grid stability and resilience.

A major limitation of this approach stems from the assumption that the electricity demand profile can be mean-scaled using the current demand profile. In a future scenario where gas demand has been decarbonized and heating is largely electrified, the electricity

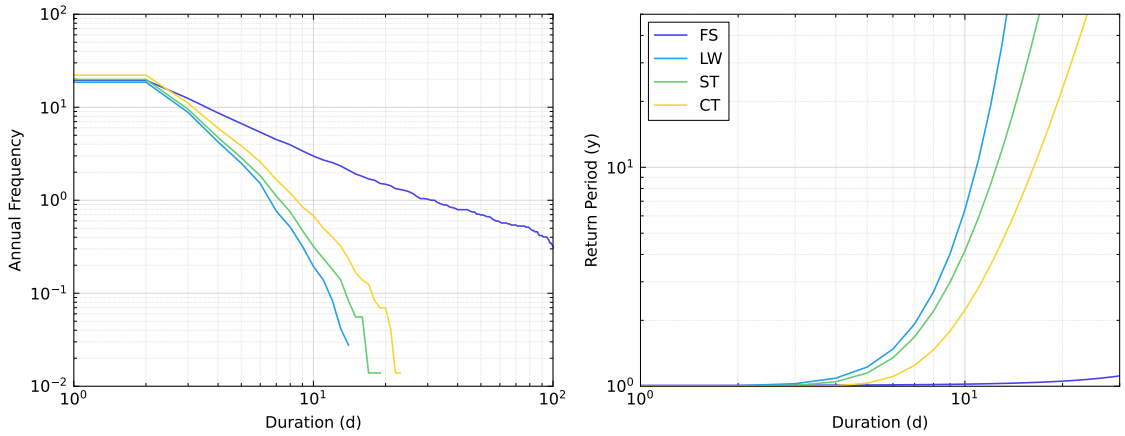


Figure 5.20: Frequency-duration curve (left) and return period (right) of electricity system stress events for each FES scenario

demand profile is likely to exhibit increased seasonality, more closely resembling the current seasonal variability of gas demand, where winter demand is approximately four times higher than summer demand [18]. This assumption risks underestimating future winter electricity peaks and seasonal demand variability, which are critical factors for planning grid capacity, infrastructure upgrades, and energy storage requirements. Addressing this issue will require incorporating the effects of electrified heating into future demand models to better capture these potential seasonal shifts.

5.4 Conclusions

A frequency analysis and an extreme value analysis were carried out on the GB-aggregated CF time series of the Near-future (2030) wind farms fleet based on the REPD. It was found that the Near-future fleet demonstrates a marginally higher level of power output and a lower level of power output variability than the current fleet. More importantly, the reduced frequency at the lower tail of the CF distribution led to a significant decrease in the frequency of low wind power events, particularly for those lasting longer than a week. As a result, the return period of extreme low wind power events is estimated to increase notably, suggesting a reduction in the risk of such events. This improvement stems from the development of wind farms in regions with higher wind power potential, such as the Dogger Bank or further north, as well as a slight increase in the fleet's spatial diversity.

However, these are aspects that can be further improved, as evidenced by the fact that the risk of shorter low wind power events has not been adequately addressed.

Looking further into the future at the Far-future (2050) wind farms fleet, an investigation was conducted to explore the various scenarios that the GB wind farms fleet could potentially adopt. The analysis was driven by two variables: the possible spatial distributions of wind farms and the projected total wind capacity/electricity demand from National Grid ESO's FES report. Considering the relationship between wind energy supply and electricity demand, it was found that limiting electricity demand is as important as adding wind farm capacity. This finding is evidenced by the Leading the Way scenario, where wind capacity is at a moderate level but is complemented by a lower electricity demand level, leading to the lowest risk of system stress events.

Furthermore, it was found that the spatial distribution of wind farms can have a significant impact on the risk profile of the wind farms fleet regarding extreme low wind power events. The following observations can be made. First, allocation of capacity further offshore leads to an improved risk profile due to higher power output potential and lower output variability, although diminishing returns in this improvement are observed with increasing distance. Second, although it may pose technical and economic challenges, building wind farms in the West allows greater spatial diversification, making it key to improving the risk profile. Third, Northern offshore regions hold greater power output potential than Southern regions, making resource allocation to the North more attractive than to the South. Fourth, the Northwest and the Southwest are two unexplored regions with significant power output potential. Allocating resources to these regions can considerably improve the resilience of the GB wind farms fleet. All in all, a spatially balanced allocation of resources is desirable, but such a scenario may not be practical. As economic and technological trends in offshore wind energy advance, these conclusions offer insights into development plans that potentially lead to a more resilient wind farms fleet.

References

[1] Department for Energy Security and Net Zero. Renewable Energy Planning Database, 2022. Accessed: 2022-12-15.

[2] National Grid ESO. Future Energy Scenarios 2022. Technical report, July 2022.

[3] D. J. Cannon, D. J. Brayshaw, J. Methven, P. J. Coker, and D. Lenaghan. Using reanalysis data to quantify extreme wind power generation statistics: A 33 year case study in Great Britain. *Renewable Energy*, 75:767–778, 2015.

[4] D. R. Drew, D. J. Cannon, D. J. Brayshaw, J. F. Barlow, and P. J. Coker. The impact of future offshore wind farms on wind power generation in Great Britain. *Resources*, 4(1):155–171, 2015.

[5] S. Abdelaziz, S. N. Sparrow, W. Hua, and D. C. Wallom. Assessing long-term future climate change impacts on extreme low wind events for offshore wind turbines in the UK exclusive economic zone. *Applied Energy*, 354:122218, 2024.

[6] J. Giddings, H. Bloomfield, R. James, and M. Blair. The impact of future UK offshore wind farm distribution and climate change on generation performance and variability. *Environmental Research Letters*, 19(6):064022, 2024.

[7] G. Sinden. Characteristics of the UK wind resource: Long-term patterns and relationship to electricity demand. *Energy Policy*, 35:112–127, 1 2007.

[8] P. Potisomporn and C. R. Vogel. Spatial and temporal variability characteristics of offshore wind energy in the United Kingdom. *Wind Energy*, 25(3):537–552, 2022.

[9] T. Poulsen and H. G. Beyer. Spectral characteristics and spatial smoothing of wind power–a case study of the Faroe Islands. *Meteorologische Zeitschrift*, 29:427–438, 2020.

[10] J. Wohland, D. Brayshaw, and S. Pfenninger. Mitigating a century of European renewable variability with transmission and informed siting. *Environmental Research Letters*, 16(6):064026, 2021.

[11] C. M. Grams, R. Beerli, S. Pfenninger, I. Staffell, and H. Wernli. Balancing Europe's Wind-Power Output Through Spatial Deployment Informed by Weather Regimes. *Nature Climate Change*, 7:557–562, 2017.

[12] Regen. Go West! An analysis of the energy system benefits and implication of a more geographically diverse offshore wind portfolio. Technical report, 2022.

[13] S. C. Pryor, R. J. Barthelmie, M. S. Bukovsky, L. R. Leung, and K. Sakaguchi. Climate change impacts on wind power generation. *Nature Reviews Earth & Environment*, 1 (12):627–643, 2020.

[14] H. Nissan, L. Goddard, E. C. de Perez, J. Furlow, W. Baethgen, M. C. Thomson, and S. J. Mason. On the use and misuse of climate change projections in international development. *Wiley Interdisciplinary Reviews: Climate Change*, 10(3):e579, 2019.

[15] S. Cavazzi and A. Dutton. An Offshore Wind Energy Geographic Information System (OWE-GIS) for assessment of the UK's offshore wind energy potential. *Renewable Energy*, 87:212–228, 2016.

[16] M. Shafiee, F. Brennan, and I. A. Espinosa. A parametric whole life cost model for offshore wind farms. *The International Journal of Life Cycle Assessment*, 21:961–975, 2016.

[17] U. Government. Offshore wind net zero investment roadmap, 2023. URL `https://www.gov.uk/government/publications/offshore-wind-net-zero-investment-roadmap`. Accessed: 2024-07-12.

[18] I. G. Wilson, A. J. Rennie, Y. Ding, P. C. Eames, P. J. Hall, and N. J. Kelly. Historical daily gas and electrical energy flows through great britain's transmission networks and the decarbonisation of domestic heat. *Energy Policy*, 61:301–305, 2013.

Appendix A - FES Scenarios

The following descriptions outline the four scenarios as taken from the FES report 2023 [2].

- **Falling Short**: *This scenario does not meet the net zero by 2050 target. There is still progress on decarbonisation compared to today, however it is slower than in the other scenarios. While home insulation improves, there is still heavy reliance on natural gas, particularly for domestic heating. Electric Vehicle take-up grows more slowly, displacing petrol and diesel vehicles for domestic use. Decarbonisation of other vehicles is slower still with continued reliance on diesel for Heavy Goods Vehicles (HGVs). In 2050 this scenario still has significant annual carbon emissions, short of the 2050 net zero target.*

- **Leading the Way**: *The net zero target is met by 2046. We assume that GB decarbonises rapidly with high levels of investment in world-leading decarbonisation technologies. Our assumptions in different areas of decarbonisation are pushed to the earliest credible dates. Consumers are highly engaged in reducing and managing their own energy consumption. This scenario includes more energy efficiency improvements to drive down energy demand, with homes retrofitted with measures such as triple glazing and external wall insulation, and a steep increase in smart energy services. Hydrogen is used to decarbonise some of the most challenging areas such as some industrial processes, produced mostly from electrolysis powered by renewable electricity.*

- **System Transformation**: *The net zero target is met in 2050. The typical domestic consumer will experience less change than in Consumer Transformation as more of the significant changes in the energy system happen on the supply side. A typical consumer will use a hydrogen boiler with a mostly unchanged heating system and an Electric Vehicle or a fuel cell vehicle. They will have had fewer energy efficiency improvements to their home and will be less likely to provide flexibility to the system. Total hydrogen demand is high, mostly produced from natural gas with Carbon*

Capture, Usage and Storage (CCUS).

- **Consumer Transformation**: *The net zero target is met in 2050 with measures that have a greater impact on consumers and is driven by higher levels of consumer engagement. They will have made extensive changes to improve their home's energy efficiency and most of their electricity demand will be smartly controlled to provide flexibility to the system. A typical homeowner will use an electric heat pump with a low temperature heating system and an Electric Vehicle (EV). The system will have higher peak electricity demands managed with flexible technologies including energy storage, Demand Side Response (DSR) and smart energy management.*

Appendix B - Zones determination

The zones used in this analysis were defined with consideration of existing onshore transmission zones, which provide a logical framework for dividing the UK into regions relevant to energy generation and distribution. These onshore boundaries were then extrapolated offshore to encompass areas within the UK Exclusive Economic Zone (EEZ), ensuring continuity between onshore and offshore regions. Additionally, an effort was made to create an approximately equal number of zones in the dimensions of interest, balancing spatial representation across the study area while maintaining relevance to the key variables being analyzed.

The shift of focus from individual wind farms to wind farm zones in the Far-future analysis necessitates the use of zone-aggregated power output time series instead of wind farm power output time series. As mentioned in Section 5.3.1, this process involves the aggregation of wind speed from ERA5's grid points that are confined within the boundary of a zone. Consequently, one key consideration of the zones determination is the size of the zones. While the number of zones should not be too great to avoid unnecessary complexity, the zone size should not be too large for two reasons. First, if the zone size is too large, the zone-aggregated wind speed may not be well correlated with the wind speed from individual grid points. Second, if the zone size is too large, the zone-aggregated wind speed may be overly smoothed out and lose variance.

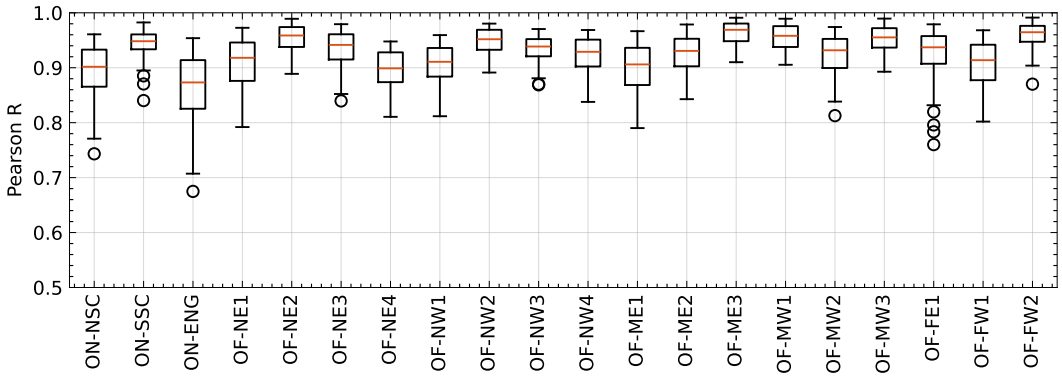


Figure 5.21: Correlation (Pearson R) of each zone-aggregated wind speed time series with wind speed time series from individual grid points confined within the zone boundary.

A simulation was carried out to determine the maximum area (number of grid points)

enclosed by a zone boundary. Two key metrics were used: first, the correlation (Pearson R) of the zone-aggregated wind speed series with wind speed series from individual grid points, and second, the coherence between the zone-aggregated wind speed series and wind speed series from individual grid points at various frequencies. This approach ensures that the aggregated wind speed time series is representative of the zone in both time and frequency domains. The resultant number of grid points was found to be 144, or approximately 172,000 km^2, and the segmentation of the UK EEZ into 20 zones was carried out accordingly.

For each of the final 20 zones, the correlations of the zone-aggregated wind speed time series with wind speed time series from individual grid points are summarized in Figure 5.21. As shown, the median correlation for any zone is higher than 0.85, and the minimum correlation is above 0.7. An exception to this trend is the *ON-ENG* zone, i.e., onshore England, which displays the lowest correlation out of all the zones. However, given the limited influence of onshore zones on the analysis, this was deemed acceptable. Furthermore, the coherence of the zone-aggregated wind speed time series with wind speed time series from individual grid points at multiple frequencies is summarized in Figure 5.22. For all zones, a reduction in coherence is observed at a frequency corresponding to a period of 4 days, resulting from the averaging of wind speed time series that smooths out fluctuations at these higher frequencies. However, across all zones, it can be seen that the coherence at the frequency corresponding to a 1-day period is within a sufficiently high range of 0.6-0.8. Given that extreme low wind power events are of duration greater than 1 day, further declines in coherence beyond this frequency have limited impacts on the results. Therefore, these analyses in the time and frequency domains confirm that, first, the zone-aggregated series are representative of the wind speed within the zone, and second, the loss of information is limited to fluctuations with a frequency higher than that associated with a 1-day period.

Although the loss of information is shown to be limited to higher-frequency signals, this loss still introduces significant differences in the final zonally or nationally aggregated capacity factor (CF) time series compared to those aggregated directly from wind farm power output. To illustrate these differences, Figure 5.23 presents the CF distribution and

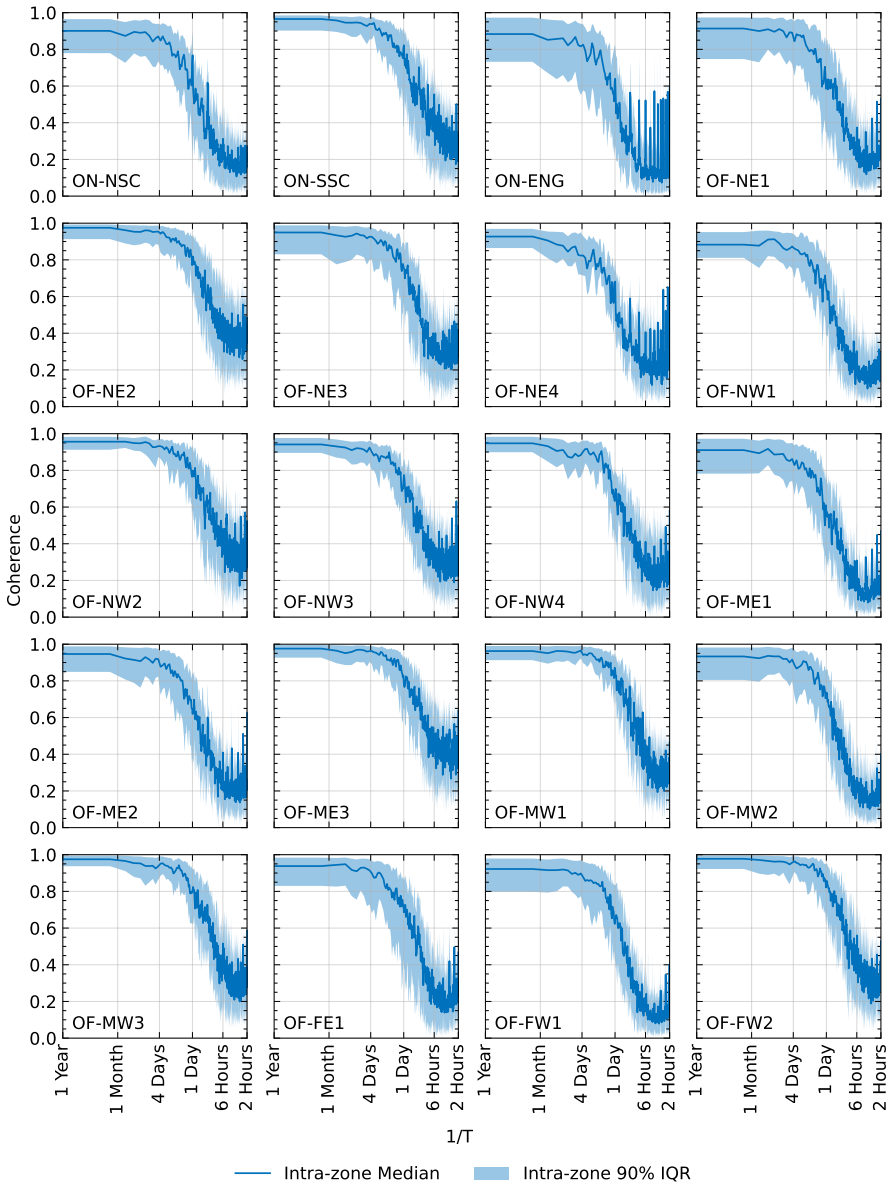


Figure 5.22: Coherence of each zone-aggregated wind speed time series with wind speed time series from individual grid points confined within the zone boundary.

the frequency-duration curve of low wind power events, identified using a CF threshold of 0.1, for each approach. In this figure, *Farm* represents the aggregation of power output directly from wind farms, while approach 1 (*App1*) involves aggregating wind speed from grid points within a zone, converting this to power output for each zone, and then aggregating power output across all zones. Notably, the distribution under *App1* shows significantly less variability in the CF time series compared to the *Farm* approach. Consequently, the frequency of longer low wind power events is substantially underestimated

under *App1*. For further comparison, approach 2 (*App2*) involves converting wind speed at each grid point to power output before aggregating power output across all grid points within a zone, and subsequently aggregating power output from all zones. The CF distribution and frequency-duration curve under *App2* show even larger deviations from the *Farm* approach than those observed under *App1*.

In light of these findings, it is clear that low wind power events identified from CF time series based on approaches 1 and 2 are underestimated in both frequency and duration compared to the farms-based approach. Two key determinations were made from these results. First, approach 1—where wind speed is aggregated within a zone before being converted into a zone-representative power output time series—was selected as the preferred method for intra-zone aggregation over approach 2. Second, since the results obtained from the farms-based approach and approach 1 are not directly comparable, results from the Far-future analysis, which relies on intra-zone aggregations, are compared only within themselves and not against the Near-future analysis, which is based on the farms-based approach.

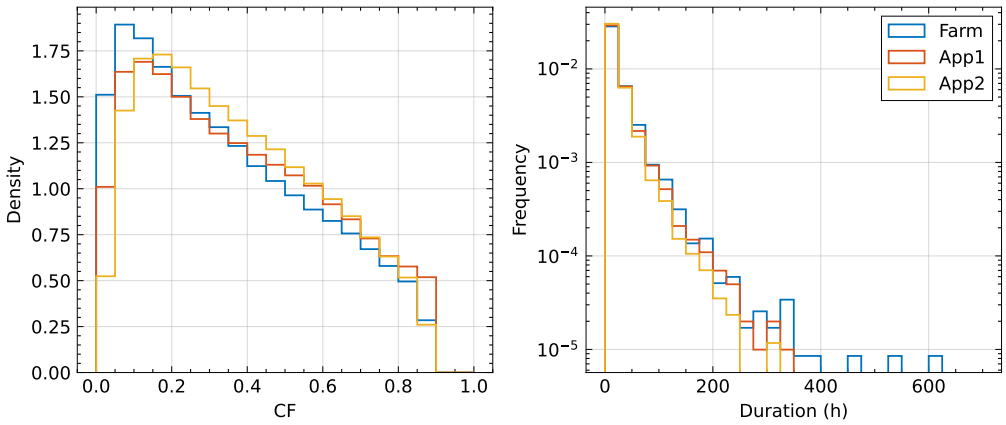


Figure 5.23: (Left) Capacity factor distribution of GB-aggregated CF time series for the 2022 wind farms distribution under different methods of aggregation. *Farm* refers to aggregating power output directly from wind farms. *App1* refers to aggregating wind speed from grid points within a given zone first before converting to wind power output, and aggregating the resultant power output from all zones. *App2* refers to converting wind speed to power output at a grid point before aggregating wind power output from all grid points within a zone, and aggregating the resultant power output from all zones. (Right) Frequency-duration curves of low wind power events identified using CF threshold of 0.1 from the CF time series resulting from these aggregation approaches.

Appendix C - Return periods and confidence intervals

Offshore distance		3 days	5 days	7 days
Unchanged	**Fit**	1.085	2.015	4.338
	0.025	1.030	1.880	3.710
	0.975	1.108	2.185	5.533
Zone-bal.	**Fit**	2.017	10.915	100.523
	0.025	1.861	8.042	56.288
	0.975	2.236	18.490	289.176
Near-1.0	**Fit**	1.085	2.362	5.879
	0.025	1.030	2.157	4.815
	0.975	1.108	2.668	8.148
Medium-1.0	**Fit**	2.241	10.813	72.397
	0.025	2.058	8.207	44.258
	0.975	2.507	17.348	176.291
Far-1.0	**Fit**	3.482	18.694	122.749
	0.025	3.091	13.777	74.087
	0.975	4.177	32.062	310.032
Cluster-bal.	**Fit**	3.216	17.424	115.538
	0.025	2.865	12.881	69.945
	0.975	3.816	29.579	288.725

Table 5.4: Fitted return periods and 95% confidence intervals of low power events with durations of 3, 5, and 7 days for each scenario in the *Offshore Distance* dimension.

East vs West		3 days	5 days	7 days
Unchanged	**Fit**	1.085	2.015	4.338
	0.025	1.030	1.880	3.710
	0.975	1.108	2.185	5.533
Zone-bal.	**Fit**	2.017	10.915	100.523
	0.025	1.861	8.042	56.288
	0.975	2.236	18.490	289.176
East-1.0	**Fit**	1.326	3.313	11.897
	0.025	1.295	2.871	8.796
	0.975	1.334	4.115	19.985
West-1.0	**Fit**	2.248	11.304	77.516
	0.025	2.058	8.535	47.193
	0.975	2.523	18.266	189.677
Split	**Fit**	1.930	7.918	45.980
	0.025	1.804	6.211	29.375
	0.975	2.092	11.920	102.770
Cluster-bal.	**Fit**	2.184	11.080	82.773
	0.025	2.006	8.310	49.095
	0.975	2.441	18.169	213.417

Table 5.5: Fitted return periods and 95% confidence intervals of low power events with durations of 3, 5, and 7 days for each scenario in the *East vs West* dimension.

North vs South		3 days	5 days	7 days
Unchanged	**Fit**	1.085	2.015	4.338
	0.025	1.030	1.880	3.710
	0.975	1.108	2.185	5.533
Zone-bal.	**Fit**	2.017	10.915	100.523
	0.025	1.861	8.042	56.288
	0.975	2.236	18.490	289.176
North-1.0	**Fit**	1.736	6.227	32.722
	0.025	1.645	5.008	21.530
	0.975	1.839	8.943	69.157
South-1.0	**Fit**	1.327	3.157	10.638
	0.025	1.298	2.760	7.992
	0.975	1.332	3.863	17.374
Cluster-bal.	**Fit**	2.046	10.790	93.687
	0.025	1.888	7.997	53.300
	0.975	2.270	18.082	261.609

Table 5.6: Fitted return periods and 95% confidence intervals of low power events with durations of 3, 5, and 7 days for each scenario in the *North vs South* dimension.

Nw. vs Sw.		3 days	5 days	7 days
Unchanged	**Fit**	1.085	2.015	4.338
	0.025	1.030	1.880	3.710
	0.975	1.108	2.185	5.533
Zone-bal.	**Fit**	2.017	10.915	100.523
	0.025	1.861	8.042	56.288
	0.975	2.236	18.490	289.176
NW-1.0	**Fit**	1.848	5.996	25.393
	0.025	1.750	4.930	17.689
	0.975	1.961	8.291	48.314
SW-1.0	**Fit**	1.311	3.053	10.850
	0.025	1.285	2.668	8.010
	0.975	1.315	3.747	18.355
Other-1.0	**Fit**	1.331	3.136	8.926
	0.025	1.301	2.779	7.053
	0.975	1.331	3.738	13.227
Cluster-bal.	**Fit**	2.492	16.845	178.575
	0.025	2.240	11.899	95.725
	0.975	2.895	30.917	558.369

Table 5.7: Fitted return periods and 95% confidence intervals of low power events with durations of 3, 5, and 7 days for each scenario in the *Northwest vs Southwest* dimension.

CHAPTER 6

Conclusions

This thesis has investigated the spatiotemporal variability of extreme low wind power events in Great Britain. ERA5 reanalysis data was evaluated with respect to low wind speed events on a large scale, and the results informed the development of a wind power generation model that formed the basis of subsequent research. In a novel approach, pooling procedures from hydrology were applied to the identification of low wind power events and electricity system stress events, leading to a more practical, relevant, and statistically robust definition of extreme events. The methodology provided the foundation for the ensuing frequency analysis and extreme value analysis conducted on simulated nationally aggregated wind power output of the current, near-future, and far-future GB wind farm fleet. Given the current farm fleet, findings suggest that the March 2021 event may not have been as extremely rare as it was described at the time. However, the near-future distribution of wind farms in 2030 has been shown to demonstrate higher power output potential and have a lower risk of extreme wind events. Looking further into the future, unexplored offshore regions offer the potential for higher power output and spatial diversification of the GB wind farms fleet. The deployment of resources into such regions has been projected to offer significant improvements to the resilience of the wind-dominated electricity system. Detailed conclusions of this thesis are summarised in three parts, corresponding to the three thesis research objectives and the chapter concludes with suggestions for future work.

6.1 Summary and Conclusions

GB wind power output and electricity demand modelling from reanalysis data

Reanalysis datasets can offer superior spatiotemporal coverage and reliability compared to observed wind speed or power output data and are calibrated using observational data through the process of data assimilation. Therefore, they are often used as the ground truth in many climate studies [1], including those on extreme wind events. However, biases and uncertainties arising from modelling processes warrant a thorough assessment prior to their usage. The 10-m wind speed data from ECMWF's state-of-the-art ERA5 reanalysis was evaluated against measured wind speed from 205 observation stations [2, 3] in the onshore and offshore domains of the United Kingdom from the year 1997-2020. A positive mean wind speed bias of 0.166 m/s was found in the onshore domain and a negative mean wind speed bias of 0.136 m/s was found in the offshore domain, while generally, ERA5 wind speed demonstrates an underestimation of hourly variability of wind speed. As a result, the frequency of low wind speed events shorter than 12 hours is significantly underestimated. However, the frequency of longer low wind speed events, which are the focus of this thesis, is substantially more accurately represented. These findings suggest that using ERA5 as ground truth without first addressing these biases or acknowledging their limitations can distort the accuracy of the conclusions drawn.

Modelling national wind power output aggregated from diverse wind farms necessitates an approach that is not overly granular but still preserves the nuances required for an accurate presentation. Results obtained from the evaluation of ERA5 reanalysis data were used to inform its bias correction as a necessary first step. Mean-variance scaling, a simple bias correction technique compared to those with slightly higher sophistication like quantile mapping and CDF transform, proved to be sufficient in obtaining an accurate characterisation of low wind speed events. The corrected surface wind speed data was then extrapolated to hub height using Multi-layer Perceptron regression, which demonstrated substantially higher accuracy than the conventionally used logarithmic wind profile, corroborating findings from smaller-scale studies [1, 4]. A farm power curve was formulated

based on a five-parameter logistic curve, empirically calibrated to take farm-level losses, and applied to hub-height wind speed. The resultant nationally aggregated wind power output data showed a high level of agreement with electricity system data, achieving an increase in accuracy by over 60% as measured by the reduction in RMSE.

Frequency and extreme value analyses of low wind power events

Defining and identifying a low wind power event is a crucial first step in characterising drought frequency and duration. While runs analysis is a basic and useful approach, in the context of fulfilling electricity demand through wind energy, the Sequent Peak Algorithm provides a more relevant definition based on the energetic content of the time series. This technique identifies longer low wind power events, where wind power generation may not consistently fall below a given threshold, but the cumulative energy deficit still significantly impacts the electricity system. According to this definition, a low wind power event associated with a capacity threshold of 0.1 can last up to 26 days from the 72-year simulated GB power output data, a duration substantially longer than previously reported [5]. Furthermore, these pooling procedures facilitate the grouping of mutually dependent events, providing greater confidence that the events in the sample are independent of each other. Such an approach, therefore, enhances the statistical robustness of the procedure, ensuring that the identified risks are accurately estimated. Nevertheless, the choice of threshold to define these events is a key parameter in determining their frequency, duration, and associated risk. Therefore, practitioners using this method should select thresholds that best reflect the nuances and objectives of their specific studies, ensuring that the results are meaningful and relevant to the analyses.

To quantify the risk of extreme wind events, an extreme value analysis was carried out on low wind power events identified by the Sequent Peak Algorithm from 72 years of simulated GB-aggregated wind power output data. Findings show that an extreme low wind power event lasting 1 week is expected to occur as frequently as once every 2 years, while an extreme event lasting 2 weeks has a return period of only 10 years. A parallel analysis was also conducted on extreme electricity system stress events identified from the demand-net-wind time series, revealing that the current estimated energetic capacity of

energy storage in GB is equipped to address only very short events with a return period of just over 1 year. Under this characterisation, the return period associated with the March 2021 event is approximately 2 years. Therefore, in contrast to the characterisation found in the literature [6], such an event may not be considered particularly rare. This highlights the critical necessity of preparing the electricity system for the growing integration of wind energy to ensure stability and reliability in the future.

Spatial variability of extreme low wind power events

By 2030, it is projected that up to 38 GW of additional onshore and offshore wind capacity will be installed. While the majority of offshore capacity will remain concentrated in the North Sea, large wind farms such as Dogger Bank and Cerulean will be situated further north and farther offshore. Using data from 1950-2021 to simulate aggregated power output in 2030, it is projected that the major improvement of the fleet's resilience to extreme wind events stems not from higher wind power output but rather from a reduction in wind power output variability. While the frequency of short low wind speed events does not exhibit significant changes, the frequency of events longer than 7 days demonstrates a substantial reduction in frequency. Consequently, the return periods of these longer events display a meaningful increase. Although improvements in the system's resilience have been observed, further enhancements could be achieved, especially considering that the total wind capacity is projected to more than double by 2030. Technical and economic constraints may continue to be significant limiting factors for these improvements.

Hence, the exploration of 2050 wind farm distributions based on FES scenarios aimed to assess the sensitivity of the resilience and reliability of the future electricity system to the spatial deployment of wind capacity. Findings indicate that regions further offshore while offering higher wind power potential and greater opportunities for spatial diversification, exhibit diminishing advantages with increasing distance. Given the concentration of planned offshore wind farms in the Southeast, the less developed Western and Northern regions also present opportunities for higher spatial diversity, enhancing the resilience of the wind farm fleet to low wind events. Furthermore, the Northwestern and Southwestern regions, currently unexplored, show significant potential in reducing the risk of extreme

low wind power events. Overall, the spatial diversification of wind farms proves to be as crucial as the deployment of resources into regions with high power output potential, as also noted by Giddings et al. [7].

These findings underscore the critical role of strategic spatial planning in wind farm deployment, not only for maximising energy production but also for bolstering electricity system resilience against extreme wind events. While it is clear that positioning wind farms in the currently unexplored regions may demand more advanced technology and incur higher economic costs, the resulting benefit in system resilience has been clearly demonstrated. Nonetheless, even with such strategic placement, the risk of low wind events cannot be entirely mitigated. Thus, the outcomes from various deployment scenarios provide guidance for future energy storage planning, ensuring the electricity system remains reliable and resilient against these extreme events.

6.2 Future work

6.2.1 Power output modelling

Although the current wind farm power curve model yields wind power output that exhibits an acceptable level of agreement with observed power output, it can be more robustly applied with additional refinements. The current model is based on empirical calibrations informed by only two low-capacity wind farms and so, such calibrations may not be representative of a larger sample of wind farms or higher-capacity wind farms where there is significant aerodynamic interaction between the farm and the wind resource. Improvements to the model could follow two approaches. The first approach can be characterised as an extension of the current empirical approach; additional wind farm data, particularly from these larger wind farms, can be incorporated to increase the size and faithfulness of the sample used to inform the calibration process. However, the limited availability of such data remains a major constraint. The second potential approach is more analytical in nature. Improvements in analytical wind farm models can be leveraged to include farm level losses like wake and blockage effects so that the resultant farm power curve is grounded in physical principles, capable of better predicting power output under a wider range of

scenarios. Additionally, both approaches should also incorporate the large-scale interaction between the farms and the wind resource. Given the increasing number and size of wind farms, the impacts of farm-farm wake interactions and farms' cumulative resistance can significantly alter the available wind resource. To fully capture these dynamics, integrating numerical weather prediction simulations into the analysis could be valuable. Such simulations would include large-scale wind farms, enabling a comprehensive assessment of both local and regional impacts on wind patterns and power generation potential.

6.2.2 Weather regimes

The study of weather regimes provides a comprehensive understanding of the climatic drivers behind extreme wind events and, therefore, represents an important and compelling avenue for future research. Although there is a growing body of literature on these meteorological drivers of *Dunkelflaute* events, the investigation of weather regimes with a particular focus on the duration and severity of extreme wind events will offer clearer insights in the context of wind energy. Two potential aspects regarding weather regimes and extreme wind events have been identified. First, the relationship between different weather regimes and extreme wind events under the influence of climate change can be examined. The possible variations in the profiles of wind energy supply and electricity demand may result in the identification of weather regimes that present a risk to future electricity systems. Second, predicting extreme wind events through the prediction of weather regimes will provide essential information for the management of the electricity system in anticipation of extreme electricity system response events. Preliminary work has been completed in exploring these relationships, laying the groundwork for further detailed investigations into the correlations between weather regimes and extreme wind events.

6.2.3 Climate change

In this thesis, reanalysis data from 1950-2021 is used to simulate power output for future distributions of wind farms due to the scope of the study and on the basis that datasets grounded in observations are more reliable and accurate than projections. Although several studies in the literature have highlighted that the inter-annual variability of mean wind

speed remains more significant than climate-change-induced variation, far fewer studies have investigated this variation in the context of extreme events. Therefore, the use of climate projections to simulate power output from future distributions of wind farms allows the impacts of climate change to be investigated in parallel with the spatial aspects. The changing patterns of electricity demand will also drive the variation of these extremes. This approach necessitates a thorough evaluation of climate projections, which includes the selection of appropriate datasets, the quantification of biases and their influences on low wind events, and the temporal down-scaling of certain datasets. As a result, the analysis will become non-stationary, requiring the replacement of ordinary extreme value analyses with dynamic extreme value analyses.

6.3 Concluding remarks

It is now evident that the weather conditions experienced by Great Britain's wind farm fleet and electricity system in March 2021 are not particularly rare occurrences. The expansion of the wind farm fleet into less developed regions with higher power output potential will enhance the fleet's energy yield, spatial diversity, and ultimately, resilience to such extreme events. However, the immutable fact is that the wind resource remains an inherently intermittent and variable source of energy. Wind energy will undoubtedly play an increasingly important role in the electricity system. Therefore, without significant advancements across various domains, similar wind conditions to those of March 2021 will have an even greater impact on the electricity system. Technological innovations and economic measures will be necessary to support fleet expansion. Limiting electricity demand and improving energy storage solutions will be essential to manage periods of supply-demand imbalance. Further research is required to better forecast the occurrences of such events, as well as how they will be impacted by climate change. In light of these multifaceted challenges, further collaborations between meteorologists, engineers, system operators, and policymakers are crucial for the complete decarbonisation of the GB electricity system.

References

[1] L. Dawkins and I. Rushby. Characterising adverse weather for the UK electricity system, including addendum for surplus generation events, 2020. URL www.metoffice.gov.uk.

[2] Met Office. Met Office Integrated Data Archive System (MIDAS) Land and Marine Surface Stations Data (1853-Current), 2012. URL http://catalogue.ceda.ac.uk/uuid/220a65615218d5c9cc9e4785a3234bd0.

[3] Crown Estate. Marine Data Exchange. URL https://www.marinedataexchange.co.uk.

[4] M. A. Mohandes and S. Rehman. Wind Speed Extrapolation Using Machine Learning Methods and LiDAR Measurements. *IEEE Access*, 6:77634–77642, 2018.

[5] D. J. Cannon, D. J. Brayshaw, J. Methven, P. J. Coker, and D. Lenaghan. Using reanalysis data to quantify extreme wind power generation statistics: A 33 year case study in Great Britain. *Renewable Energy*, 75:767–778, 2015.

[6] I. Staffell, R. Green, T. Green, and M. Jansen. Electric Insights Quarterly. Technical report, Drax Group, 2021. URL https://reports.electricinsights.co.uk/wp-content/uploads/2021/05/Drax-Electric-Insights-Q1-2021-Report.pdf.

[7] J. Giddings, H. Bloomfield, R. James, and M. Blair. The impact of future UK offshore wind farm distribution and climate change on generation performance and variability. *Environmental Research Letters*, 19(6):064022, 2024.